THE RHEOLOGICAL AND STRUCTURAL PROPERTIES OF BLENDS OF POLYETHYLENE WITH PARAFFIN WAX

A Dissertation
Presented to
The Academic Faculty

By

Ian Douglas Winters

In Partial Fulfillment
Of the Requirements for the Degree
Doctor of Philosophy in Polymer Engineering

Georgia Institute of Technology

December 2012

THE RHEOLOGICAL AND STRUCTURAL PROPERTIES OF BLENDS OF POLYETHYLENE WITH PARAFFIN WAX

Approved by:

Dr. Donggang Yao
School of Materials Science and Engineering
Georgia Institute of Technology

Dr. Karl Jacob
School of Materials Science and Engineering
Georgia Institute of Technology

Dr. David Bucknall
School of Materials Science and Engineering
Georgia Institute of Technology

Dr. Yonathan Thio
School of Materials Science and Engineering
Georgia Institute of Technology

Dr. Kevin Kit
School of Materials Science and Engineering
University of Tennessee

Date Approved: August 23, 2012

ACKNOWLEDGEMENTS

The author takes this opportunity to express his sincere gratitude to the special other people who made this accomplishment possible. Specifically he owes great thanks to his Advisor, Dr. Donggang Yao, Associate Professor of Materials Science and Engineering at the Georgia Institute of Technology; and his Co-advisor Dr. David Bucknall, Professor of Materials Science and Engineering at the Georgia Institute of Technology. Additional thanks go out to his thesis committee members: Dr. Karl Jacob, Professor of Materials Science and Engineering at the Georgia Institute of Technology; Dr. Kevin Kit, Associate Professor of Materials Science and Engineering at the University of Tennessee (Knoxville); Dr. Meisha Shofner, Assistant Professor of Materials Science and Engineering at the Georgia Institute of Technology; and Dr. Yonathan Thio, Assistant Professor of Materials Science and Engineering at the Georgia Institute of Technology.

Of course, I could never have gotten through this without my understanding lab-mates, past and present: Dr. Jun Jia, Dr. Ruihua Li, Dr. Ramasubramani Kuduba Raman Thanumoorty, and Dr. Wei Zhang; Sarang V. Deodhar, Xudong Fang, Yifeng Hong, and Thomas Wyatt.

I do not know who is more cordially pleased that this is over, they or myself.

TABLE OF CONTENTS

ACKNOWLEDGEMENTS iii
LIST OF TABLES vi
LIST OF FIGURES viii
LIST OF SYMBOLS AND ABBREVIATIONS xiv
SUMMARY xvi
CHAPTER 1: INTRODUCTION 1
CHAPTER 2: LITERATURE REVIEW 5
2.1. History of Polyethylene/Polyethylene Blends 5
2.2. Theories and Equations 11
2.2.1. Polymer Solutions 11
2.2.2. Miscible Polymer Blends and Mixtures 21
2.2.3. Thermodynamics of Polymer Blends and Solutions 29
CHAPTER 3: RHEOLOGICAL AND THERMAL BEHAVIOR OF PE/PE MELT MIXTURES 31
3.1. Rheological and Thermal Behavior: Introduction 31
3.2. Material Preparation and Characterization 32
3.2.1. Melt Mixing 32
3.2.2. Thermogravimetric Analysis 35
3.2.3. Differential Scanning Calorimetry 37
3.2.4. Compression Molding 38
3.2.5. Parallel Plate Rheometry 40
3.3. Thermal and Phase Behavior 41
3.3.1. Concerning TGA 42
3.3.2. Thermal Results and Phase Behavior 43
3.3.3. Phase Diagrams 59
3.4. Rheological Behavior 66
3.5. Conclusions 102

3.5.1. Thermal Overview....102
3.5.2. Rheological Overview....104
CHAPTER 4: DEFORMATION INDUCED PHASE SEGREGATION....105
4.1. DIPS: Introduction....105
4.2. Material Preparation and Characterization....111
4.2.1. Melt Mixing....111
4.2.2. Thermogravimetric Analysis....112
4.2.3. Compression Molding....113
4.2.4. Etching and Microscopy....118
4.3. Results and Discussion....120
4.3.2. DIPS Investigated....120
4.3.3 Compression Overview....139
4.4. Conclusions....144
CHAPTER 5: RECOMMENDATIONS FOR FURTHER STUDY....146
REFERENCES....149

LIST OF TABLES

Table 1: Summary of equations for different concentrations and solvent types for polymer solutions. Equations 17 a-g(column 1) describe athermal solvents, Equations 18 a-g (columndescribe good solvents, and Equations 19 a-g (column 3) describe theta solvents 20

Table 2: Grades of polyethylene used 33

Table 3: Linear fits to the melting and recrystallization temperatures of the PE and wax phases as a function of composition for blends of 41K PE and wax. 47

Table 4: Linear fits to the melting and recrystallization heats of the PE and wax phases as a function of composition for blends of 41K PE and wax.....48

Table 5: Linear fits to the melting and recrystallization temperatures of the PE and wax phases as a function of composition for blends of 72K PE and wax. 50

Table 6: Linear fits to the melting and recrystallization heats of the PE and wax phases as a function of composition for blends of 72K PE and wax.....51

Table 7: Linear fits to the melting and recrystallization temperatures of the PE and wax phases as a function of composition for blends of 115K PE and wax.....52

Table 8: Linear fits to the melting and recrystallization heats of the PE and wax phases as a function of composition for blends of 115K PE and wax.....53

Table 9: Linear fits to the melting and recrystallization temperatures of the PE and wax phases as a function of composition for blends of 125K PE and wax.....54

Table 10: Linear fits to the melting and recrystallization heats of the PE and wax phases as a function of composition for blends of 125K PE and wax.....55

Table 11: Linear fits to the melting and recrystallization temperatures of the PE and wax phases as a function of composition for blends of UHM_wPE and wax. 56

Table 12: Linear fits to the melting and recrystallization heats of the PE and wax phases as a function of composition for blends of UHM_wPE and wax. 57

Table 13: Concentration of PE (% PE) for which the wax is completely absorbed into the PE-rich phast for the different grades of PE. 61

Table 14: Linear and exponential factors of the power law fits of Figure 30.....77

Table 15: Linear and exponential factors of the power law fits of Figure 31.....78

Table 16: Linear and exponential factors of the power law fits of Figure 33.....80

Table 17 Linear and exponential factors of the power law fits of Figure 34.....81

Table 18 Linear and exponential factors of the power law fits of Figure 36.....83

Table 19: Linear and exponential factors of the power law fits of Figure 37.....84

Table 20: Linear and exponential factors of the power law fits of Figure 39.....86

Table 21: Linear and exponential factors of the power law fits of Figure 40.....87

Table 22: Linear and exponential factors of the power law fit of Figure 42 90

Table 23: Linear and exponential factors of the power law fit of Figure 43 91

Table 24: Power law fit exponent z for the concentrated regime and Φ* critical concentration for the grades of PE 93

Table 25: Power law fit exponent α for the concentrated regimes and critical effective molecular weights M_{eff}* of the grades of PE.....96

Table 26: Power law fit exponent a for the concentrated regime and Φ* critical concentration for the grades of PE 98

Table 27: Temperatures for compression and region of thermal behavior. T_m(PE rich) is the melting temperature of the PE rich phase while T_m(PE) is the melting temperature of the pure PE. 109

Table 28: Blend compositions and melting temperatures for compression molding 112

Table 29: Compression ratios and temperatures used for examination of DIPS 114

LIST OF FIGURES

Figure 1: Chemical structure (left) and typical specimen (right) of polyethylene. Pellets are of Sigma Aldrich 428019 HDPE. 2

Figure 2: Concentration dependence of specific viscosity for linear poly(ethylene oxide) with M_w = 5 x 10^6 g/mol in water at 25.0 °C. Water is a θ solvent for PEO. [75, p. 328] 19

Figure 3: Typical plots of zero-shear viscosity as a function of molecular weight for polymer melts. Note the change in slope from 1 to 3.4 at a critical molecular weight, M_c. [75, p. 340].....26

Figure 4: TGA temperature ramp in nitrogen of 5 °C/min to 600 °C for pure paraffin wax, pure UHM_wPE, and a 75% UHM_wPE / 25% wax mixture. 36

Figure 5: TGA heat-and-hold scans of pure paraffin wax and 12K PE. The samples were heated in nitrogen to 350 °C at 50°C/min and held at that temperature. Blue is for paraffin wax; red for 125K PE. The black line indicates the time at which the system reached 350 °C 37

Figure 6: Typical DSC scan for paraffin wax 45

Figure 7: Typical DSC scan of HDPE (125 K g/mol M_w PE) 45

Figure 8: Typical DSC scan for a 50/50 blend of wax/HDPE. The peaks corresponding to the paraffin wax (blue) and PE-rich phases are encircled.....46

Figure 9: Melting and recrystallization temperatures vs. composition (% PE) for the PE-rich and wax phases of 41K PE / wax blends with associated linear fits 47

Figure 10: Melting and recrystallization heats (normalized) vs. composition (% PE) for the PE-rich and wax phases of 41K PE /wax blends with associated linear fits.....48

Figure 11: Melting and recrystallization temperatures vs. composition (% PE) for the PE-rich and wax phases of blends of 72K PE / wax blends with associated linear fits 50

Figure 12: Melting and recrystallization heats (normalized) vs. composition (% PE) for the PE-rich and wax phases of 72K PE / wax blends with associate linear fits. 51

Figure 13: Melting and recrystallization temperatures vs. composition (% PE) for the PE-rich and wax phases 115K PE / wax blends with associated linear fits. 52

Figure 14: Melting and recrystallization heats (normalized) vs. composition (% PE) for the PE-rich and wax phases of 115K PE / wax blends with associated linear fits.....53

Figure 15: Melting and recrystallization temperatures vs. composition (% PE) for the PE-rich and wax phases of 125K PE / wax blends with associated linear fits. 54

Figure 16: Melting and recrystallization heats (normalized) vs. composition (% PE) for the PE-rich and wax phases of 125K PE / wax blends with associated linear fits. 55

Figure 17: Melting and recrystallization temperatures vs. composition (% PE) for the PE-rich and wax phases of UHM_wPE / wax blends with associated linear fits. 56

Figure 18: Melting and recrystallization heats (normalized) vs. composition (% PE) for the PE-rich and wax phases of UHM_wPE / wax blends with associated linear fits. 57

Figure 19: Typical phase diagram for a mixture which exists as an ideal solution in the melt, but non-ideal solution in the solid. R. A. Matkar and T. Kyu, *J. Phys. Chem. B* 2006, 110, 16059-16065, page 16063 (Fig 5).....62

Figure 20: Phase diagram for 41K PE and wax 63

Figure 21: Phase diagram for 72K PE and wax 63

Figure 22: Phase diagram for 115K PE and wax 64

Figure 23: Phase diagram for 125K PE and wax 64

Figure 24: Phase diagram for UHM_wPE and wax.....65

Figure 25: Zero-shear viscosity as a function of molecular weight for the neat HDPE grades used in blending. The red solid line is a power-law fit to all the data. The blue line omits the 125K g/mol PE. 67

Figure 26: Zero-shear viscosity vs. effective molecular weight (M_{eff}) for blends of 41K PE and 125K PE with a power-law best-fit applied.....69

Figure 27: Zero shear viscosity (η_0) vs. composition (% 125K PE) for blends of 41K PE and 125K PE, with the curves predicted for the Christov, Tsenoglou, and log-additive model 70

Figure 28: Zero shear viscosity (η_0) vs. composition (% 125K PE) for blends of 125K PE and 41K PE, with the curves predicted for the Christov, Tsenoglou, and log-additive models, following adjustment for best-fit. 72

Figure 29: Zero shear viscosity (η_0) vs. composition (% PE) for blends of 41K PE and wax, with the curves predicted for the Christov, Tsenoglou, and log-additive models. An exponent of 6.1 was arbitrarily generated in order to obtain the lowest possible R^2 between the values predicted by the Christov equation and the data collected. 76

Figure 30: Specific viscosity (η_{sp}) vs. volume fraction of PE (Φ_{PE}) for blends of 41K PE and wax with power law fits 77

Figure 31: Zero shear viscosity (η_0) vs. effective molecular weight (M_{eff}) for blends of 41K PE and wax with power law fits 78

Figure 32: Zero shear viscosity (η_0) vs. composition (% PE) for blends of 72K PE and wax, with the curves predicted for the Christov, Tsenoglou, and log-additive models. An exponent of 4.3 was arbitrarily generated in order to obtain the lowest possible R^2 between the values predicted by the Christov equation and the data collected. 79

Figure 33: Zero shear viscosity (η_0) vs. effective molecular weight (M_{eff}) for blends of 72K PE and wax with power law fits 80

Figure 34: Specific viscosity (η_{sp}) vs. volume fraction of PE (Φ_{PE}) for blends of 72K PE and wax with power law fits 81

Figure 35: Zero shear viscosity (η_0) vs. composition (% PE) for blends of 115K PE and wax, with the curves predicted for the Christov, Tsenoglou, and log-additive models. An exponent of 4.2 was arbitrarily generated in order to obtain the lowest possible R^2 between the values predicted by the Christov equation and the data collected. 82

Figure 36: Zero shear viscosity (η_0) vs. effective molecular weight (M_{eff}) for blends of 115K PE and wax with power law fits 83

Figure 37: Specific viscosity (η_{sp}) vs. volume fraction of PE (Φ_{PE}) for blends of 115K PE and wax with power law fits 84

Figure 38: Zero shear viscosity (η_0) vs. composition (% PE) for blends of 125K PE and wax, with the curves predicted for the Christov, Tsenoglou, and log-additive models. An

exponent of 4.6 was arbitrarily generated in order to obtain the lowest possible R^2 between the values predicted by the Christov equation and the data collected. 85

Figure 39: Zero shear viscosity (η_0) vs. effective molecular weight (M_{eff}) for blends of 125K PE and wax with power law fits 86

Figure 40: Specific viscosity (η_{sp}) vs. volume fraction of PE (Φ_{PE}) for blends of 125K PE and wax with power law fits 87

Figure 41: Zero shear viscosity vs. % PE for blends of UHM_wPE and wax. 88

Figure 42: Zero shear viscosity (η_0) vs. effective molecular weight (M_{eff}) for blends of UHM_wPE and wax with power law fit 90

Figure 43: Specific viscosity (η_{sp}) vs. volume fraction of PE (Φ_{PE}) for blends of UHM_wPE and wax and power law fit.....91

Figure 44: Overlay of the power law fits of specific viscosity (η_{sp}) vs PE concentration (Φ_{pe}) for all the blends of PE and wax.....93

Figure 45: Exponents z from the power law fits of $\eta_{sp} = Y\ \Phi^z$ for the different PE molecular weights.....94

Figure 46: Overlay of the power law fits for zero shear vistcosity (η_0) vs effective molecular weight (M_{eff}) for all the blends 95

Figure 47: Exponents α from the power law fits of $\eta_0 = K\ M_{eff}^{\alpha}$ for the different PE molecular weights.....96

Figure 48: Overlay of the power law fits for zero shear vistcosity (η_0) vs PE concentration (Φ_{pe}) for all the blends 98

Figure 49: Master curve of the solution $\eta_0 = 6.538\text{x}10^{-16}\ M_w^{3.799}\Phi^a$ fitted for all PE systems used in this study. The solid lines are linear fits to the data. 100

Figure 50: Cross-section of jet drawn fiber produced from a blend of 70% PP 350 / 30% C105 PE wax.....106

Figure 51: Wax content of compressed discs of a 30% UHM_wPE / 70% wax blend as a function of radial distance.....109

Figure 52: DSC sweep of a film of 25% UHM_wPE / 75% wax compressed at 130 ºC. The sample is taken from a half-radius distance. 110

Figure 53: Simple schematic of the set-up used for testing DIPS samples. Grey is the underlying aluminum sheet. Black is the mold that determines the compression ratio, and white is the sample to be compressed. 115

Figure 54: A sample of 10% UHMwPE and 90% wax compressed at 100 °C and a compression ratio of 20, then quenched in water. Scale bar is in inches. 117

Figure 55: Absolute % PE composition of P75 samples at different compression ratios 121

Figure 56: Absolute change in % PE composition of P75 samples at different compression ratios 122

Figure 57: relative change in % wax composition of P75 samples at different compression ratios 122

Figure 58: Morphology of P75 samples taken by SEM at 5K magnification and 6 kV. 123

Figure 59: Absolute % PE composition of 50 samples at different compression ratios .124

Figure 60: Absolute change in % PE composition of P50 samples at different compression ratios 125

Figure 61: relative change in % wax composition of P50 samples at different compression ratios 125

Figure 62: Morphology of P50 samples taken by SEM at 5K magnification and 6 kV. 126

Figure 63: Morphology of P25 samples taken by SEM at 5K magnification and 6 kV. 128

Figure 64: As-quenched sample of P25 compressed to a ratio of 20 at 100 C 129

Figure 65: Absolute % PE composition of X35 samples at different compression ratios 130

Figure 66: Absolute change in % PE composition of X35 samples at different compression ratios 131

Figure 67: relative change in % wax composition of X35 samples at different compression ratios 131

Figure 68: Morphology of X35 samples taken by SEM at 5K magnification and 6 kV 132

Figure 69: Absolute % PE composition of X25 samples at different compression ratios 133

Figure 70: Absolute change in % PE composition of X25 samples at different compression ratios 134

Figure 71: relative change in % wax composition of X25 samples at different compression ratios 134

Figure 72: Morphology of X25 samples taken by SEM at 5K magnification and 6 kV 135

Figure 73: Absolute % PE composition of X10 samples at different compression ratios 136

Figure 74: Absolute change in % PE composition of X10 samples at different compression ratios 137

Figure 75: relative change in % wax composition of X10 samples at different compression ratios 137

Figure 76: Morphology of X10 samples taken by SEM at 5K magnification and 6 kV .138

Figure 77: Absolute % PE composition of all X# samples at different compression ratios 139

Figure 78: Absolute % PE composition of P# samples at different compression ratios 140

Figure 79: SEM images taken at 2500, 500, and 100 x (row 1, 2, and 3 respectively) for blends X10, X25, and X35 respectively 142

Figure 80: SEM images taken at 2500, 500, and 100 x (row 1, 2, and 3 respectively) for blends P25, P50, and P75 respectively 143

LIST OF SYMBOLS AND ABBREVIATIONS

c: Mass Concentration

c*: Overlap Concentration *or* Critical Concentration for Overlap (mass)

DIPS: Deformation Induced Phase Segregation

DSC: Differential Scanning Calorimetry

DMA: Dynamic Mechanical Analysis

H: heat

H_m: heat of fusion (melting)

H_r: heat of recrystallizatoin

HDPE: High Density Polyethylene

LCB: Long Chain Branch

LDPE: Low Density Polyethylene

LLDPE: Linear Low Density Polyethylene

m-: prefix indicating metallocene catalyzed

M_c: critical molecular weight *or* entanglement molecular weight in melt

M_w: weight average molecular weight

M_{eff}: effective molecular weight

M_{eff}*: critical effective molecular weight

OM: Optical Microscopy

PE: Polyethylene

SAXS: Small Angle X-ray Scattering

SEM: Scanning Electron Microscopy

T: Temperature

$T_{m:}$ Melting Temperature

$T_{r:}$ recrystallization temperature

TGA: Thermogravimetric Analysis

UHM_wPE: Ultra-High Molecular Weight Polyethylene

WAXD: Wide Angle X-ray Diffraction

Φ: Volumetric Concentration

Φ^*: Overlap Concentration

Φ_e: Entanglement concentration (volumetric)

η: Viscosity

η_0: Zero Sheer Viscosity

η_{sp}: Specific Viscosity

SUMMARY

Motivations

Direct industrial requirements motivated this research. Frequently in polymer processing, pairs of polymers are mixed or blended to achieve certain desirable properties or characteristics. While most industrially relevant polymer combinations consist of *immiscible* components, many systems employ *miscible* polymers. One such case is that of polyethylene (PE). Improved processability and/or mechanical performance are obtained by combining different grades of polyethylene. A substantial portion of all polyethylene is, in fact, marketed in already-blended form.

However, the rheological, morphological, and thermal characteristics of such miscible polymer combinations were not previously well understood, for cases in which both components had the same chemical formula but different molecular weights and particularly where the ratio of molecular weights comprised several orders of magnitude. The matters were further complicated if the lower molecular weight component had a molecular weight, M_w, less than that of the critical molecular weight for entanglement, M_c, and the higher molecular weight component had a molecular weight much greater than M_c.

For dealing with PE mixtures, two sets of theories have been available: those applicable to solutions and those applicable to blends.

Both theory sets are limited in application. Solution theories generally break down as concentrations of high molecular weight polymer solutes *increase* beyond certain levels in low molecular weight polymer solvents. Blend theories suffer similar failure as ratios of component molecular weights (or viscosities) *increase*. Research has thus far treated such systems only as *solutions* in which very high concentrations were neglected or as *blends* in which very low concentrations were neglected.

This study provides a much-needed bridge between the two theories by identifying crossover points between them, and the behaviors exhibited therein. It accomplishes this by production and analysis of cases in which the solute and solvent, although chemically identical, comprise a wide range of molecular weight ratios and blend compositions. Results demonstrate that this "bridge" realm offers significant manufacturing applications and advantages.

Means and Outcomes

Several polyethylene blends were employed in this study. The low molecular weight component is fixed as 3134 paraffin wax, which possesses a molecular weight well below that of entanglement, but is solid at room temperature. The wax was blended with several grades of high-density polyethylene with widely varying molecular weights from 41 kg/mol to 2,000 kg/mol. The blends were prepared by melt-mixing the components across a wide range of compositions, and quenching them in ice water. The zero-shear viscosities were then determined at a fixed temperature.

Within the purview of polyethylene/wax blends, of particular interest is that of ultra-high molecular weight polyethylene (UHM_wPE) and paraffin wax. UHM_wPE is of great value as it provides the best mechanical properties of the PE grades. However, it is notoriously difficult to process due to its incredibly high viscosity in melt. Because of this high viscosity, it is usually processed only in solution. Solution processing brings with it a significant problem in that the solvents employed are usually both expensive and environmentally unfriendly. This study indicates paraffin wax to be a viable, inexpensive, safe and "green" alternative to these problem solvents.

For blends of PE and paraffin, the paraffin typically remains to some degree not fully intercalated into the PE, though the PE is partially miscible with the paraffin. This behavior was demonstrated by melting and observing endotherms of the blends. In doing so, the wax heat peak remained at a fixed temperature but changed in intensity as a function of composition. The PE rich heat peak changed in both temperature and intensity as a function of composition. From these peaks, it is possible to determine the fraction of wax in the sample that was intercalated into the PE. This was further evidenced by examination of the blends under microscopy whereby after dissolving away the wax component of the blend, a web-like co-continuous structure was observed.

Exploiting this phenomenon, a new means of separating wax from the blend is also discerned and demonstrated. This is an important commercial capability, for once the wax has performed its function in the manufacturing process, its recovery is desirable for both economic and material performance reasons.

It was demonstrated that a substantial portion of the wax can be literally squeezed out of a sample by rapidly applying mechanical stress to an UHM_wPE/wax blend (either

tensile or compressive) at a temperature above the melting point of the wax but below the melting point of the polyethylene. Viability of this method was verified by compressing a cylindrical sample at such a temperature, then determining the composition by TGA of the resulting film at different radial distances. The interior wax content proved lower than the neat blend; and the exterior wax content, higher. The sample remains mechanically intact.

This technique potentially permits production of UHM_wPE films and fibers by melt processing, thereby eliminating need of toxic chemicals while yet retaining adequate mechanical properties. This process was examined in detail under widely different compressive stress conditions and compositions. Of particular interest are the local compositions and morphologies. These were determined respectively by thermal (TGA, DSC) means and microscopy of etched samples. Further development of this technology is warranted.

CHAPTER 1: INTRODUCTION

Polyethylenes are frequently modified with other polyethylenes to improve processability, mechanical performance, or other material properties as compared to neat resins. Significant industrial benefit can be realized by such binary mixing or blending to instill qualities or characteristics not otherwise economically achievable. Indeed, a substantial portion of polyethylene production is commercially distributed only after such blending.

Most industrially relevant polymer blends consist of immiscible components. However, blends of *miscible* polymers are also exploited. Polyethylene (PE) is frequently one such case.

Industry trends require mixtures of PE in ever increasing viscosity ratios. This practice led to unexplored areas and unpredictable outcomes. For polyethylene blends wherein components' molecular weights differ by several orders of magnitude, phase behavior has been little examined and is even less understood. This is particularly true for binary blends in which the molecular weight of one polyethylene is *less* than the entanglement molecular weight and the molecular weight of the other is *greater* than the entanglement molecular weight.

The rheological, morphological, and thermal characteristics of such miscible polymer blends were not previously well determined, particularly in the case of blends of components having the same chemical formula but different molecular weights, and, again, particularly where the ratio of molecular weights covered several orders of

magnitude. Depending on miscibility, such combinations can produce extremely complex rheological results with behaviors and concentrations spanning a range from those normally considered characteristic only of solutions, to those normally considered characteristic only of blends

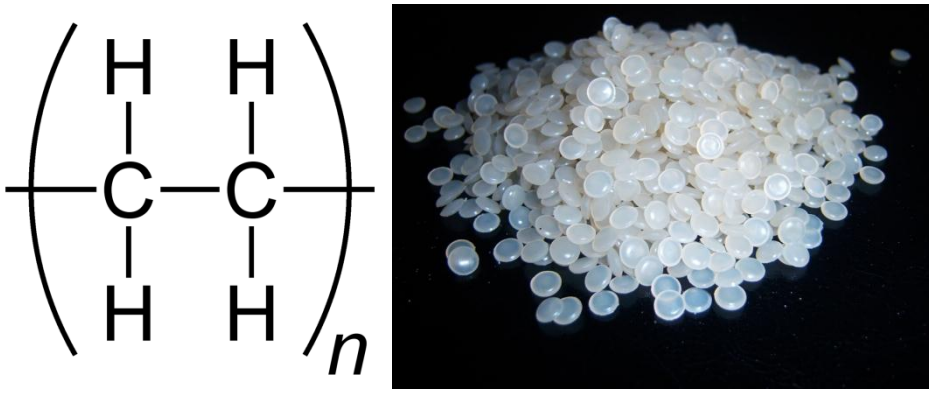

Figure 1: Chemical structure (left) and typical specimen (right) of polyethylene. Pellets are of Sigma Aldrich 428019 HDPE.

For working with such mixtures, two sets of theories exist:

- those applicable to solutions

  and

- those applicable to blends.

Each set has inherent limitations. *Solution* theories break down when *high* molecular weight polymer solute concentrations *increase* beyond certain levels in solvents of the *low* molecular weight polymers. *Blend* theories demonstrate similar issues in that behaviors become less predictable as the ratios of component molecular weights (or viscosities) *increase* beyond certain values.

Research had thus far treated mixtures exclusively as *solutions* in which the *high* concentrations were neglected or exclusively as *blends* in which the *low* concentrations were neglected. This study unifies the two. By creating a system in which the solute and solvent are more nearly chemically identical, the cross-over points between the two theories and the associated behaviors have been identified and more clearly defined. The exhaustive examinations document PE/wax blend behaviors over a broad spectrum of PE molecular weights and composition ratios.

The examinations are rheological, thermal, mechanical, and morphological in nature, delving into both neat blends and blends after various processings. Through these new methods a more thorough understanding of the rheology and phase behavior is revealed.

Thereby this exploration provides a universal model of mixture rheology and phase behavior, creating a bridge between the concepts applied in solution and the concepts applied in blends. This greater comprehension of the factors relevant to such mixtures should enable production of more complex targeted combinations.

Additionally, by applying certain post processing techniques, a phase segregation technique that potentially eliminates the need for environmentally unfriendly, expensive manufacturing solvents is demonstrated. Furthermore, it does so without significantly sacrificing mechanical properties. This phase segregation technique can permit production by simple melt mixing.

Within the purview of polyethylene/wax blends, of particular interest is that of ultra-high molecular weight polyethylene (UHM_wPE) and paraffin wax. UHM_wPE is of great value as it provides the best mechanical properties of the PE types, but is

notoriously difficult to process due to its incredibly high viscosity in melt. Because of its viscosity, most processing of this material is done in solution. The problem is that the solvents used are usually both expensive and environmentally unfriendly. This study demonstrates paraffin wax as a viable alternative to these chemicals in processing.

This is achieved by producing mixtures of several different high density polyethylene grades mixed with a specific, set grade of paraffin wax over the full range of compositions possible in melt mixing. These blends are then examined to determine their miscibility, morphology, crystal structure, and composition by parallel plate rheology, differential scanning calorimetry, thermogravimetric analysis, and microscopy.

It was found that under certain thermal and morphological conditions, it is possible to cause phase segregation in a blend through application of tensile or compressive mechanical stress and deformation. This new process is called Deformation Induced Phase Segregation (DIPS). Knowledge of this behavior makes it simpler both to produce existing blends, and to achieve controlled production of more targeted mixtures.

This thesis is organized as follows: Chapter 2 is a literature survey covering the state of the art of PE/PE blends, and the rheological and thermal theories applied to miscible polymer solutions and melts. Chapter 3 details the examination of the thermal and rheological characteristics of the blends. Chapter 4 details the Deformation Induced Phase Segregation study. Chapter 5 suggests future courses of research.

CHAPTER 2: LITERATURE REVIEW

2.1. History of Polyethylene/Polyethylene Blends

Polymer blending has been used in material production for some time now, providing a large range of benefits that would otherwise be unattainable or prohibitively expensive. From the standpoint of the material itself, blending can provide an entire range of desirable properties at low cost, extension of an engineering resin's performance, improvement of targeted properties (chemical, mechanical, etc.), and enhancement of recyclability of resultant products. From a manufacturer's standpoint, blending can improve a material's processability and final uniformity, reduce fraction-to-scraps, generating byproducts that are inherently recyclable, increase the range of products a given plant can produce, and reduce the range of specific grades of resin that need to be manufactured and stockpiled. [1, p. 13]

Normally, such commercial blends comprise immiscible or at least dissimilar polymers. Polyethylene (PE), while it can be modified by other polymers or used as a means of modifying other polymers, is frequently blended with other forms of itself. These forms include low density polyethylene (LDPE), linear low density polyethylene (LLDPE), high density polyethylene (HDPE), paraffin oils and waxes (a category of low molecular weight PE), and ultra-high molecular weight polyethylene (UHM_wPE), along with variations within those categories (i.e. molecular weight, degree of branching).

Blending two forms of polyethylene can improve the finished product's processability and mechanical performance without sacrificing compatibility. (Note however, that, though compatible, not all PE forms are miscible.) In some countries, up to 70% of all PE is wholesaled in already blended form. [1, p. 51] In these mixing processes, polymer viscosity ratios of 1000 or greater are frequently employed to modify the material. [2] These intense ratios are employed with the understanding that the greater the viscosity ratio, the less modifier needed to produce a given property and the greater the range of properties that can be produced merely by altering the composition. [1, p. 51]

The broad range of available polyethylene chain types and structures may be used to produce various blend types for various applications. Mixtures of LDPE with LLDPE are known to improve a thin film's processability, stiffness, resistance to abrasion and tear, and water vapor permeability. [3] [4] [5] [6] [7]

Blends combining two grades of LLDPE produce improved processability, impact strength, and generally enhance mechanical performance. [8] Mixtures combining HDPE with LLDPE produce improved strength, transparency and crack resistance in films. [9] [10] As a general rule, molecular weight blends of PE improve processability and physical properties of materials. [11] It is this last category of molecular weight blends that is of particular interest in this project.

For commercial polymer blends, rheological studies of miscible polymer systems have been relatively rare compared with immiscible systems. [12, p. 482] However, some research has been pursued concerning rheological and thermal behaviors of PE/PE blends, covering the same range of combinations of different polyethylene types as listed

above with varying outcomes and results. As early as the 1960's, researchers have used PE/PE blends to study miscible systems. [13]

When contemplating polymers in use from an industrial/commercial point of view, a key factor to consider is the means by which they were produced. Metallocene (denoted with an m- prefix) and Zeigler-Nata catalyzed polymers possess significantly fewer and shorter branches than their conventional equivalents at the same molecular weight, and have narrower molecular weight distributions and therefore less polydispersity [14]. Although polydispersity plays a smaller role for MPEs than it does for conventional polyethylenes, branching remains important in determining properties of the polymer. [15] [16]

Blends of LLDPE with LDPE have been heavily studied under a range of conditions and with a variety of characterization techniques. Melt behavior of this blend category has been studied by a number of authors under oscillatory shear conditions. [17] [18] [19] [20] [21] [22] These studies show such systems to be rheologically complex in shear and elongational flow, and to develop shark-skin like features under capillary flow. [23] [24] [25]

Though immiscible under flow, an LLDPE/LDPE blend nevertheless behaves as a compatible combination. [26] The assertion of immiscibility of LLDPE/LDPE is supported by previous thermal studies of the combination under differential scanning calorimetry (DSC), generating the melting and recrystallization temperatures and creating the associated enthalpies, and degrees and types of crystallinity. [19] [27] [28] These studies have yielded distinct phase diagrams of the upper critical system temperature (UCST) form. [29] [30] [31] Indeed, UCST proved the applicable phase diagram type for

all PE/PE blends. Additional studies examined the blends' steady-state and dynamic tensile mechanical properties in the solid state. [17] [32]

Similarly to LLDPE/LDPE blends, LLDPE/HDPE and LDPE/HDPE blends have been studied in melt under conditions of oscillatory shear flow, [17] [19] [33] [34] elongational flow [24] [33] [35], DSC [19] [34], and steady state tensile elongation in the solid state. [17] [34]

HDPE/HDPE (a like/like combination) blends have been examined, specifically targeting the effects of different molecular weights and the use of m-HDPE, using oscillatory shear flow [25] [36], DSC [36], and solid-state mechanical testing [36]. The significance of this blend type is that it is considered miscible by all characterization techniques across all compositions and conditions used.

A blend type of particular interest under the purview of PE/PE mixtures is of PE with paraffin wax. Thus far, studies have considered only mixtures wherein each component possesses a molecular weight substantially above the critical molecular weight for entanglement of linear polyethylene (M_c = 3660-3800 g/mol) [25] [37] [38] [39]. However, the molecular weights of paraffin oils and waxes are significantly below this value. Indeed, in order to examine any PE/PE mixture as if it were a solution, at least one of the components must have a molecular weight below this M_c. Wax has been combined with or used as a modifier for LLDPE, LDPE, and HDPE, with studies performed targeting the rheological [40] [41], thermal [40] [42] [43] [44], and solid-state mechanical properties [42] [45]. Additionally, wide angle x-ray diffraction (WAXD) has been employed to examine the crystallization of wax/wax blends, with the intensity pattern used to estimate the apparent degree of wax crystallinity. [45] Small angle x-ray

scattering (SAXS) has been used to study the phase structures in elongated HDPE/wax blends. [46] Both WAXD and SAXS (in-situ) have been employed to study shear-induced crystallization precursors in model PE blends under flow conditions. [40]

UHM_wPE has been combined with every form of polyethylene at one time or another. The properties resolved from these blends are heavily dependent on the degree of branching present in the grade of PE with which the UHM_wPE is combined. The lower the fraction of molecular weight taken up by branching, the more miscible the two PE will become.

Generally, unless otherwise specified, LLDPE, HDPE, and UHM_wPE have relatively low branching content and exhibit a high degree of miscibility, resolving a single crystal structure under WAXD, a single melting and recrystallization peak from DSC, and a uniform phase structure in microscopy. [47] [48] However, these blends frequently must be produced by solution mixing rather than melt mixing [46] [49] [50] [51] [52], as viscosity of the resulting mixture is too high to successfully process in melt. These solution-produced mixtures have combined UHM_wPE with LDPE [50], LLDPE [51], and HDPE [46] [48].

When working with UHM_wPE blends, much of the focus has been on the solid-state mechanical properties of films, and the processing used to produce them. Drawing and so-called ultra-drawing processes produce films and fibers with the best tensile properties. In production of samples from solutions, the solvent used (typically xylene or decaline) is extracted from the sample prior to or during its processing into useful form (fiber or film). Of these, the films have been experimentally characterized through DMA

[51] [52], solid state tensile draw [49] [52], DSC [46] [49] [50] [51] [52], and WAXD [51].

Though it is possible to melt mix using higher viscosity forms of polyethylene [53], most melt mixing of UHM_wPE is done with paraffin wax. Paraffin wax has been used as a processing additive to UHM_wPE since 1985 when Mitsui Petrochemicals patented a process for producing ultra-drawn blends of UHM_wPE and paraffin. [54] [55] Since then, studies have examined UHM_wPE and paraffin wax as a semi-dilute solution in which paraffin is the solvent and UHM_wPE the solute, using both oscillatory and steady state shear flow. [56] It has been found that even for miscible semi-dilute UHM_wPE/paraffin solutions there is, during melt flow when near the critical melting temperature, a shear rate that causes instabilities. This results in local shear-induced phase separation and crystallization of UHM_wPE from solution. (This effect was identified using small angle light scattering and microscopy in-situ with rheology, a useful tool set for determining miscibility and cloud points in melts and solutions.) [57] [58]

Blending UHM_wPE or HDPE and wax has uses other than improvement of processability and mechanical properties. Some researchers have used the technique to produce micro-porous structures by dissolving away the paraffin oil employed during processing, leaving the UHM_wPE framework intact. [59] [60] [61] Other researchers have proposed UHM_wPE/paraffin wax gels as energy storage media for heat in which the paraffin can melt, but not leak out of the UHM_wPE matrix or alter the surrounding architecture. [62] [63]

2.2. Theories and Equations

Combinations of paraffin wax and high molecular weight polyethylene will be examined in two modes:

- as a solution

  and

- as a polymer blend.

A distinct set of theories is associated with behaviors of each form. However, there is only limited cross-over capability between the two theory sets. This lack of cross-over is a primary motivator for this research.

2.2.1. Polymer Solutions

In understanding these mixtures as solutions, three states must be considered: the dilute, the semi-dilute, and the concentrated. In a dilute solution, polymer chains interact with their solvent individually and without the coils of separate chains overlapping. In a semi-dilute solution, polymer chains may overlap but are not considered entangled. In the concentrated solution, the polymer chains are entangled. Each of these conditions is examined separately.

Dilute solutions

In the dilute state, the chains of polymers in the solution may be treated as discrete particles. The limiting value of this condition is the overlap concentration, c^* (mass-concentration), beyond which the solution can no longer be considered dilute. **[64]**

Equation 1

$$c^* = \frac{1}{k_H[\eta]}$$

Here, k_H is the Huggins coefficient and $[\eta]$ is the intrinsic viscosity.

In terms of the molecular weight M_w and radius of gyration R_g, the overlap concentration may be articulated as: [46]

Equation 2

$$c^* = \frac{M_w}{(4/3)\pi \left\langle R_g^2 \right\rangle^{3/2} N_A}$$

The intrinsic viscosity of a solution is determined from a relationship between the specific viscosity, η_{sp}, of the solution and the mass concentration c. [64]

Equation 3

$$\frac{\eta_{sp}}{c} = [\eta] - k_H[\eta]^2 c + \ldots$$

The specific viscosity of the solution is given by.

Equation 4

$$\eta_{sp} = \frac{\eta - \eta_s}{\eta_s}$$

Here, η is the viscosity of the solution and η_s, is the viscosity of the solvent. [65, pp. 189-191]

Considering this, intrinsic viscosity is defined as the limit of the ratio of the specific viscosity to the concentration as the concentration approaches zero. [66]

Equation 5

$$[\eta] = \lim_{c \to 0} \left(\frac{\eta_{sp}}{c} \right)$$

A useful form of Equation 3, based on volume fraction of a suspended particle (i.e. the volumetric concentration of the polymer molecules in the solution), Φ, rather than mass concentration may be employed to generate.

Equation 6

$$\eta_{sp} = 2.5\phi + 6.2\phi^2 + \ldots$$

The Φ first (linear) term in Equation 6 is based on Einstein's equations on Brownian motion [67]; the second (quadratic) was developed by Batchelor. [68] By using the linear term of Equation 6, one may estimate the intrinsic viscosity by.

Equation 7

$$[\eta] = 2.4\left(\frac{\phi}{c}\right) = 2.5\frac{N_a v_{per}}{M_n} = \frac{10\pi}{3}\frac{N_a R_g^3}{M_n}$$

In this, N_a is Avagadro's number, v_{per} is the pervaded volume of the polymer, M_n is the number average molecular weight, and R_g is the radius of gyration of a single polymer chain. [69]

By combining Equation 7 with Equation 1, intrinsic viscosity is found to be inversely proportional to the overlap concentration and directly proportional to the pervaded volume. This is known as the Fox-Flory equation:

Equation 8

$$[\eta] \sim \frac{v_{per}}{M} \sim \frac{R_g^3}{M}$$

All of these relationships thus far expressed assume monodispersity, i.e. every molecule of polymer in solution possesses the same molecular weight. However, except for low molecular weight polymers (where chain length is more easily controlled) or very high grade polymeric materials, a given sample of most polymers will be polydisperse, comprising molecules of various molecular weights. Following this line of thinking, by

employing the linear term in Equation 3 [64], one may approximate the specific viscosity of a molecular mixture comprised of polymers all having with the same chemistry but possessing discretely different molecular weights (a polydisperse polymer in solution) by

Equation 9

$$\eta_{sp} = \sum [\eta]_i c_i$$

Here, $[\eta]_i$ is the specific viscosity of polymer *i* and c_i is the mass concentration of polymer *i*, and the Huggin's coefficient is set as $k_H = 0.99$. [65, p. 219]

In the dilute state, an empirical power law relationship between intrinsic viscosity and viscosity-average molecular weight (M_v) has long been established. This relationship is known by the Mark-Houwink equation [70] [71] [72] [73] [74]:

Equation 10

$$[\eta] = K' \overline{M}_v^{\alpha}$$

So long as the two Mark-Houwink constants *K'* and α are known, this equation enables an indirect approximation of the average molar mass of a given polymer from the measurement of its intrinsic viscosity. From a derivation of the Fox-Flory equation, the Mark-Houwink exponent α is related to the exponent describing the molar mass dependence of coil size in solution *v*, as:

Equation 11

$$\alpha = 3v - 1$$

The coil size *v* is also known as the swelling exponent or the Flory exponent. [75, p. 103] This factor comes into play for temperatures at which the excluded volume interactions within each chain in a polymer solution exceeds the thermal energy *kT*. [75, p. 176] The exponent α becomes increasingly significant as the semi-dilute and concentrated regimes are entered in solutions.

There are two limits for unentagled polymer dynamics, the Zimm Limit and the Rouse Limit. The first case, the Zimm Limit (which is of greater significance in this discussion of solutions), applies to dilute solutions. In this situation, the solvent is hydrodynamically coupled to the polymer within its pervaded volume. [75, p. 325] These dynamics are described by the Zimm model [75, p. 316]:

Equation 12

$$[\eta] \approx \frac{R^3 N_a}{M_0 N} \approx \frac{b^3 N_a}{M_0} N^{3v-1}$$

Here, *b* is the length of Kuhn monomer, *R* is the coil size of a random-walk chain, M_0 is the molar mass of a Kuhn monomer, and *N* is the number of Khun monomers in a strand ($N_e(l)$ is the number of Khun monomers of an entangled strand in the melt). [75, p. 54]

The second case, the Rouse limit, applies to unentangled polymer melts. In this state, hydrodynamic interactions (along with excluded volume interactions) are screened

because the concentration φ=1. [75, p. 325] These dynamics are described by the Rouse model for short, unentangled chains [75, p. 315]:

Equation 13

$$[\eta] \approx \frac{b^3 N_a}{M_0} N$$

Semi-dilute Solutions and Entangled Solutions

Once a solution passes the critical concentration for overlap (c^* in mass concentration, Φ^* in volumetric concentration), the viscous behavior of the solution alters significantly as the chains of the separate polymer molecules begin to heavily interact with each other. Polymer chain overlap begins when the chains' volume fraction Φ exceeds the volume fraction of monomers inside each isolated coil. This is the *semi-dilute* or *unentangled* regime.

The behavior of the solution alters again once it surpasses a concentration at which it enters the entangled regime (c_e in mass concentration, Φ_e in volumetric concentration). This is also known as the *concentrated* regime. Polymers are considered to begin entanglement when the coil size R is equal to or greater than the diameter of the tube in which a chain's motion or "reptation" is confined. In a melt, this contemplated tube diameter, *a*, is given by

Equation 14

$$a(l) \approx b[N_e(l)]^{1.2}$$

Dilute solutions are in practice classified according to their *intrinsic viscosity*. However, most solutions of greater than overlap concentration are rheologically considered in terms of *specific viscosity*. For a semi-dilute, unentangled solution, the specific viscosity is articulated as [75, pp. 329-330]

Equation 15

$$\eta_{sp} \approx N\phi^{(1/(3v-1))} \approx \left(\frac{\phi}{\phi^*}\right)^{1/(3v-1)}$$

In turn, the overlap concentration is given by [75, p. 369]

Equation 16

$$\phi^* \approx \frac{Nb^3}{R^3} \approx N^{1-3v}$$

The three types of solvents addressed in this discussion are athermal solvents, good solvents and theta solvents. An *athermal solvent* is chemically identical to the monomers in solution with it, resulting in no energy difference between interactions of the solvent with itself, and the solvent with the solute. [75, p. 98] This condition occurs at higher temperatures where the excluded volume v is equal to b^3.

A *good solvent* exists below the athermal limit, where the monomer-monomer attraction is slightly stronger than the monomer-solvent attraction because dispersion

forces usually favor identical species. In a good solvent, the excluded volume v of a polymer is between 0 and b^3.

A *theta solvent* exists only at a specific temperature (T_θ) for which there is no penalty for monomer-monomer contact, resulting in a net excluded volume of zero, the polymer chains in solution having near ideal conformations. [75, p. 101]

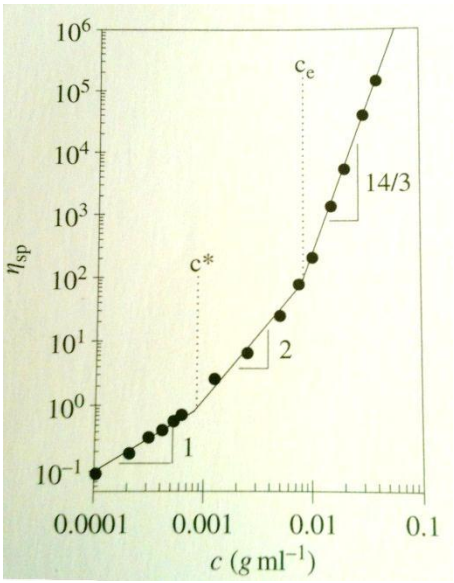

Figure 2: Concentration dependence of specific viscosity for linear poly(ethylene oxide) with M_w = 5 x 10^6 g/mol in water at 25.0 °C. Water is a θ solvent for PEO. **[75, p. 328]**

The different solvent forms have different inherent values and equations associated with them. These values are summarized in Table 1.

Table 1: Summary of equations for different concentrations and solvent types for polymer solutions. Equations 17 a-g(column 1) describe athermal solvents, Equations 18 a-g (columndescribe good solvents, and Equations 19 a-g (column 3) describe theta solvents

	Athermal Solvent	*Good solvent*	*Theta solvent*
Coil size, ν [75, p. 104]	$\nu = 0.588$	Similar to athermal	$\nu = 0.5$
Excluded volume, v [75, p. 101]	$v = b^3$	$0 < v < b^3$	$v = 0$
Tube diameter, a (semidilute) [75, pp. 366-367]	$a \approx a(l)\Phi^{-0.76}$	$a \approx a(l)\Phi^{-\nu/(3\nu-1)}$	$a \approx a(l)\Phi^{-2/3}$
Overlap concentration, Φ^* [75, p. 369]	$\Phi^* = N^{-0.76}$	$\Phi^* = N^{1-3\nu}$	$\Phi^* = N^{-1/2}$
Entanglement concentration, Φ_e [75, p. 369]	$\Phi_e = [N_e(l)/N]^{0.76}$	$\Phi_e = [N_e(l)/N]^{(3\nu-1)}$	$\Phi_e = [a(l)/b]^{3/2}N^{-3/4}$ $\Phi_e = [N_e(l)/N]^{0.75}$
Specific viscosity, η_{sp}, Semi-dilute $\Phi^* < \Phi < \Phi_e$ [75, p. 330]	$\eta_{sp} \approx N\Phi^{1.305}$	$\eta_{sp} \approx N\Phi^{(1/(3\nu-1))}$	$\eta_{sp} \approx N\Phi^2$
Specific viscosity, η_{sp}, Entangled $\Phi_e < \Phi < 1$ [75, p. 373]	$\eta_{sp} \approx \frac{N^3}{[N_e(l)]^2}\phi^{3.914}$	$\eta_{sp} \approx \frac{N^3}{[N_e(l)]^2}\phi^{3/(3\nu-1)}$	$\eta_{sp} \approx \frac{N^3}{[N_e(l)]^2}\phi^{14/3}$

Note that for the entangled regime, the general equation for specific viscosity does not carry forward from good solutions into theta solutions. This is due to differing

concentration dependencies in length scales, as is exhibited by the dependencies of tube diameter on concentration in the semi-dilute regime.

2.2.2. Miscible Polymer Blends and Mixtures

Most interpretation of blend theory for miscible systems has been concerned with components that possess relatively similar densities, viscosities, molecular weights, and/or glass transition temperatures T_g. Such systems are relatively simple in comparison to their immiscible counterparts. However, as differences in these properties significantly increase, the viscoelastic characteristics of blends become increasingly complex.

For a system in which the glass transition temperatures of the two components are separated by more than 60 ºC, the dynamics of the individual components within the blend is preserved. This results in a more complex rheometry. However, the system remains miscible. Interestingly, the further apart the glass transition temperatures become, the less a mixture behaves like a miscible blend and the more it behaves like a miscible solution. Achievement of greater understanding with respect to this important conversion zone forms a core component of this thesis work.

When considering the behavior of polymer blends, several types of behavior have been observed, all in reference to the classic log-additive rule defined formulated by Arrhenius in the nineteenth century. The modern version of this law is:

Equation 20

$$\ln \eta_0 = \sum (\phi_i \ln \eta_{0i}) + \ln \eta^E$$

where η_0 is the zero-shear viscosity of the blend, Φ_i is the mass fraction of polymer *i* in a polymer mixture, η_{0i} is the zero-shear viscosity of polymer *i*, and η^E is a term that describes the excess viscosity. [12, p. 457] When the natural log of the excess viscosity approaches zero, the blend may be considered miscible and is described by the simplified form [13] [76] [77]:

Equation 21

$$\ln \eta_0 = \sum \phi_i \ln \eta_{0i}$$

While adherence to the behavior described by Equation 21 may be used as a rule-of-thumb for determining miscibility, the reality is that the viscosities of miscible polymer blends can vary from the log-additive with positive deviation, negative deviation, or a sequence of the two. Utracki further developed Equation 20 to account for all types of deviation behavior away from the log-additive rule as:

Equation 22

$$\ln \eta_0 = \ln \eta_L + \Delta \ln \eta^E$$

The first term in Equation 22 accounts for any negative deviation in the blend behavior while the second demonstrates any positive deviation. For a binary blend, the terms are further broken down as

Equation 23

$$\ln \eta_L = -\ln[1 + \beta(\phi_1\phi_2)^{1/2}] - \ln\left(\frac{\phi_1}{\eta_1} + \frac{\phi_2}{\eta_2}\right)$$

And

Equation 24

$$\Delta \ln \eta^E = \eta_{max}\left[1 - \frac{(\phi_1 - \phi_{1I})^2}{\phi_1\phi_{2I}^2 + \phi_2\phi_{1I}^2}\right]$$

where Φ_{iI} is the phase inversion concentration of polymer *i*, β is the interlayer slip factor, and η_{max} is a parameter that determines the magnitude of the positive deviation behavior. [78][1]

The range over which positive or negative deviation can be observed for binary blends may be characterized by a simple mixing rule [76]:

Equation 25

$$\eta_0 = \phi_a\eta_{0a}^n + \phi_b\eta_{0b}^n$$

[1]Note that Equation 23 and Equation 24 apply only to immiscible polymer blends. However, they form the basis for many further developments in the understanding of miscible blend behavior.

where $-1 \leq n \leq 1$. When $n = -1$, the formula is considered to be in parallel when $n = 1$, in series. [79] More recently, Tsenoglou has taken a closer examination of binary molecular weight blends, developing a positive-deviation predictive equation [80]:

Equation 26

$$\eta_0 = \eta_{0a}\phi_a^2 + \eta_{0b}\phi_b^2 + 4\phi_a\phi_b\left(\frac{\eta_a\eta_b}{\eta_a + \eta_b}\right)$$

Within the purview of miscible polymer blends, of particular relevance is the molecular mixture, in which all components of a blend have the same chemical formula and architecture, but differ in molecular weight. (Polydisperse polymers are frequently considered as molecular mixtures.) Within such a framework, an empirical power-law relationship similar to the Mark-Houwink equation (Equation 10) is frequently observed for zero-shear viscosity as a function of molecular weight in polymer melts. However, this relationship is broken into two distinct regimes for homopolymers:

- one regime below the critical molecular weight for the effect of entanglement on polymer melts M_c

  and

- one regime above critical molecular weight for the effect of entanglement on polymer melts M_c. [81]

Below M_c, the zero shear viscosity is given by

Equation 27

$$\eta_0 = k'\overline{M}_w$$

Above M_c, the zero shear viscosity is given by

Equation 28

$$\eta_0 = k\overline{M}_w^{\alpha}$$

where M_w is the weight average molecular weight, α is a constant (further on this parameter later), and k and k' are constants related to each other at the critical molecular weight by [82]

Equation 29

$$k' = k \cdot M_c^{\alpha-1}$$

As first predicted by Fox and Flory, for typical monodisperse polymers when the weight average molecular weight is less than the critical molecular weight, α is 1; when $M_w > M_c$, α is 3.4. [83] Later research has found varying degrees of deviation from these relations. For example, conventional commercial polyethylenes have α values ranging from 3.2 to 3.6 [25] [84] [85] [86], while metallocene-catalyzed polyethylenes with long chain branching are reported to have α values as high as 4.2. [19] [25]

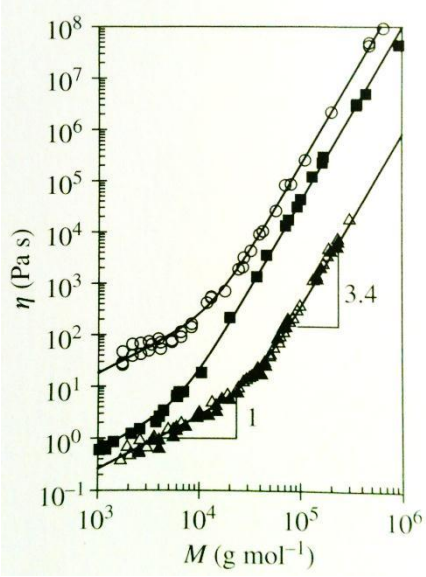

Figure 3: Typical plots of zero-shear viscosity as a function of molecular weight for polymer melts. Note the change in slope from 1 to 3.4 at a critical molecular weight, M_c. **[75, p. 340]**

A derivation of Equation 28 by Friedman and Porter further develops those theories from monodisperse polymers to encapsulate polydisperse polymers and molecular mixtures. The relation is described by the Christov equation [87]:

Equation 30

$$\eta_0 = k\left[\sum(\phi_i M_i)\right]^{\alpha} = \left[\sum(\phi_i \eta_{0i}^{1/\alpha})\right]^{\alpha}$$

This predicts a positive deviation from the log-additive rule for binary miscible molecular blends.

Another value frequently used in the determination of system miscibility is the stress relaxation modulus G, and more specifically the plateau modulus, G_N^0. For

entangled polymers, there is a wide range of frequencies over which the modulus is constant in an oscillatory shear flow. [75, p. 362] (Note: Unlike zero-shear viscosity, the relaxation modulus may be determined only by dynamic rheological testing. This places certain limits upon the materials for which the plateau modulus may be determined.) Also known as the rubbery plateau, the plateau modulus is related to the average molecular weight between entanglements M_e by: [88] [89] [84]

Equation 31

$$G_N^0 = \frac{\rho RT}{M_e}$$

It is important to note that the critical molecular weight for entanglement M_c is always a factor of 2-4 times larger than M_e. Most frequently, $M_c = 2M_e$ is used as a rule of thumb. [75, p. 341]

Several theories exist to relate the plateau modulus of a blend to that of the blend's constituents. Based on the single-reptation model, Doi and Edwards postulated a linear additive rule for the athermal case in which specific inter-chain interactions exert little influence on entanglement probability, as that probability remains unperturbed with respect to individual components. [89] These linear additive rules are given as:

Equation 32 a-c

$$G_N^0 = \sum G_{Ni}^0 \phi_i \qquad \eta_0 = \sum \eta_{0i} \phi_i \qquad J_e^0 \eta_0^2 = \sum J_{ei}^0 \eta_{0i}^2 \phi_i$$

where G_N^0 is the platue modulus, η_0 is the zero shear viscosity, and J_e^0 is the recoverable shear compliance.

Alternatively, Tsenoglou proposed a double-reptation model in which there is a random formation of chain entanglements between chains of the components in a miscible blend:

Equation 33

$$G_N^0 = \left[\sum (G_{Ni}^0)^{1/2} \phi_i\right]^2$$

This may be extended further to incorporate zero shear viscosity and recoverable shear compliance. For a binary mixture, the following equations result: [90]

Equation 34

$$\eta_0 = \eta_{0a}\phi_a^2 + \eta_{0b}\phi_b^2 + 4\phi_a\phi_b \frac{(G_{Na}^0 G_{Nb}^0)^{1/2}}{(G_{Na}^0/\eta_{0a}) + (G_{Nb}^0/\eta_{0b})}$$

Equation 35

$$J_e^0\eta_0 = J_{ea}^0\eta_{0a}^2\phi_a^2 + J_{eb}^0\eta_{0b}^2\phi_b^2 + 8\phi_a\phi_b \left[\frac{(G_{Na}^0/G_{Nb}^0)^{1/4}}{(J_{ea}^0\eta_{0a}^2)^{1/2}} + \frac{(G_{Nb}^0/G_{Na}^0)^{1/4}}{(J_{eb}^0\eta_{0b}^2)^{1/2}}\right]^{-1}$$

2.2.3. Thermodynamics of Polymer Blends and Solutions

As most of this work is concerned with rheology, the thermodynamic studies were focused on the determination of the presence and degree of miscibility in a given system, along with some crystallinity studies. The basis for measurements of miscibility by thermodynamic means is the Flory-Huggins equation for mixing:

Equation 36

$$\Delta G_M = kT\left(\frac{\phi_a}{v_a N_a}\ln\phi_a + \frac{\phi_b}{v_b N_b}\ln\phi_b + \frac{\chi\phi_a\phi_b}{v}\right)$$

where ΔG_M is the free energy change of mixing per unit volume, k is the Boltzmann constant, T is the absolute temperature, Φ_i is the volume fraction of component i in the mixture, v_i is the volume of each monomer in chain i, N_i is the number of monomers in chain i, χ is the Flory-Huggins interaction parameter, and v is an arbitrary reference parameter. [91] [92] Originally developed for polymer/solvent interactions, the theory was later extended to include polymer blends and other multi-component systems. [93]

A means of measuring miscibility of a system (assuming it is miscible in the specified range) is determination of the shift in the melting temperature of the mixture as a function of temperature. In the context of mean-field approximation as applied to a polymer solution at the high molecular weight limit, the melting peak of a solution may be calculated by

Equation 37

$$\frac{1}{T_s^0} - \frac{1}{T_m^0} \cong \frac{R}{\Delta H_u}[(1-\phi_p) - \chi(1-\phi_p)^2]$$

where T_s^0 is the melting point of the solution, T_m^0 is the melting point of the bulk polymer, R is the gas constant, ΔH_u is the heat of fusion per mole of repeating unit, Φ_p is the volume fraction of the polymer, and χ is the Flory-Huggins interaction parameter. [58] [94] For a polymer in a theta solvent, $\chi = 0$.

In the case of polymer blends, a simple, linear rule of mixture is frequently used to verify miscibility of a binary blend. (However, this simplified rule does not take into account any curve in the data resulting from ternary phase interactions, intermediate phases, non-linear changes in crystallite size, etc.)

Equation 38

$$T_m = \phi_a T_{ma} + \phi_b T_{mb}$$

T_m is the melting temperature of the blend, Φ_i is the volume fraction of component *i*, and T_{mi} is the melting temperature of component *i*. [18] [19] [29] [47] [32] [36] Similarly, heat of fusion can be used to trace the degree of independence of a component i.e. how much of polymer A is incorporated into polymer B in a blend. [32] [44] [60]

CHAPTER 3: RHEOLOGICAL AND THERMAL BEHAVIOR OF PE/PE MELT MIXTURES

3.1. Rheological and Thermal Behavior: Introduction

In this study of the properties of blends of different grades of polyethylene and paraffin wax, several features will be examined, splitting into the thermal and the rheological, with complementary features arching between both.

To understand the miscibility of a blend, it is useful to have an idea of the overall phase diagram of a given mixture. In this case, the phase diagram will be examined at atmospheric pressure and a nitrogen atmosphere across a full spectrum of composition (0 – 100% PE) and a range of temperatures from below the initiation of melting for the wax to well above the melting point of the PE (0 °C to 180 °C). These phase diagram may be generated and cross validated using a number of techniques including transmission electron microscopy (which can directly image crystal structures), x-ray and neutron diffraction, and others. However, the most simple and traditional method for determining a mixtures phase diagram is differential scanning calorimetry (DSC). In this method a sample is heated and then cooled at constant temperature rates and the heat flows are measured. From this, the phase transition temperatures and the heats of those transitions may be determined. This technique is best complemented by some form of microscopy as DSC does not give any data as to the morphology of the blend.

To understand the behavior of a mixture in the melt, the samples should be measured by some form of rheometry, of which there are many (cone-and-plate,

capillary, rotational) with different regimes of usefulness. In this case, a parallel-plate rheometer shall be used in steady-state shear. The rheological property of interest is the zero-shear viscosity, η_0, or the viscosity of the melt at low shear rates, when it still behaves as a Newtonian fluid. The manner in which a mixture's zero-shear viscosity behaves as a function of its composition gives great detail as to the state of the mixture in melt, i.e. miscible or immiscible and concentrated or dilute (for solutions). These details, when combined with the results from DSC, allow a more complete understanding of the behaviors of PE/wax mixtures.

3.2. Material Preparation and Characterization

3.2.1. Melt Mixing

A broad range of high density polyethylenes have been used in this study, all of which are blended with a single grade of paraffin wax. It is important to note that the molecular weight of the paraffin wax of 405 g/mol is well below the estimated critical molecular weight for entanglement linear PE (3660-3800 g/mol). [25] [37] [38] [39]

The materials examined are listed in Table 2. The densities of all materials are approximately 0.95 g/cm^3. The paraffin wax and given PE grades were combined over a range of compositions for all grades, from 0-100% PE content for every grade except UHM_wPE. In melt mixing, it is not possible to go employ compositions having above a certain proportion of UHM_wPE because the material's viscosity becomes too great. It causes significant viscous heating, resulting in material degradation even when using

antioxidant and nitrogen gas. This limit has been found to be approximately 35% UHM_wPE for the given mixing conditions.

Table 2: Grades of polyethylene used

PE grade	*Abbreviation*	*Molecular Weight M_w (g/mol)*	*Melting Temperature (°C)*
3134 paraffin wax	Wax	405	57
SA 420819 PE	41K PE	41,000	127
SA 427985 PE	72K PE	72,000	129
SA 547999 PE	115K PE	115,000	129
SA 181900 PE	125K PE	125,000	131
XM-220 UHM_wPE	UHM_wPE	$2x10^6$	142

The paraffin wax was acquired in 10 lbs. slabs from Endless Possibilities, a division of Hobby Lobby Manufacturing. (Note: this grade of wax is widely used in candle production.) The four grades of high density polyethylene (HDPE) were acquired in pellet form from Sigma-Aldrich, Co. The UHM_wPE was acquired in powder form from Mitsui Chemicals America, Inc, under the trade name Mipelon XM-220.

The mixer used was a Brabender Prep Center with the Prep-Mixer attachment using dual roller blades. The blends were mixed at 180 ºC for 30 minutes and 150 rpm under a nitrogen atmosphere [27] with the inclusion of 0.5 wt% antioxidant (Alfa Aesar 2,6-Di-tert-butyl-4-methylphenol). [18] The use of an antioxidant and a nitrogen atmosphere reduces any thermomechanical degradation and/or decomposition that might incur. [95] After 30 minutes, the resulting blend was removed from the mixer and immediately quenched in ice water.

The temperature selected for mixing was well above the melting temperature of any of the materials used herein and consequently above the temperature at which phase separation between the wax and the polyethylene might occur. Previous studies of the development of required torque in mixing as a function of time for HDPE blends indicate a plateau to develop in a range from 5 to 20 minutes depending on the materials being used, the blend composition, the temperature, and the rotor speed. [2] [48] Based on that and experiences developed during this study, 30 minutes at 180 ºC was determined a safe time frame for use across all blends to develop homogeneity. The mixture must be homogeneous for valid testing.

When mixing HDPE materials, which are in pellet form, the polymer was fed into the mixer before the wax. This alleviated an issue that might otherwise occur with particularly low viscosity fluids, wherein the wax tends to leak out of the mixer.

For UHM_wPE blends, a certain degree of special preparation was required prior to loading the materials in the mixer. First, the wax was melted in a glass beaker over a hot plate at 100 ºC. This temperature is above the wax's melting temperature but well below that of the UHM_wPE. The UHM_wPE was then dispersed in powder form into the liquid paraffin by manual stirring. The resulting slurry was immediately fed into the mixer, and any residue remaining in the beaker was scraped into the mixer. This prevented any variations of mixture ratios from being introduced because of the material transfer.

From that point forward, the procedure employed was the same as is normally used for mixing HDPE materials. Failure to observe this procedure can cause the aforementioned wax leak issues and cause the initial composition of the blend to deviate

from the intended ratios. Because of this, independent determination of the blends composition was essential.

3.2.2. Thermogravimetric Analysis

Thermogravimetric Analysis (TGA) was performed using a both a Thermal Analytics Q5000 TGA and a Thermal Analytics Q500 TGA. This analysis was done for two reasons:

1. to identify any decomposition effects [19] [44]
2. *and* to independently verify a given sample's composition [60].

To gauge decomposition effects, a small sample (~25 mg) of a blend was placed in the TGA under an inert nitrogen atmosphere. The temperature was then ramped up at a rate of 5 ºC/min to a level of 600 ºC. The peaks in the derivative of the change in weight percentage as a function of temperature ($d\%_m/d\mathrm{T}$) for a blend gave the approximate decomposition temperatures of the components (see Figure 4). Additionally, by heating to 180 ºC and holding for an hour, any decomposition effects that occur at that temperature (the temperature used for mixing, molding, and extrusion) were identified. (As it turns out, such effects are minimal.)

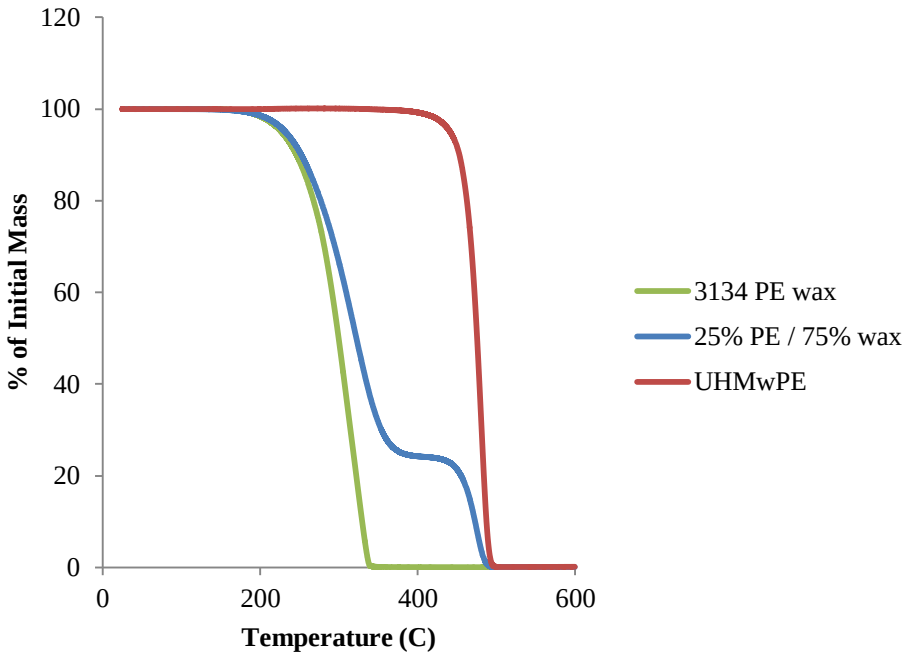

Figure 4: TGA temperature ramp in nitrogen of 5 °C/min to 600 °C for pure paraffin wax, pure UHM_wPE, and a 75% UHM_wPE / 25% wax mixture.

In order to measure a blend's composition, a sample is heated at a rate of 20 ºC/min until it reaches 350 ºC in a nitrogen atmosphere. The temperature is held there until the rate of change in the percent mass is less than 0.2 %/min or 30 minutes has elapsed, whichever occurs first. At 350 ºC, the wax will decompose completely within the specified period with minimal decomposition occurring for the PE (see Figure 5). The remaining percent of mass is the fraction of PE in the blend. This technique was validated by placing two unmixed samples of the pure PE and pure wax with known masses together in TGA. The material was heated to 350 ºC and held as described above. The final mass percentage matched that of the initial PE used.

This technique is useful not only for determining the compositions of the neat blends but also for determining those of any materials that have undergone post-processing steps such as extrusion, compression, or partial dissolution of a component.

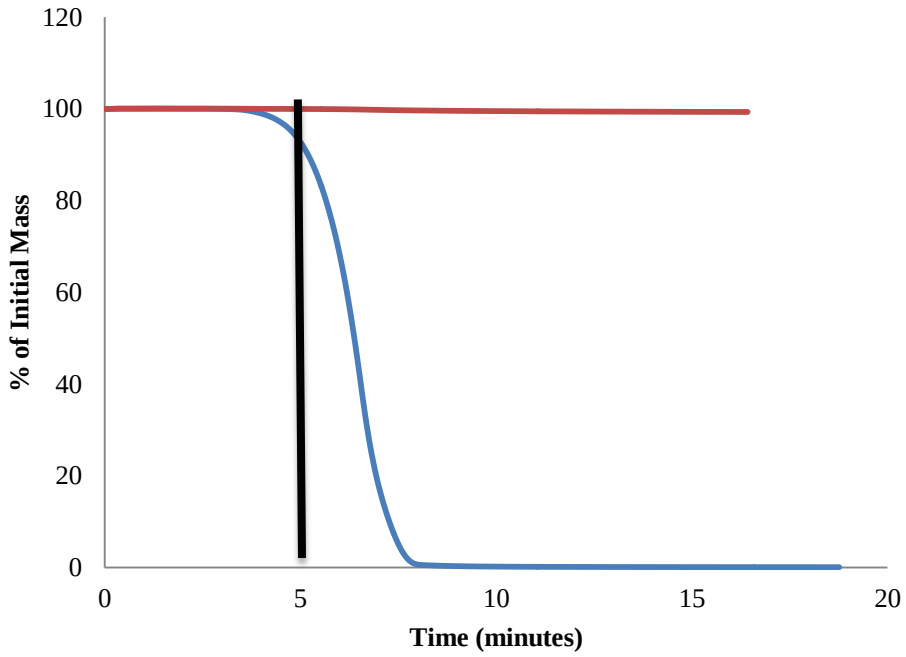

Figure 5: TGA heat-and-hold scans of pure paraffin wax and 12K PE. The samples were heated in nitrogen to 350 °C at 50°C/min and held at that temperature. Blue is for paraffin wax; red for 125K PE. The black line indicates the time at which the system reached 350 °C

3.2.3. Differential Scanning Calorimetry

Differential Scanning Calorimetry (DSC) was performed using a Thermal Analytics Q200 DSC. The applications of such a characterization are numerous. However, the technique employed follows a constant pattern.

A small sample of material (< 10 mg) is placed in a hermetically sealed aluminum pan. This pan is placed in the DSC with an identical empty pan as reference. Under a nitrogen atmosphere, the temperature is reduced to and equilibrated at 0 ºC. Once equilibrium is achieved, the temperature is ramped up at 10 ºC per minute to 180 ºC, and held isothermal for 2 minutes. Then the temperature is ramped back down to 0 ºC. From the resulting heat-flow curve, a number of values may be determined including melting temperatures and crystallization temperature, enthalpies of melting and recrystallization, and percent crystallinity. These values have wide range of applications including determination of blend composition and homogeneity, identification of crystal structures present, and measurement of any processing effects. [44] [51] [60]

After mixing, samples frequently underwent additional processing. However, minimal alteration of the initial blend structure is essential unless otherwise specified. By performing additional DSC sweeps on these materials, inconsistencies (or the lack thereof) in a material between stages of processing may be identified.

3.2.4. Compression Molding

To prepare samples for use in parallel plate rheometry, the neat polymer blends must be first molded into sheets. This was accomplished using a Carver 4389 Hot Press with both the top and bottom plates heated. Without this prior preparation, the material will not sufficiently conform to the rheometer. The exception to this is blends of exceptionally high wax content. If molding is attempted on the high wax content samples using the Carver Hot Press, the resulting slabs will too brittle to remove from the mold

intact. Fortunately, the high wax blend samples will conform themselves between the plates of the rheometer without prior shaping.

The press and the mold itself are preheated to 180 ºC. The mold comprises a rectangular steel sheet having a thickness of 1.0 mm and two Teflon sheets. In the center of the steel sheet is a rectangular orifice of dimensions 100 mm by 150 mm. This orifice forms the four side walls of the mold. During the molding process, the Teflon sheets are positioned one above and one below the steel sheet, completely covering the rectangular orifice from both sides. Teflon was chosen for use in the top and bottom surfaces of the mold because it manifests low surface energy.

After heating the press and mold, a sample that will completely fill the mold space [in one or more pieces of sufficient combined mass (~15 g)] is placed in the metal frame on top of the lower Teflon sheet. To obtain successful and uniform results, these sample pieces should consistently be thin, no thicker than half a centimeter when lying in the mold.

The second Teflon sheet is then placed on top of the sample and the plates of the press are brought together so that the top plate makes only slight contact with the top Teflon sheet, this contact just sufficient to permit heat transfer. The system is maintained in this configuration for approximately 10 minutes, allowing the sample to heat completely. Then, the plates are gently pressed together, putting the mold under increasing compression and tightening the Teflon plates against the steel, until the pressure steadies at one metric ton, as indicated by an installed analog pressure gauge. This contact is just sufficient to permit heat transfer while driving the sample to conform to the mold and removing any air remaining in the samples.

This pressure is maintained for ten minutes. [33] The entire mold is then released, removed from the press, and quenched in water. Finally, the resulting sample slab is removed from the mold.

During the molding process, structural or compositional changes may in occur in some instances. Indeed, compression molding may be used for specifically that purpose. However, in the procedure described above, the structure and composition remained unchanged as consistently verified by DSC and TGA respectively, using the neat material as a standard.

3.2.5. Parallel Plate Rheometry

Rheological examinations of the blends were performed using a Thermal Analytics AR2000ex rheometer with parallel plate geometry. Specifically, the zero shear viscosities of the blends at 180 ºC were determined.

This was accomplished as follows. Molded samples were placed between the plates and allowed to equilibrate for 10 minutes. The plates were then brought together to the designated testing gap +5%. Excess material was then scrapped from around the plates.

The chosen testing gap itself was dependent on the samples viscosity. Most samples were tested at 1 mm thickness, but the lower viscosity samples needed a thinner gap - as low as 250 μm for the pure wax - in order to develop reliable data. After excess material was removed, the plates were brought to the testing gap, and the sample was allowed to equilibrate for an additional 10 minutes. This permitted any stress developed

due to the compression to relax out of the sample. Finally, a steady state shear rate sweep was performed. The range of shear rates covered was specific to each sample. The initial test of every blend type covered the full range of shear rates from 10^{-6} 1/s to 1000 1/s. From this sweep, the range of rates over which the melt behaves as a Cross or Newtonian liquid was identified. Additional shear sweeps were performed on the blend in the specified range to determine the zero shear viscosity.

Arguably, oscillatory testing would be of much greater value than steady state testing because dynamic testing provides much more information about the sample with the storage and loss moduli. However, for most of the PEs examined, the complex viscosity could never be brought to the zero-shear range of frequencies, a common problem with HDPE. [25] This is due to the extremely low frequency/strain percentage required for it to be in the Newtonian regime. The required time for testing would be impractically long with limited benefit.

3.3. Thermal and Phase Behavior

A wide range of compositions were created for blends of polyethylene and wax. Blends of the four grades of HDPE and wax (Table 2) covered a full range of PE compositions from 0% to 100%, with a greater number of blends created at the lower concentrations. For blends with UHM_wPE, the compositions ranged from 0 to 35% UHM_wPE.

3.3.1. Concerning TGA

Though all blends were initially mixtures of pure materials at targeted ratios (i.e. were fed into the mixer at 75% wax and 25% PE), the compositions of the sample resulting from mixing frequently differed from the initial ratio. This is due to loss of wax that unavoidably leaked from the mixer as described in the mixing procedures (*3.2.1. Melt Mixing*). Therefore, prior to measurements, tests, or processing, the actual composition of the samples drawn from the mixer were determined by TGA.

While the samples with higher concentrations of PE showed little variance in composition from the initial ratio, those mixed using lower concentrations of PE differed significantly. For example, a sample that started as 1% PE before mixing may come out as 2% after mixing. While this percent difference matters little at the greater PE concentrations, its effects are amplified at the lower PE concentrations, particularly when concentration values are converted to effective molecular weights.

Additionally, in low PE concentration samples, TGA measurements indicated significantly greater relative variance in composition within given mixed samples as compared to variances noted within high PE concentration samples. This is attributed in part to decreased sensitivity of the measuring instrument at lower masses, but is primarily due to actual concentration fluctuations within a given sample. The lower the concentration of PE in wax, the greater the mobility of the PE molecules, particularly at concentration levels below that of entanglement. Furthermore, the PE becomes more difficult to mix uniformly with wax at the lower compositions as the pellets of PE less frequently contact each other to form a continuous network into which the mechanical

forces of mixing may be applied. Indeed, below the critical concentration for entanglement, the PE appeared to dissolve into the wax more by diffusion than by force of conventional, shear/friction-based mixing.

3.3.2. Thermal Results and Phase Behavior

Differential scanning calorimetry is used to determine two sets of values:

- the temperatures at which phase transitions occur

  and

- the heats associated with those phase transitions.

From these values, tentative phase diagrams may be deduced.

In terms of the phase transition temperatures, different temperatures denote different phases existing in the sample. In that regards, DSC can be used to determine the types of crystals and structures present in a given sample. Furthermore, shifts in transition temperatures of a given phase as a function of composition are well established indicators of interactions between the components of a system, i.e. miscibility.

In terms of heat flow, when a phase undergoes a transition of state (i.e. solid to liquid) it either releases or absorbs heat proportional to the amount of that phase structure created or destroyed. As such, DSC heat values (the integral of an endotherm or exotherm) may be used to determine the degree to which a given phase (rather than a given component) exists in a sample [44]. In this case, it can be used to determine the concentration at which the wax is completely miscible in the PE-rich phase. This is the concentration at which there is no endotherm or exotherm associated with wax as the wax

is fully absorbed into the PE rich phase. A down side of using heat values is that they are inherently sensitive to the initial sample mass. Even when normalized to mass (J/g), any error in the initial mass measurement gets carried over into the heat measurement. This is the major source of error in heat measurements in this data. Contrariwise, the temperatures for phase transitions are independent of the sample mass, and so those measurements have one less source of possible error.

Typical DSC curves for wax (Figure 6), 125K PE (Figure 7), and a 50/50 wax/125K PE blend (Figure 8) are shown below with the peaks for the melting and the recrystallization marked. These types of curves form the basis of any thermal study of miscible or semi-miscible blends using DSC.

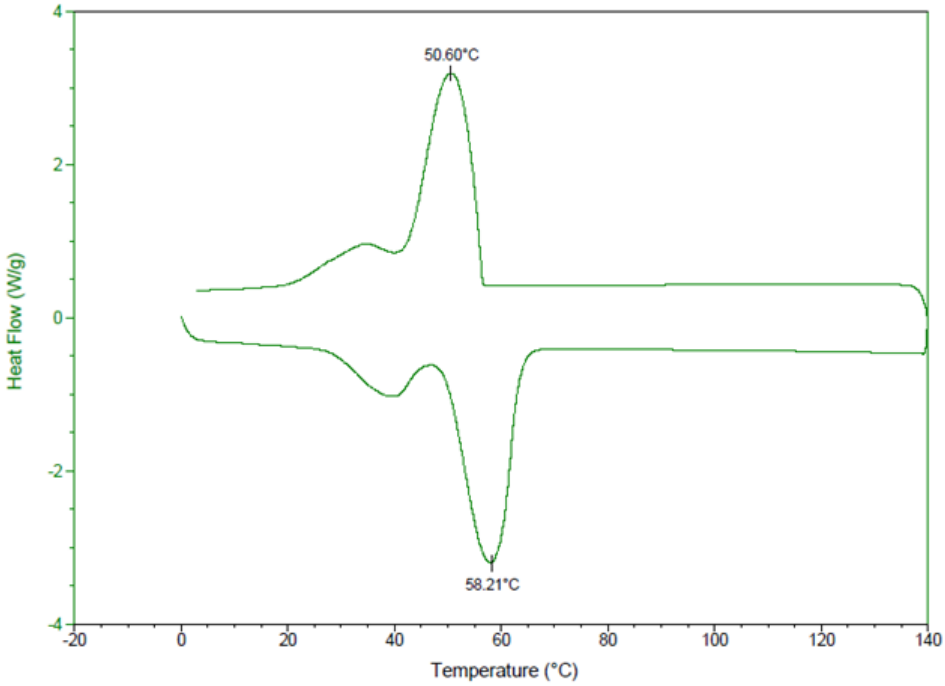

Figure 6: Typical DSC scan for paraffin wax

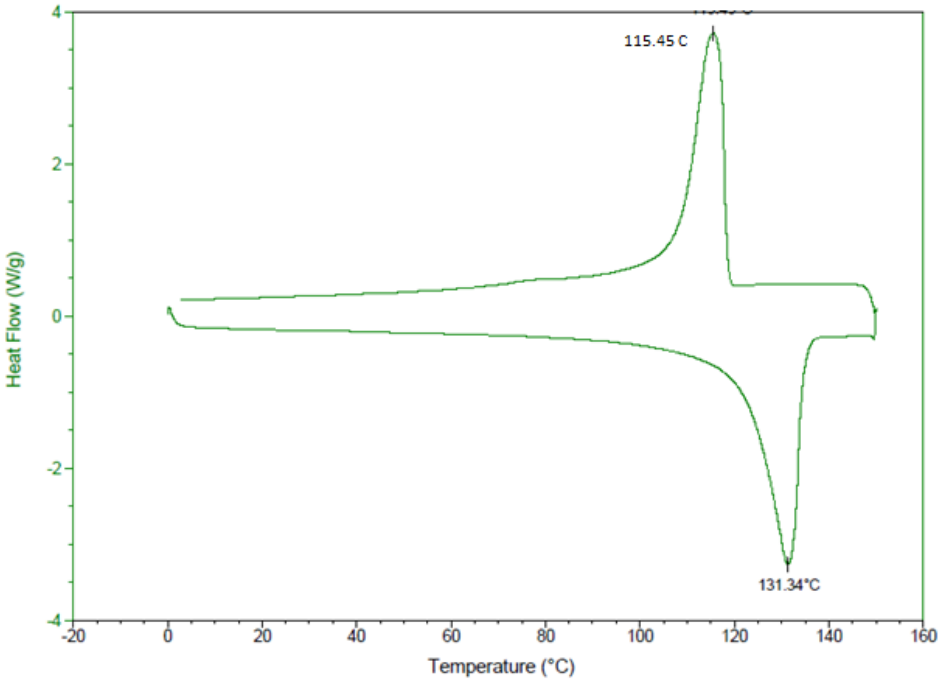

Figure 7: Typical DSC scan of HDPE (125 K g/mol M_w PE)

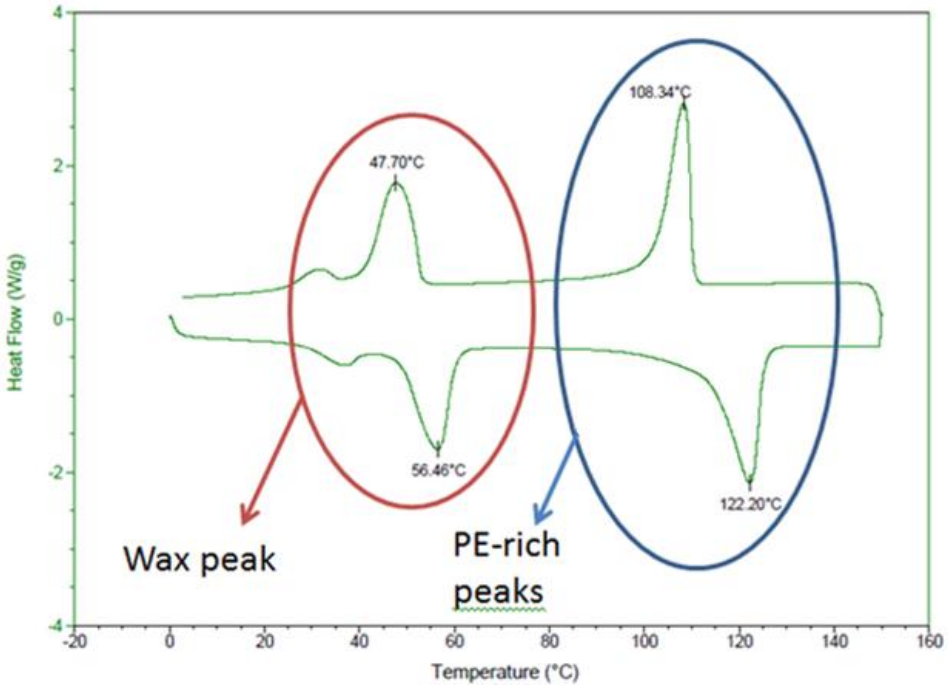

Figure 8: Typical DSC scan for a 50/50 blend of wax/HDPE. The peaks corresponding to the paraffin wax (blue) and PE-rich phases are encircled.

The first feature of note is that for both melting and recrystallization in blends, distinct peaks exist at low and high temperatures. The low temperature peaks are associated with the wax-rich phase; the high temperature, the PE rich phase. By examining the temperature shift of these two peaks as a function of temperature, the miscibility behavior may be elucidated (Figure 8).

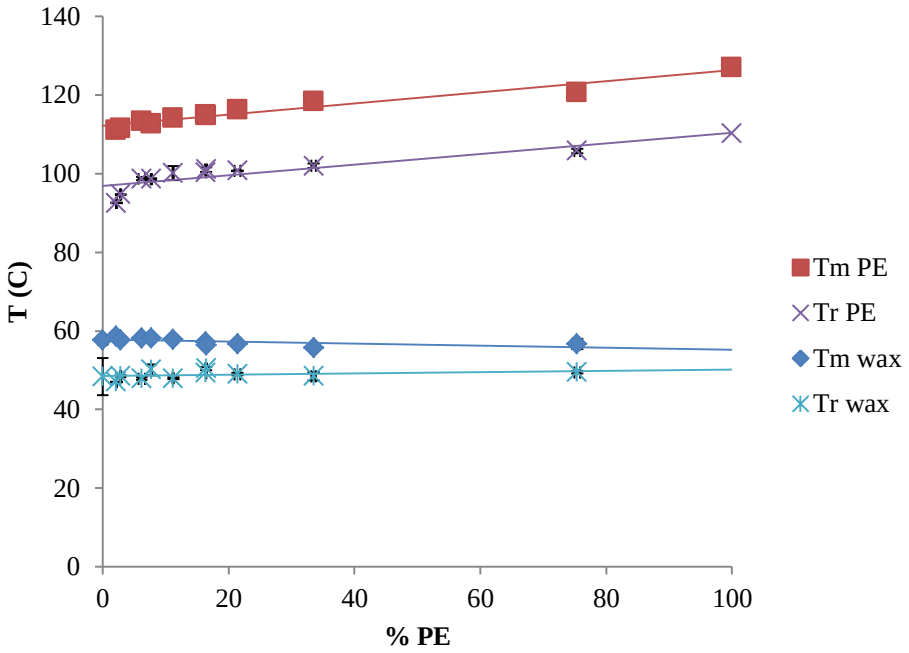

Figure 9: Melting and recrystallization temperatures vs. composition (% PE) for the PE-rich and wax phases of 41K PE / wax blends with associated linear fits

Table 3: Linear fits to the melting and recrystallization temperatures of the PE and wax phases as a function of composition for blends of 41K PE and wax.

Peak type	*Linear fit*	R^2
PE melting	T_m(PE) = 0.142 (% PE) + 112.1	0.9424
PE recrystallization	T_r(PE) = 0.135 (% PE) + 96.86	0.8209
Wax melting	T_m(wax) = -2.58x10^{-2} (% PE) + 57.79	0.3858
Wax recrystallization	T_r(PE) = -1.61x10^{-2} (% PE) + 48.49	0.1177

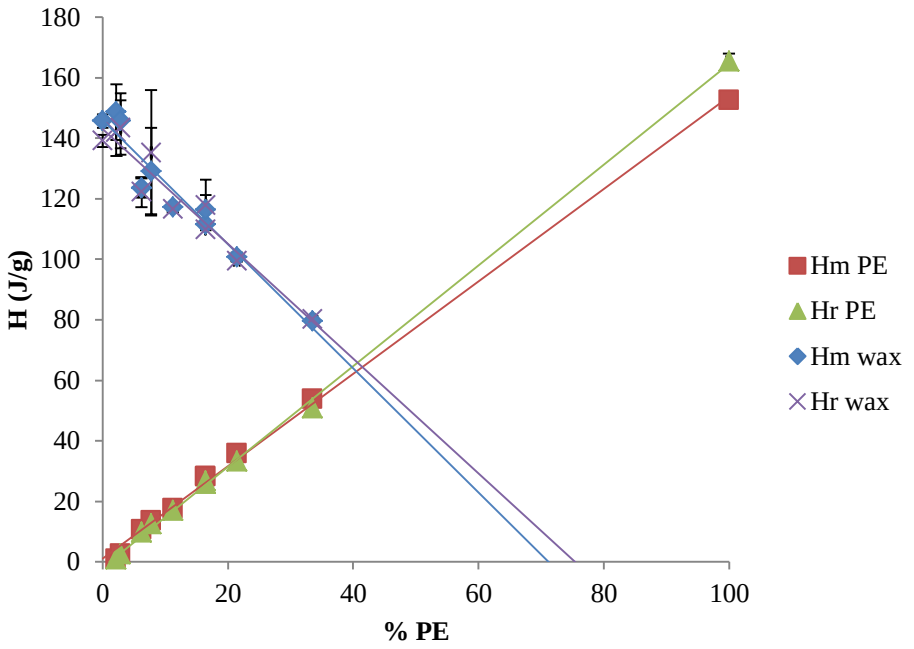

Figure 10: Melting and recrystallization heats (normalized) vs. composition (% PE) for the PE-rich and wax phases of 41K PE /wax blends with associated linear fits

Table 4: Linear fits to the melting and recrystallization heats of the PE and wax phases as a function of composition for blends of 41K PE and wax.

Peak type	*Linear fit*	R^2	*X-axis intercept*
PE melting	H_m(PE) = 1.529 (% PE) + 1.051	0.9979	-0.6874
PE recrystallization	H_r(PE) = 1.665 (% PE) – 1.836	0.9992	1.103
Wax melting	H_m(PE) = -2.052 (% PE) + 146.1	0.9450	71.17
Wax recrystallization	H_r(PE) = -1.898 (% PE) + 143.0	0.9297	75.36

Special note needs to be made with regards to the thermal data for the 41K PE and wax blends. The melting and recrystallization temperature data from the 50/50 mixture of 41K PE and wax was sufficiently poor quality as to invalidate the sample. Furthermore, the enthalpy values measured from the ~75% 41K PE / 25% wax blends

were much greater than could be possible, likely as a result of a poor measurement of sample mass. However, the 75/25 mixture's transitions temperatures (for which measurement is independent of mass) were consistent and in line with the expected trends, and so remain reported here. These inconsistencies are the likely cause of the unexpectedly low calculated wax-phase limits (71.17% from melting; 75.36% from recrystallization). Not only are these limits substantially lower than those of any of the other mixtures, these calculated limits are below that actually observed for the samples as wax melting and recrystallization peaks are still observed at ~75% PE.

72K PE and wax blends

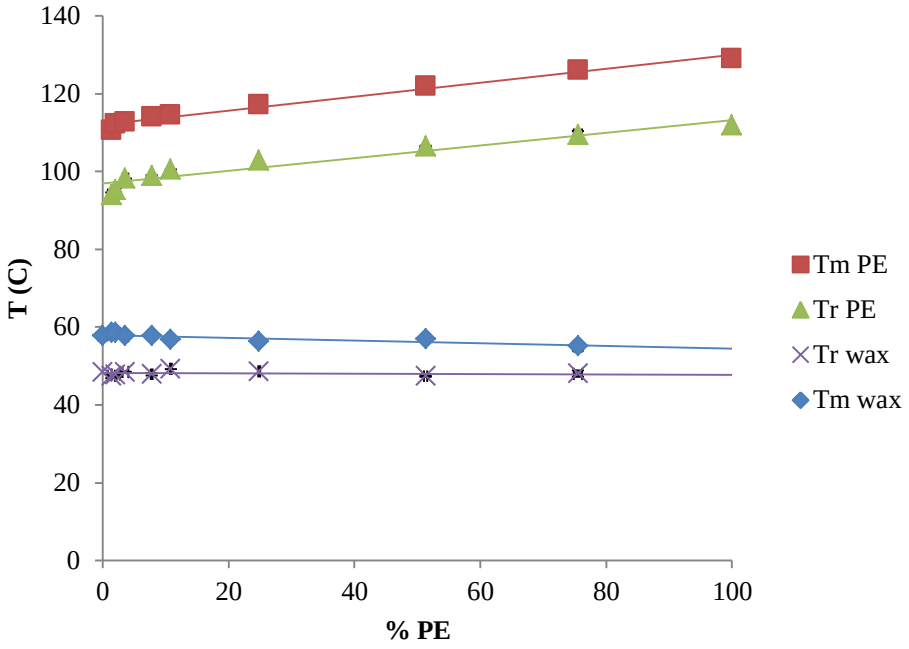

Figure 11: Melting and recrystallization temperatures vs. composition (% PE) for the PE-rich and wax phases of blends of 72K PE / wax blends with associated linear fits

Table 5: Linear fits to the melting and recrystallization temperatures of the PE and wax phases as a function of composition for blends of 72K PE and wax.

Peak type	*Linear fit*	R^2
PE melting	T_m(PE) = 0.179 (% PE) + 112.1	0.9830
PE recrystallization	T_r(PE) = 0.164 (% PE) + 96.89	0.9209
Wax melting	T_m(wax) = -3.54x10^{-2} (% PE) + 57.97	0.7058
Wax recrystallization	T_r(PE) = -4.25x10^{-3} (% PE) + 48.20	0.0360

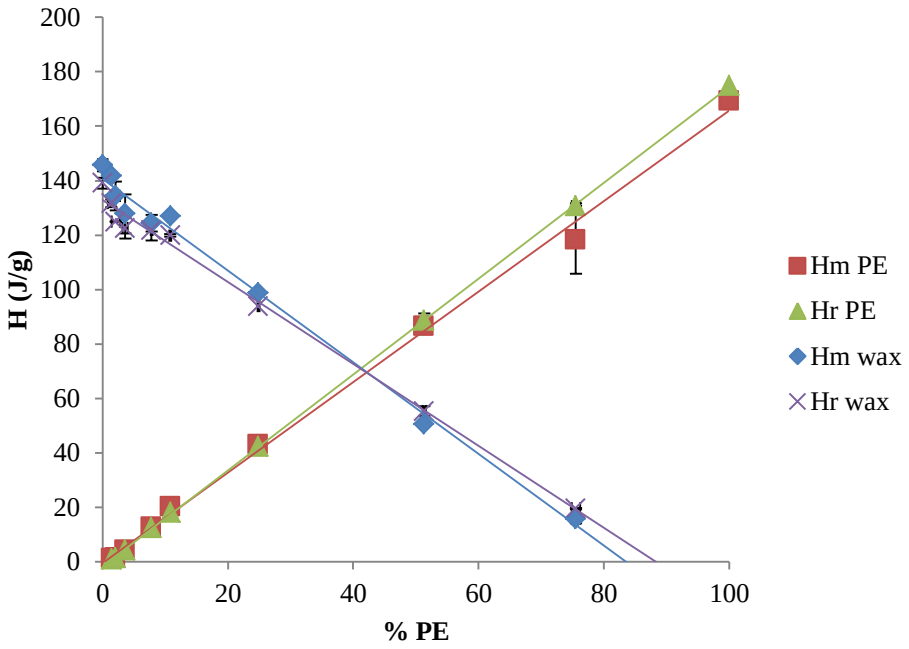

Figure 12: Melting and recrystallization heats (normalized) vs. composition (% PE) for the PE-rich and wax phases of 72K PE / wax blends with associate linear fits.

Table 6: Linear fits to the melting and recrystallization heats of the PE and wax phases as a function of composition for blends of 72K PE and wax.

Peak type	*Linear fit*	R^2	*X-axis intercept*
PE melting	H_m(PE) = 1.663 (% PE) - .489	0.9973	0.2942
PE recrystallization	H_r(PE) = 1.761 (% PE) -1.608	0.9999	0.9131
Wax melting	H_m(PE) = -1.683 (% PE) + 140.5	0.9914	83.52
Wax recrystallization	H_r(PE) = -1.506 (% PE) + 132.9	0.9922	88.24

115K PE and Wax Blends

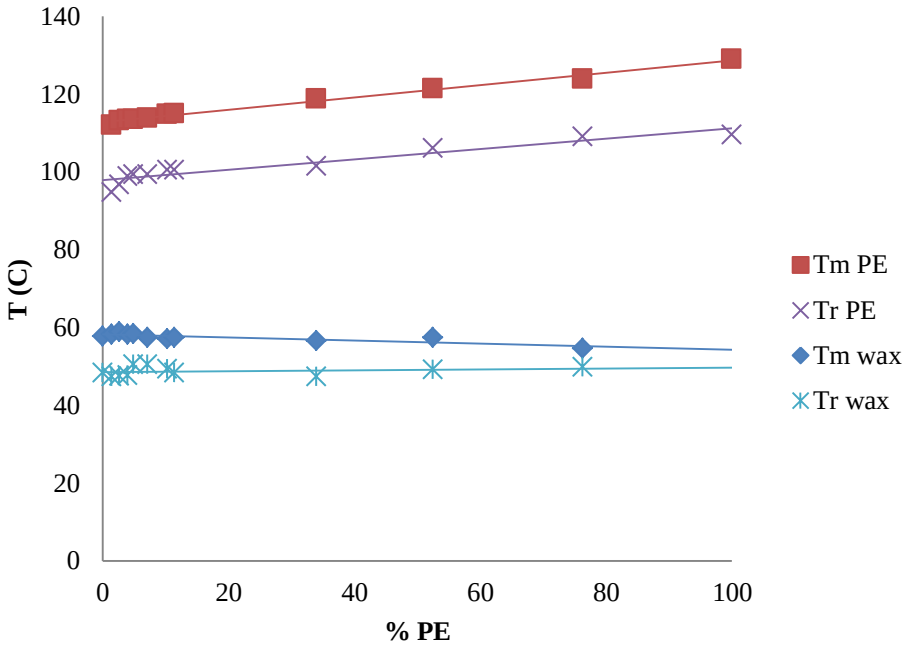

Figure 13: Melting and recrystallization temperatures vs. composition (% PE) for the PE-rich and wax phases 115K PE / wax blends with associated linear fits.

Table 7: Linear fits to the melting and recrystallization temperatures of the PE and wax phases as a function of composition for blends of 115K PE and wax

Peak type	*Linear fit*	R^2
PE melting	T_m(PE) = 0.159 (% PE) + 112.8	0.9907
PE recrystallization	T_r(PE) = 0.133 (% PE) + 97.89	0.9005
Wax melting	T_m(wax) = -3.84×10^{-2} (% PE) + 58.21	0.6996
Wax recrystallization	T_r(wax) = 1.13×10^{-2} (% PE) + 48.55	0.0539

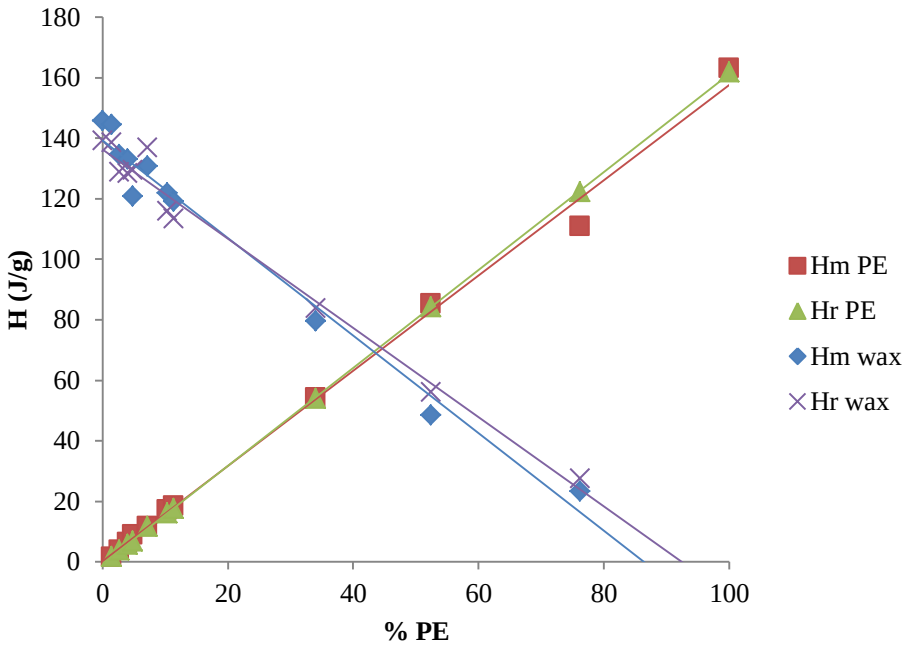

Figure 14: Melting and recrystallization heats (normalized) vs. composition (% PE) for the PE-rich and wax phases of 115K PE / wax blends with associated linear fits

Table 8: Linear fits to the melting and recrystallization heats of the PE and wax phases as a function of composition for blends of 115K PE and wax.

Peak type	*Linear fit*	R^2	*X-axis intercept*
PE melting	H_m(PE) = 1.575 (% PE) + 0.203	0.9956	-0.129
PE recrystallization	H_r(PE) = 1.620 (% PE) - 0.683	0.9999	0.397
Wax melting	H_m(PE) = -1.612 (% PE) + 140	0.9794	86.37
Wax recrystallization	H_r(PE) = -1.475 (% PE) + 136	0.9823	92.40

125K PE and Wax Blends

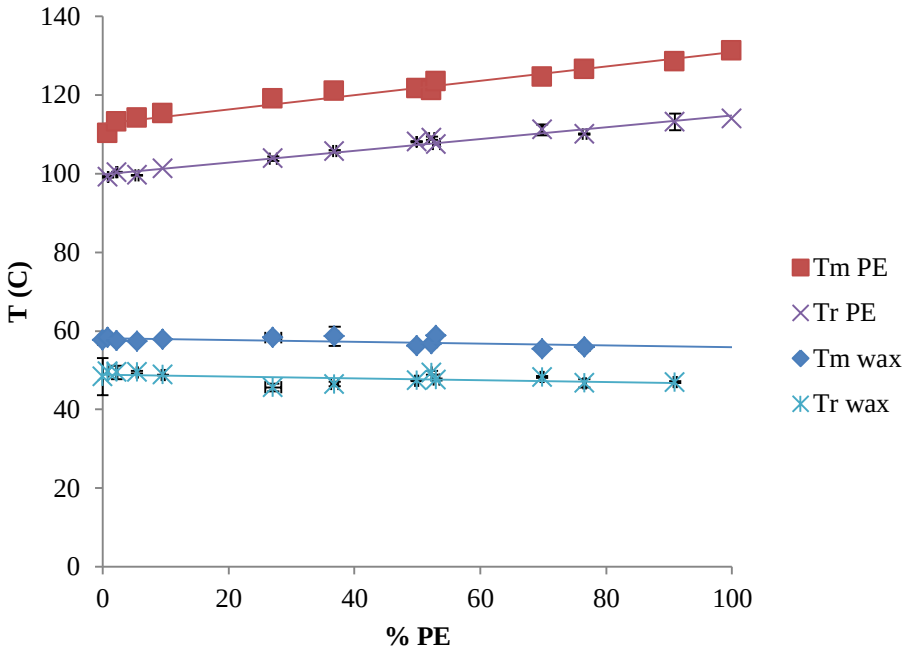

Figure 15: Melting and recrystallization temperatures vs. composition (% PE) for the PE-rich and wax phases of 125K PE / wax blends with associated linear fits.

Table 9: Linear fits to the melting and recrystallization temperatures of the PE and wax phases as a function of composition for blends of 125K PE and wax.

Peak Type	*Linear fit*	R^2
PE melting	T_m(PE) = 0.1808 (% PE) + 112.7	0.9670
PE recrystallization	T_r(PE) = 0.1501 (% PE) + 99.77	0.9768
Wax melting	T_m(wax) = -2.336x10^{-2} (% PE) + 58.12	0.3452
Wax recrystallization	T_r(PE) = -2.218x10^{-2} (% PE) + 48.87	0.2782

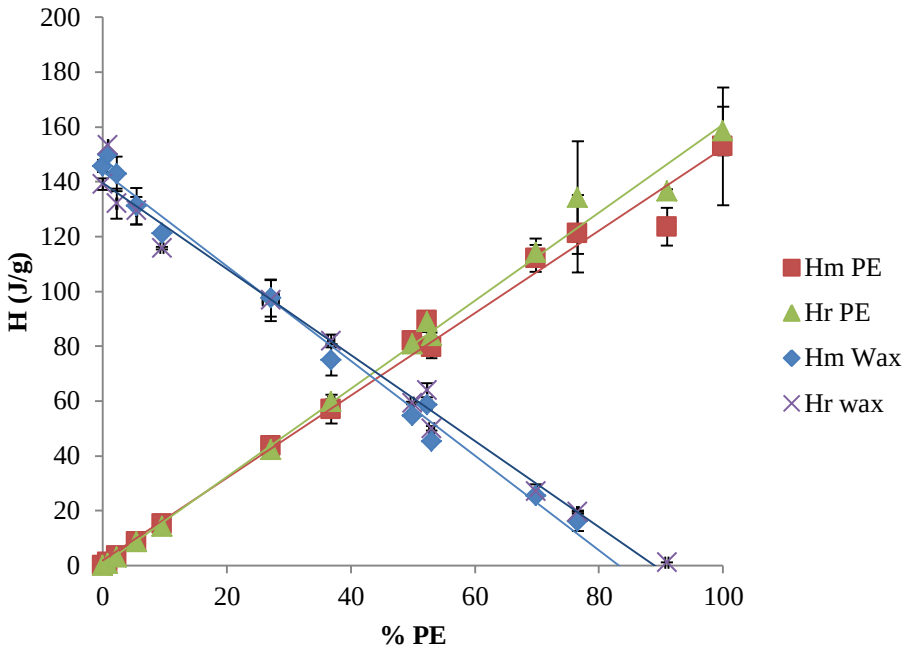

Figure 16: Melting and recrystallization heats (normalized) vs. composition (% PE) for the PE-rich and wax phases of 125K PE / wax blends with associated linear fits.

Table 10: Linear fits to the melting and recrystallization heats of the PE and wax phases as a function of composition for blends of 125K PE and wax.

Peak type	*Linear fit*	R^2	*X-axis intercept*
PE melting	H_m(PE) = 1.504 (% PE) + 1.821	0.9891	-1.211
PE recrystallization	H_r(PE) = 1.607 (% PE) + 0.1538	0.9937	-9.572×10^{-2}
Wax melting	H_m(PE) = -1.727 (% PE) + 143.8	0.9903	83.28
Wax recrystallization	H_r(PE) = -1.569 (% PE) + 139.56	0.9855	88.97

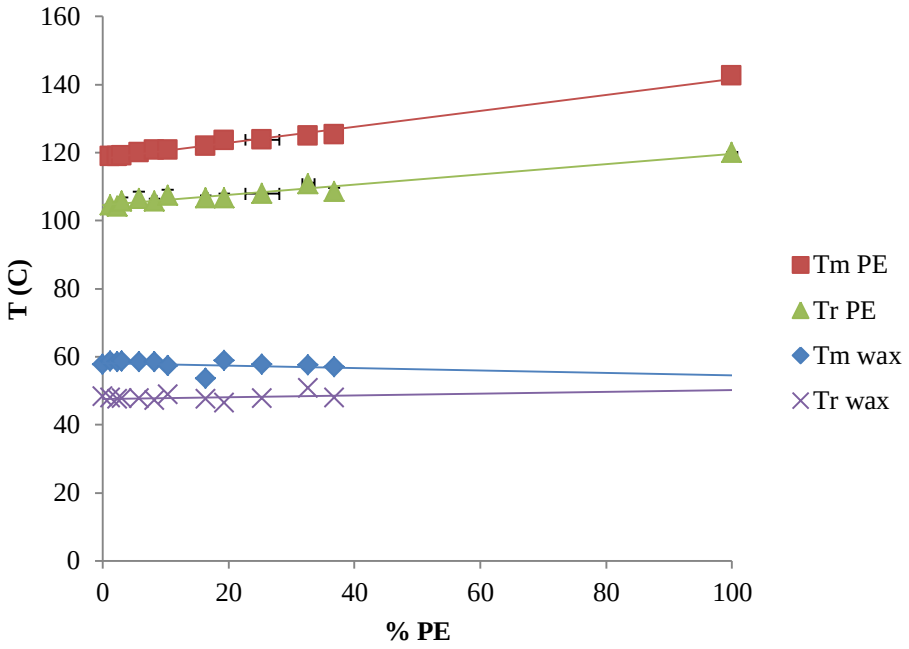

Figure 17: Melting and recrystallization temperatures vs. composition (% PE) for the PE-rich and wax phases of UHM$_w$PE / wax blends with associated linear fits.

Table 11: Linear fits to the melting and recrystallization temperatures of the PE and wax phases as a function of composition for blends of UHM$_w$PE and wax.

Peak type	*Linear fit*	R^2
PE melting	T_m(PE) = 0.234 (% PE) + 118.2	0.9873
PE recrystallization	T_r(PE) = 0.149 (% PE) + 104.6	0.9539
Wax melting	T_m(wax) = -3.61x10^{-2} (% PE) + 58.21	0.0988
Wax recrystallization	T_r(PE) = -2.56x10^{-2} (% PE) + 47.66	0.0940

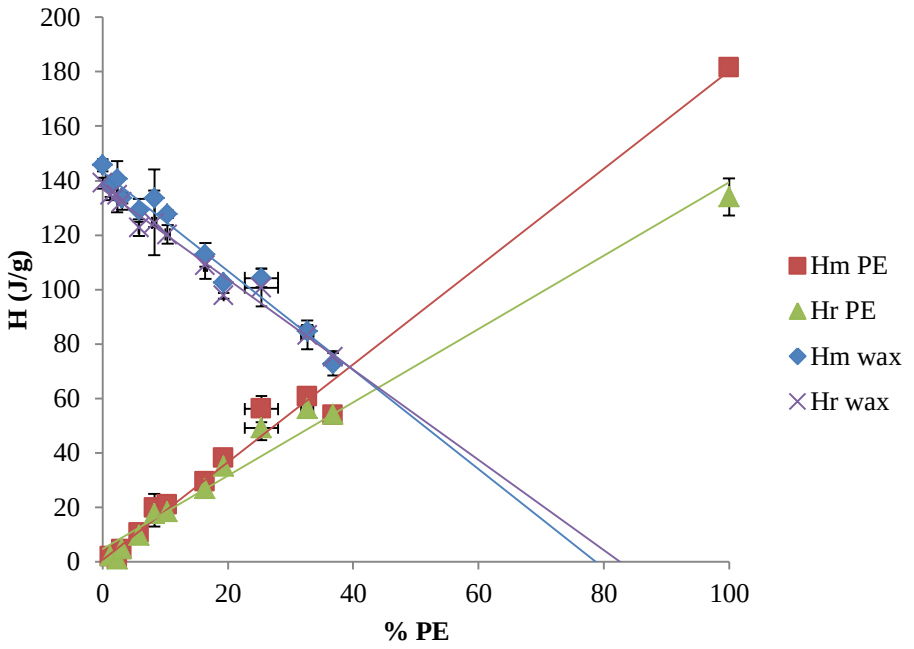

Figure 18: Melting and recrystallization heats (normalized) vs. composition (% PE) for the PE-rich and wax phases of UHM$_w$PE / wax blends with associated linear fits.

Table 12: Linear fits to the melting and recrystallization heats of the PE and wax phases as a function of composition for blends of UHM$_w$PE and wax.

Peak type	*Linear fit*	R^2	*X-axis intercept*
PE melting	H_m(PE) = 1.796 (% PE) + 0.739	0.9882	-0.4114
PE recrystallization	H_r(PE) = 1.347 (% PE) + 4.714	0.9800	-3.500
Wax melting	H_m(PE) = -1.820 (% PE) + 143.2	0.9698	78.67
Wax recrystallization	H_r(PE) = -1.658 (% PE) + 136.8	0.9764	82.52

As with the 42K PE / wax mixtures, special conditions surround the UHM$_w$PE / wax mixtures. Given the equipment and conditions used, there exists a practical limit of ~35% for the melt mixing of the UHM$_w$PE / wax blends due to the increasing force required to cause mixing and increasing viscous heating during mixing caused by higher

UHM_wPE content. However, the data for compositions above 25% begin to deviate substantially from the generated linear trend. Furthermore, this 35% limit means that no data was generated for the compositions between 35% and the pure UHM_wPE. However, as decent linear fits were generated both for the transition temperatures and for the transition enthalpies and the wax-limiting compositions were consistent with those of the other PE blends, the data shall be considered valid.

DSC Addendum

Certain ancillary features of the DSC data merit discussion. During melting, for some samples of lower PE content, a secondary peak associated with the PE-rich phase appears at a temperature lower than the primary peak. This peak is associated with a separate, minor PE-rich crystalline structure formed in the blend. The lack of a secondary peak for the PE rich phase upon recrystallization indicates that this structure only resolves during melting, and that it forms a single crystal upon recrystallization. [51] [52]

For all samples, the wax melting and recrystallization data shows two separate peaks, the larger at higher temperature. The first (lower temperature) peak occurs at the transition of one crystalline phase into another, a so-called solid-solid transition. The second, higher peak is associated with melting of the crystallites. [44]

The miscibility of the systems can be verified by identification of changes in transition temperatures (T_m, T_r) as a function of composition for the different phases. Further structure information may be interpreted from the heats of transition (H_m, H_r). In

particular, the value of composition for which a heat associated with a transition becomes zero shows the temperature window in which a phase exists independent from the other phases. In this case, there is a limit of PE concentration above which the wax no longer exists as an independent phase (Table 13).

3.3.3. Phase Diagrams

From the data of the melting temperatures and enthalpies determined by DSC of the wax and PE-rich phases, tentative phase diagrams for these systems may be generated.

A great deal of work concerning PE/PE phase diagrams has been undertaken by M.J. Hill and P.J. Barham, covering a wide range of PE types and molecular weights. Phase separation has been previously observed during isothermal crystallization in blends containing 2.5K g/mol PE (below M_c) and a high molecular weight PE, with the low molecular weight crystallizing at a constant temperature across a range of compositions, even when the composition is as low at 20%, indicating some degree of phase separation. However, the melting temperature of the PE-rich phase crystals were found to decrease substantially with increasing low molecular weight PE content, denoting some degree of co-crystallization, but only a partially miscible system. [47] (Notably, when the molecular weights of both components in a blend of linear PE with linear PE are above M_c, the blend shows no indication of phase separation, showing only a single melting peak. [47]) These findings are consistent with the results for PE mixtures contained here, wherein the melting temperature of the wax phase remain near constant for all

compositions while the melting temperature of the PE-rich phase changes substantially with composition.

In the liquid state, it has been established that such a linear PE / linear PE system forms a homogeneous melt, separation only occurring upon crystallization of said melt. [47] This has been further observed for blends of LDPE (which is lightly branched) and linear PE, for which liquid-liquid phase separation is the norm until the molecular weight of the linear PE falls below M_c, at which point no liquid-liquid phase separation is observed. [96] [31] Such isotropic liquid solutions are not surprising as the PE fractions are chemically identical, with an anticipated interaction parameter of zero in the melt. [97] Such melt homogeneity in the blends used here is supported by the rheological data (*3.4. Rheological Behavior*) and microscopy (*4.3.3 Compression Overview*). In the rheological examinations, the systems behave homogeneously, not showing any of the aberrations associated with heterogenetity (i.e. significant positive or negative deviation from the power law). In microscopy, the wax phase regions are found to be distributed randomly, in a network-like structure, again indicating crystallization from a homogenous melt. [47]

M. J. Hill and P. J. Barham give an explanation of such behavior. The low M_w PE fraction consists of shorts molecules (~23 nm in the case of the 2500 g/mol linear PE used in their study). This is on parity with the thickness of the crystals being formed (~21-23 nm). Hence, many of the low M_w PE molecules do not form co-crystals. [98] However, some of the low molecular weight PE may nevertheless be incorporated without folding into the high molecular weight PE lamellae. [99]

The wax peaks in all the blend types have a known composition limit beyond which they no longer exist. This was determined by the calculating the enthalpy of melting of the wax peak as a function of composition. These limits are shown in Table 13. (Note: For 41K PE, the calculated limit is lower than that actually observed. That is, the limit is calculated as 71.17% PE, but a wax peak is still present at 75.41%. This discrepancy is likely due to experimental error. The 41K PE system is the only one without thermal data around 50% PE.)

Table 13: Concentration of PE (% PE) for which the wax is completely absorbed into the PE-rich phast for the different grades of PE.

PE Grade	Single phase limit from melting (% PE)	Single phase limit from recrystallization (% PE)
428019	71.17	75.36
427985	83.52	88.24
547999	86.37	92.40
181900	83.28	88.97
xm220	78.67	82.52

These limits are consistent with previous work by M.J. Hato et al concerning mixtures of HDPE and paraffin wax, where 80% and 90% HDPE mixtures showed only a singled melting peak associated with the HDPE. However, at 70% and lower HDPE compositions, an independent, lower-temperature melting peak resolves from DSC. [99]

The resulting data is consistent with the phase diagram of an ideal liquid solution, but non-ideal solid solution, with liquid-liquid interaction parameter being much greater than the critical interaction parameter, as shown in Figure 19.

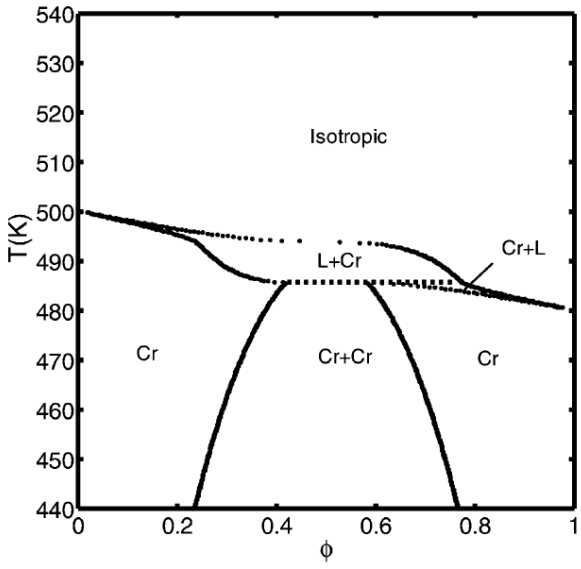

Figure 19: Typical phase diagram for a mixture which exists as an ideal solution in the melt, but non-ideal solution in the solid. R. A. Matkar and T. Kyu, *J. Phys. Chem. B* 2006, 110, 16059-16065, page 16063 (Fig 5)

Using the framework outlined in Figure 19, best-guesses are made concerning the phase transitions not associated with the melt, shown as black dotted lines in the phase diagrams. The actual data for the melting peaks are the diamonds; the fits to the melting peaks are the solid lines. (Note that the template layout and the layout of the diagrams in this thesis are reversed. That is, for the template, the high melting temperature component is associated with 0% composition; for phase diagrams herein, 100% composition.)

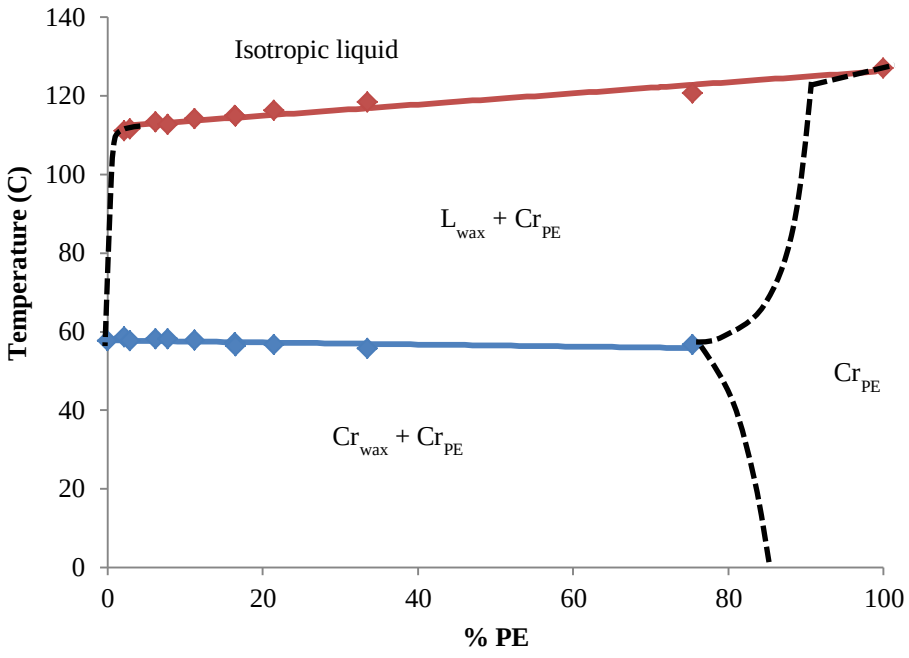

Figure 20: Phase diagram for 41K PE and wax

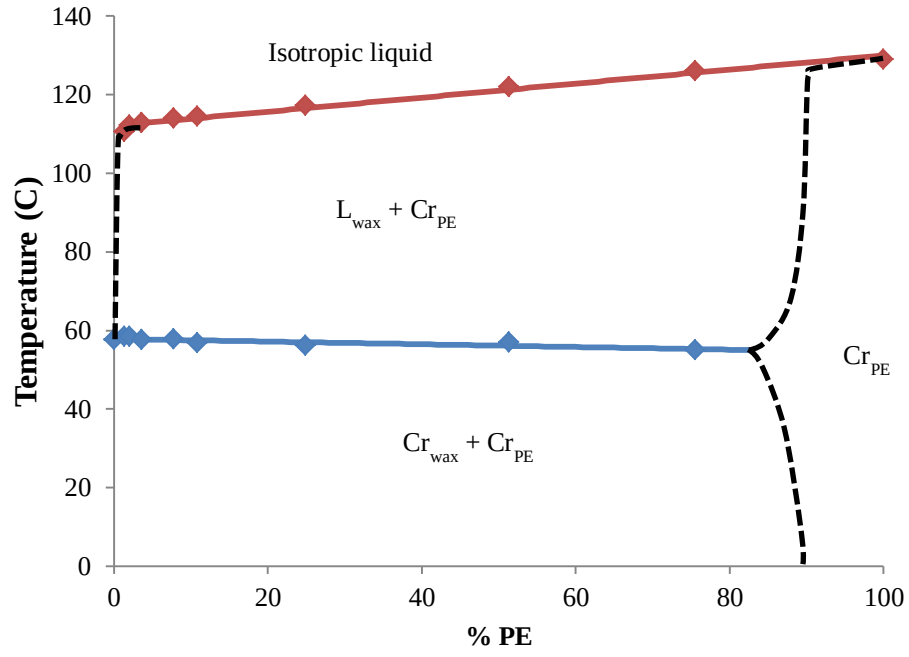

Figure 21: Phase diagram for 72K PE and wax

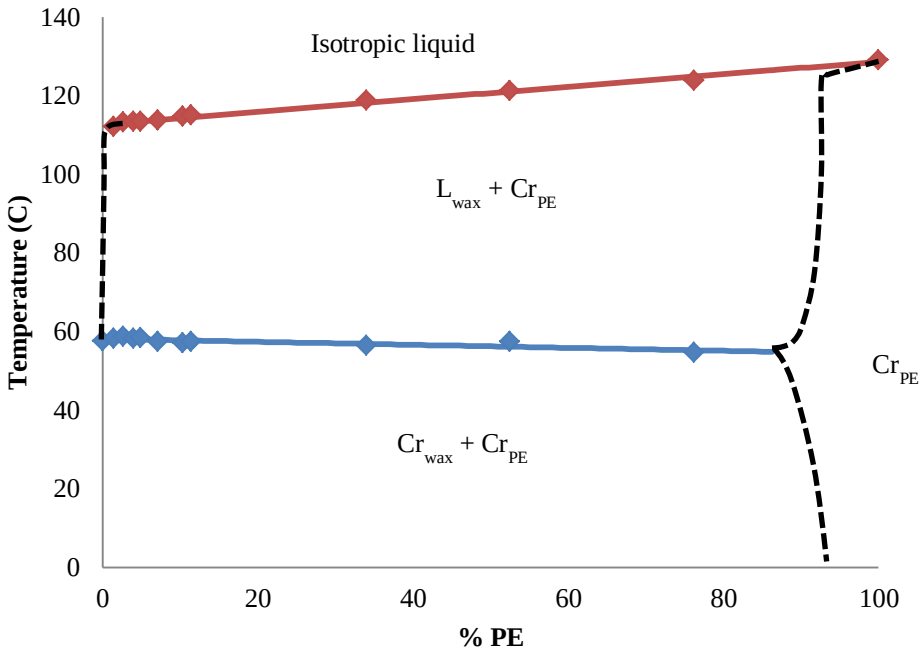

Figure 22: Phase diagram for 115K PE and wax

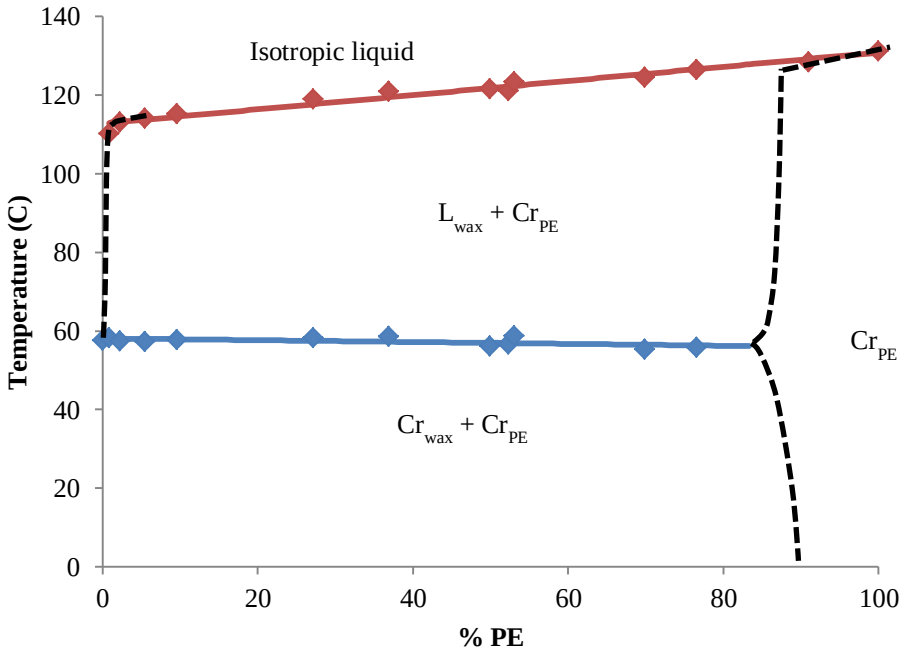

Figure 23: Phase diagram for 125K PE and wax

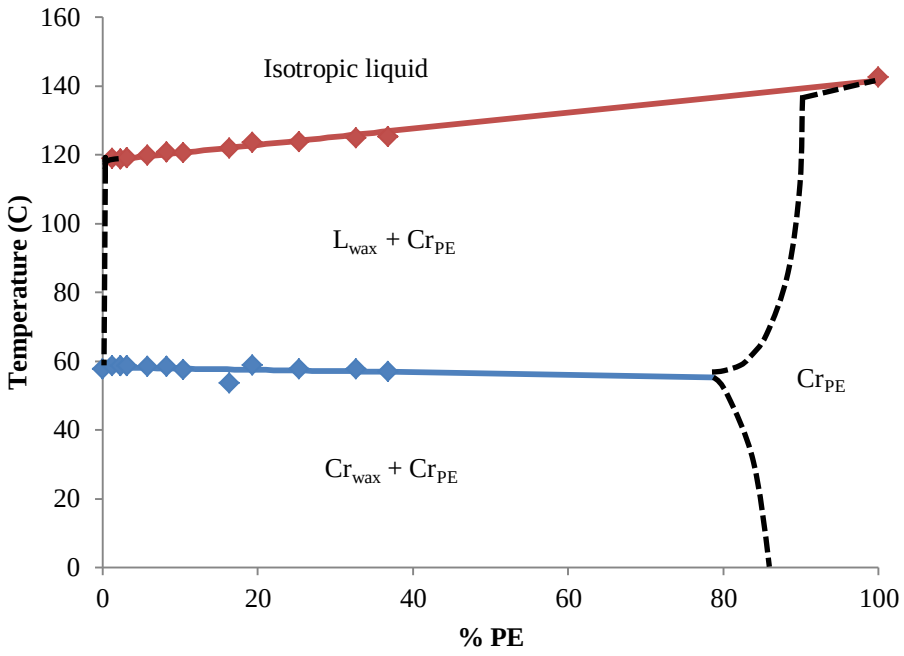

Figure 24: Phase diagram for UHM_wPE and wax

There is a slight observed down-turn of the melting temperature of the PE-rich phase as the concentration approaches 0% PE, hence the down-turn in the best-guess line associated with that region. Additionally, the melting peaks for the wax phase have been determined to have a composition limit, which is the end of the blue linear fit to the wax data (Table 13).

In order to fit the data to the template, the Cr - Cr+Cr and Cr+Cr - Cr lines (see Figure 19) have to be near vertical. In fact, on the side of 0% PE, the anticipated Cr_{wax} section does not appear at all from the thermal data, being either non-existent or existing at concentrations lower than any examined here. This also eliminates the Cr_{wax}+L_{PE} region predicted by the template.

As the composition approaches 100% PE, a thin region of L_{wax}+Cr_{PE} is expected to form. While not observed by DSC, this could be simply due to the proximity of the temperature associated with the Cr_{PE} – L_{wax}+Cr_{PE} transition to that of the melting of the PE-rich phase at those compositions. Such close peaks would not be resolved during the DSC sweeps used here.

3.4. Rheological Behavior

The same blends used during the thermal studies were used for the rheological. Previous rheological testing of blends of this nature (HDPE with wax) all have been limited to dilute or semi-dilute concentrations. In this study, the composition range is expanded to include the *entangled* regime. An additional set of blends of 125K PE with 41K PE was prepared as a control reference.

As a baseline for further rheological testing, the zero shear viscosities of the four pure HDPE's to be used in the blends have been plotted as a function of their molecular weights (Figure 25).

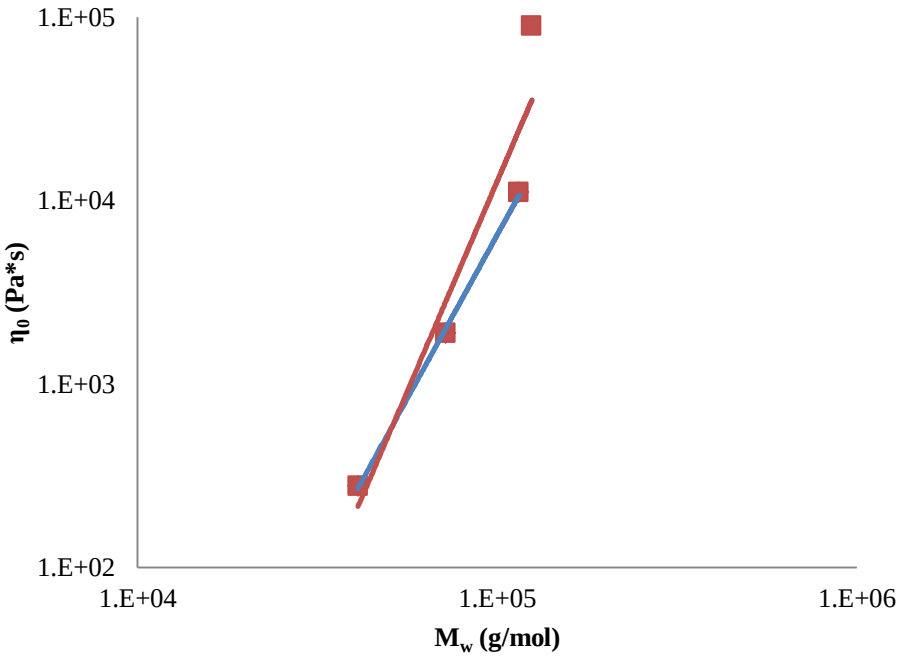

Figure 25: Zero-shear viscosity as a function of molecular weight for the neat HDPE grades used in blending. The red solid line is a power-law fit to all the data. The blue line omits the 125K g/mol PE.

A power-law function applied to these points (Equation 28) gives an equation for zero shear viscosity of $\eta_0 = 1.593 \times 10^{-19} M_w^{4.581}$ with an R^2 value of 0.9067. The exponent generated is well above that predicted for conventional PE (3.4-3.6 range) [85], with a fairly poor fit. However, if the highest value (125K PE) is removed, the low three M_w PEs conform to the expect result for conventional PEs $\eta_0 = 9.602 \times 10^{-15} M_w^{3.566}$. This inconsistency undoubtedly influences the rheological results and must be kept in mind. The paraffin wax (not shown here), has a molecular weight of 405 g/mol and a zero shear viscosity of ~9×10^{-4} Pa*s. The pure UHM$_w$PE viscosity is too high to be measured.

As a control, mixtures of 41K PE and 125K PE were prepared. No DSC or TGA results were generated from blends of these types. With respect to TGA, the

decomposition temperatures proved too similar to resolve any differences. The purpose of the TGA measurements would be to compensate for wax lost due to leakage during the mixing process. No materials leaked in the control samples mixing process. Therefore, the sample composition is the same as that which initially went into the mixer. With respect to DSC, the melting and recrystallization curves for the two grades of PE are too similar to resolve a dependable fit to the associated peak temperatures.

The miscibility of certain grades of HDPE is well established in literature. For a given blend of two linear PEs with different molecular weights, single melting and recrystallization peaks form for all compositions, with the peak temperatures being a function of composition. [48] [70] The exception to this single-peak formation is when one of the PEs has a molecular weight below the critical molecular weight for which two peaks are formed. [47] This phenomenon is manifest for most of the blends used in this research, as already described in *3.3.2. Thermal Results and Phase Behavior*.

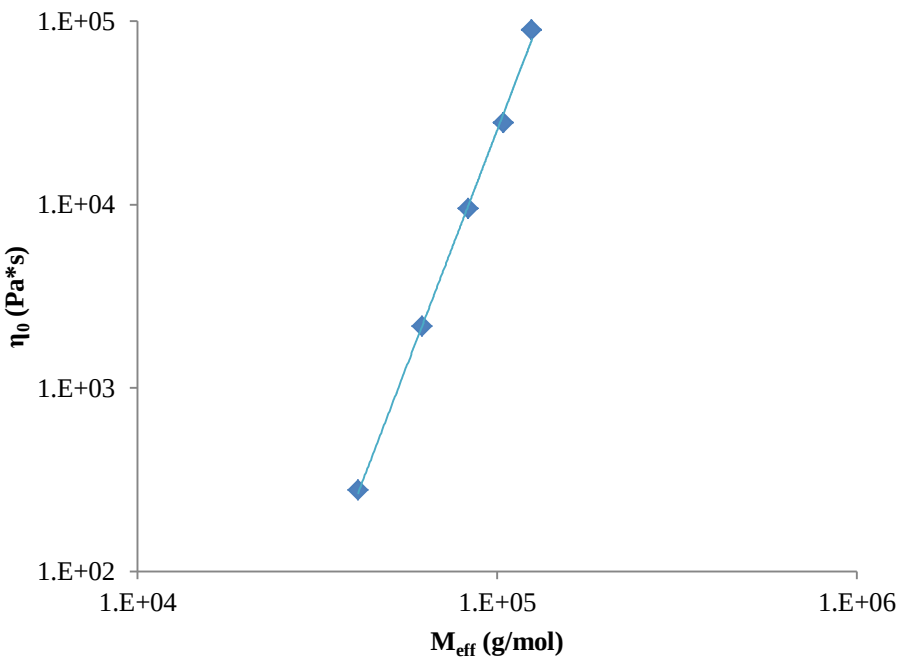

Figure 26: Zero-shear viscosity vs. effective molecular weight (M_{eff}) for blends of 41K PE and 125K PE with a power-law best-fit applied

A power fit is applied to a plot of the log of the zero-shear viscosity against the sample effective molecular weight ($M_{eff} = M_{w,a}\Phi_a + M_{w,b}\Phi_b$) for Figure 26. This gives an equation for viscosity of the blend as $\eta_0 = 6.916\text{x}10^{-22}\ M_w^{5.113}$ with an R^2 value of 0.9986. This strong fit is a good indicator of miscibility. However, the power-law exponent is well above that which is reported in literature for conventional PE-PE blends. Combined with the data in Figure 25, it is concluded that while 41K, 72K, and 115K PE are of the conventional PE structure (linear, with few short chain branches, if any), the 125K PE contains long chain branches.

Long chain branches (LCBs) are defined as a branch which has a length exceeding the critical molecular weight for entanglement for the polymer. [37] LCBs have been found to have a disproportionate effect on rheological properties, even at low

branch-densities. [100] D. Yan et al found that by increasing LCB density from 0.22 to 0.44 branches per 10,000 carbons in PE, the viscosity of the PE increase by six times [15], while the critical molecular weight for entanglement in LCB PEs remains the same as for conventional PEs. [25] In contrast to PEs that possess frequent but short branches, this low density of LCBs does not appear to effect 125K PE's miscibility with 41K PE. Nevertheless, these differences in molecular structure for 125K PE will likely further influence the rheological results in mixing with paraffin wax.

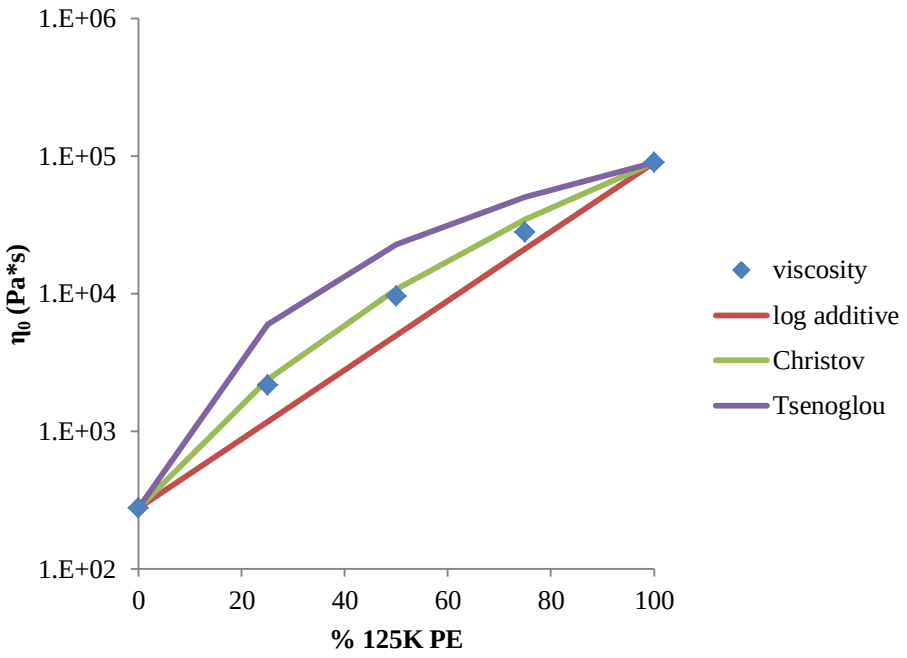

Figure 27: Zero shear viscosity (η_0) vs. composition (% 125K PE) for blends of 41K PE and 125K PE, with the curves predicted for the Christov, Tsenoglou, and log-additive model

A more conventional plot of η_0 as a function of composition for the 41K PE and 125K PE blend is presented in Figure 27. The data are most closely matched by the log-additive and Christov equations; significantly less so by the Tsenoglou equations. The exponent for the Christov equation (5.113) is the same as that which is found in the power-law fit for η_0 vs M_{eff} in, a relation from which the Christov equation is derived. Notably, all the above theoretical fits, the η_0 of the pure components must be previously defined constants. However, those pure values are as likely to contain error in measurement as any other composition. As such, adjustments for best-fit were performed for the log-additive and Christov equations. These adjusted values for the viscosities of pure 41K PE and 125K PE were obtained by a linear fit to a plot of the log-viscosity vs. % composition for the log-additive rule, and by the power law fit in Figure 26. (The Tsenoglou equation was determined to be too far from the measured values to merit adjustment.) These adjustments resulted in greatly improved fits, as seen in Figure 28.

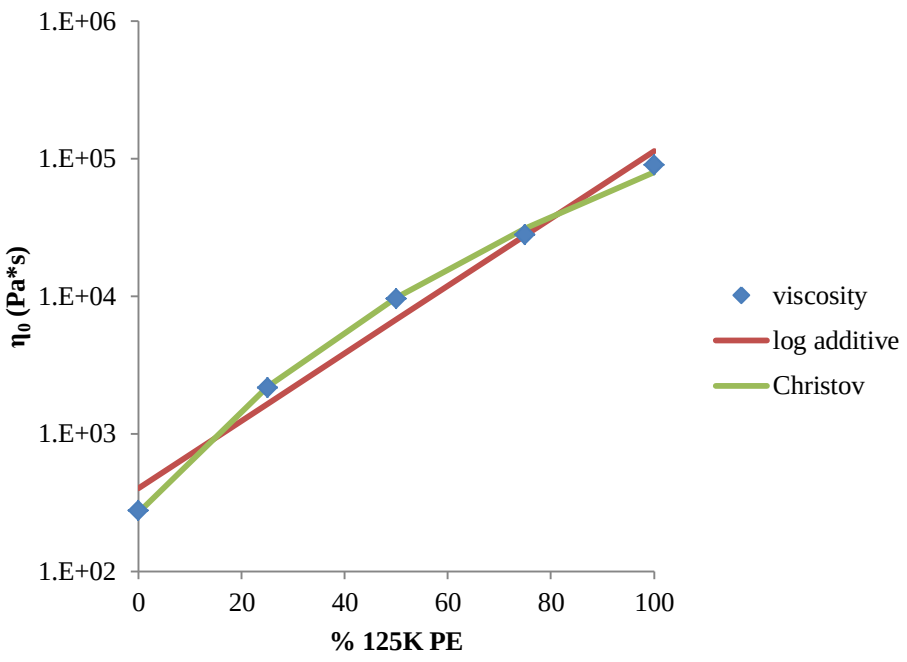

Figure 28: Zero shear viscosity (η_0) vs. composition (% 125K PE) for blends of 125K PE and 41K PE, with the curves predicted for the Christov, Tsenoglou, and log-additive models, following adjustment for best-fit.

In the coming results, it was necessary to fit two separate power-laws to a given data set, dividing data for low concentrations from data for high concentration or data for low effective molecular weights from data for high effective molecular weights. A common means of quickly determining the critical concentration for entanglement Φ^* of a polymer in an athermal solvent is given by $\Phi^*=M_c/M_w$, where M_c is the critical molecular weight in the melt for a polymer type, and M_w is the molecular of the specific polymer. [81] The literature value of the critical molecular weight M_c for polyethylene is 3800 g/mol in the melt and has been demonstrated to be near-constant for all grades of HDPE. [85] Therefore, this M_c was determined to be appropriate for defining the limits of the low and high regions.

This M_c reference point has shown itself to be valid to varying degrees of accuracy for the different blends as will be shown below. Recalling that the critical molecular weight (M_c) for PE is 3800 g/mol, when determining the applicable boundaries for power-law fits (Equation 40 and Equation 41 below) in the viscosity plots, the fit for the lower concentration regimes was applied in mixtures having effective molecular weights (M_{eff}) equaling M_0 (that of wax) to those having M_{eff} just above 3800 g/mol. The fit for the higher concentration regimes was applied in compositions wherein M_{eff} ranges from the molecular weight of the PE, down to just below 3800 g/mol as calculated by:

Equation 39

$$M_{eff} = \phi_{wax} M_{w,wax} + \phi_{PE} M_{w,PE}$$

Although, strictly speaking the above equation is accurate as to the weight average molecular weight of PE in the mixture, it does not accurately convey the dynamics of a given mixture when one component of the combination is below the critical molecular weight.

All plots of η_0 vs. % PE are referenced and compared against three existing theories for predicting the viscosity of miscible polymer melts: Christov (Equation 30), Tsenoglou (Equation 26), and the log-additive rule (Equation 21).

All plots of η_0 vs. M_{eff} are fitted to a modified form of the power law (Equation 28) wherein M_w is replaced by M_{eff}:

Equation 40

$$\eta_0 = K \times M_{eff}^{\alpha}$$

In Equation 40, K is a function of temperature. The exponent α is a function of molecular weight, linearity, branching, and entanglement, all of which are properties of the polymer which remain the same regardless of the temperature. As is also true in the case of conventional melts, this equation is applicable to two separate regimes for most of the data presented; those being regimes defined by M_c as designated above. From the intersection of the two resulting fits of Equation 40, a critical effective molecular weight M_{eff}* may be determined for each grade of PE in paraffin wax.

All plots of η_{sp} vs. Φ_{PE} (similarly, η_0 vs. Φ_{PE}) graphically depict a simplified form of the power law equations for specific viscosity as a function of concentration for the semi-dilute and concentrated regimes as defined in (Table 1). These equations are converted to the following simplified form:

Equation 41

$$\eta_{sp} = Y \times \phi^{z}$$

This equation, like Equation 40, is fitted over two separate regimes for most of the data presented (see Figure 2), using the same compositions for each regime as used for plots of η_0 vs. M_{eff}. From the intersection of the two resulting fits for Equation 41, the critical concentration Φ* for each grade of PE in paraffin wax may be determined. Note however that this critical concentration, unlike the critical molecular weight, is also a

function of temperature, quality of the solvent, and the form of the PE for any given mixture.

Other authors have attempted to predict solution properties as a function of not only their concentrations, but also the polymer's molecular weight. These equations are of the form:

Equation 42

$$\eta = K' M^{\beta} \phi^{\alpha}$$

The value of K' is a function of the temperature and the polymer solvent system being considered. The tube model predicts $\eta \sim \Phi^3 M^3$ for concentrated solutions [101]. However, experimental evidence has shown $\eta \sim \Phi^4 M^{3.5}$, [88] [102] [103] though there is some scatter in this exponent (3.5 +/- 0.2). [104]

Further work on these systems have considered a wider variety of structures of the polymer in solution, and the related spatial dimension *d* and fractal dimension d_f. [105]

Equation 43

$$\eta_0 \sim \left[M^{(d_f+2)/d_f}\right]^{(d+2)/2}$$

For concentrated polymer solutions of long flexible chains, $\eta_0 = K(cM)^{10/3}$ ($d = 3$, $d_f = 2$); for swollen chains with excluded volume, $\eta_0 = Kc^{49/12}M^{11/3}$ ($d = 3$, $d_f = 5/3$); for stiff chain, $\eta_0 \sim M^5$ ($d = 3$, $d_f = 1$). The exponent on the concentration term is additionally reliant on solvent quality, increasing as solvent quality decreases. [105]

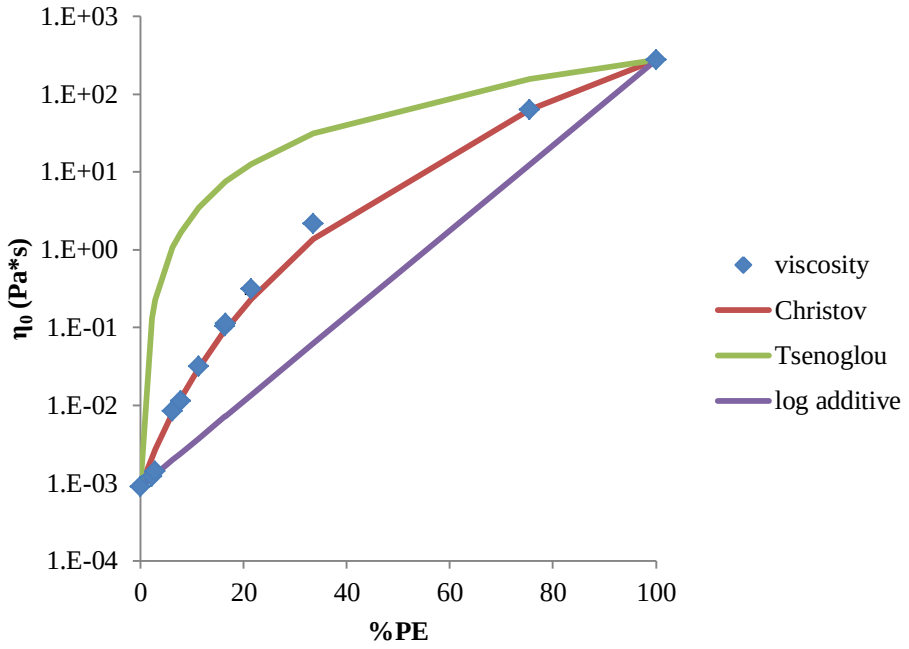

Figure 29: Zero shear viscosity (η_0) vs. composition (% PE) for blends of 41K PE and wax, with the curves predicted for the Christov, Tsenoglou, and log-additive models. An exponent of 6.1 was arbitrarily generated in order to obtain the lowest possible R^2 between the values predicted by the Christov equation and the data collected.

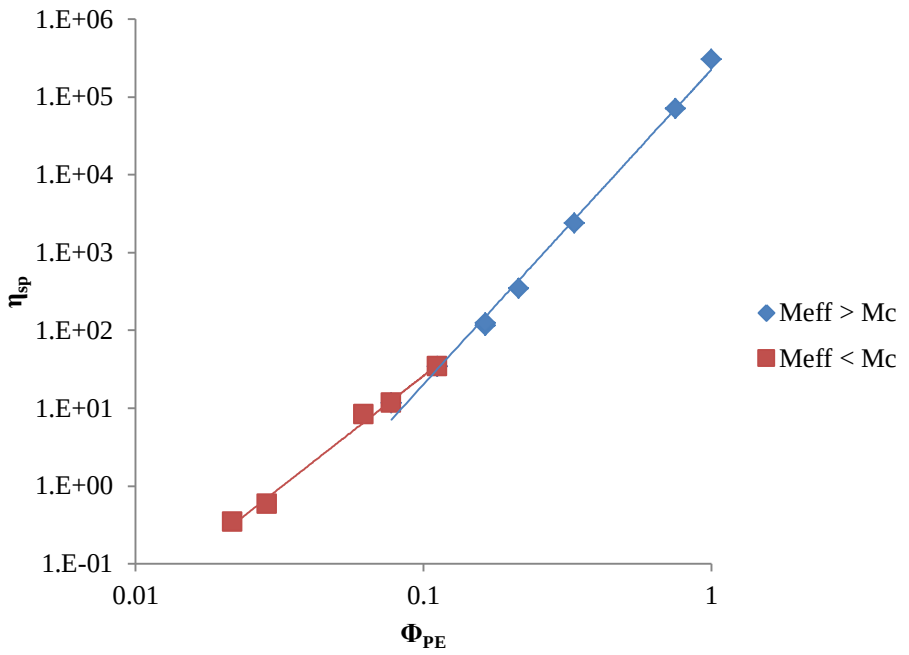

Figure 30: Specific viscosity (η_{sp}) vs. volume fraction of PE (Φ_{PE}) for blends of 41K PE and wax with power law fits

Table 14: Linear and exponential factors of the power law fits of Figure 30

	$M_{eff} > M_c$			$M_{eff} < M_c$			*Intercept,* Φ_e
	Y	z	R^2	Y	z	R^2	
$\eta_{sp} = Y\Phi^z$	2.24×10^5	4.05	0.994	2.04×10^4	2.89	0.993	0.125

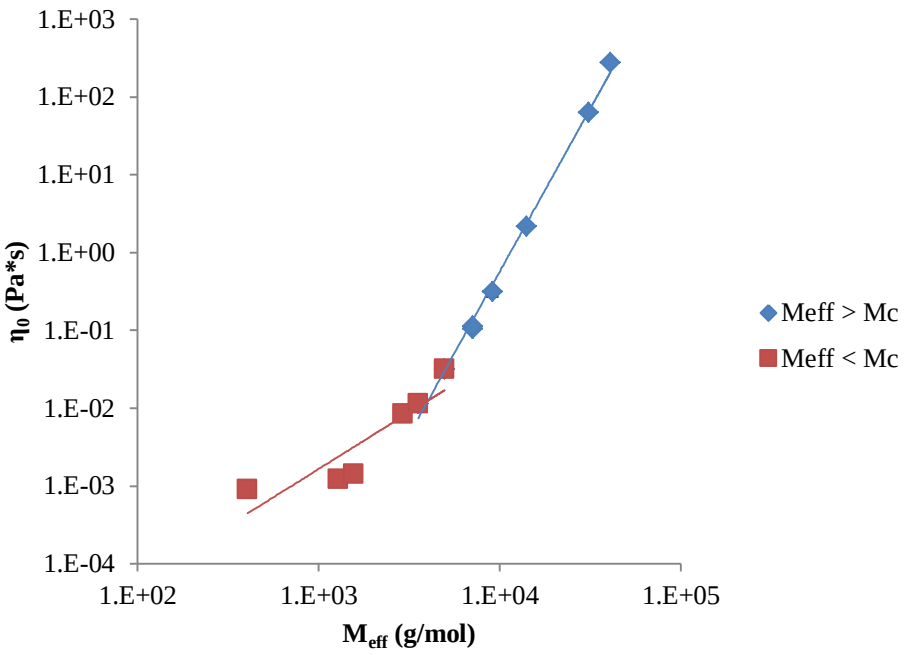

Figure 31: Zero shear viscosity (η_0) vs. effective molecular weight (M_{eff}) for blends of 41K PE and wax with power law fits

Table 15: Linear and exponential factors of the power law fits of Figure 31

	$M_{eff} > M_c$			$M_{eff} < M_c$			*Intercept,* M_{eff}*
	K	α	R^2	K	α	R^2	
$\eta_0 = KM_{eff}^{\alpha}$	9.77×10^{-13}	4.19	0.996	2.09×10^{-11}	1.46	0.8114	4016

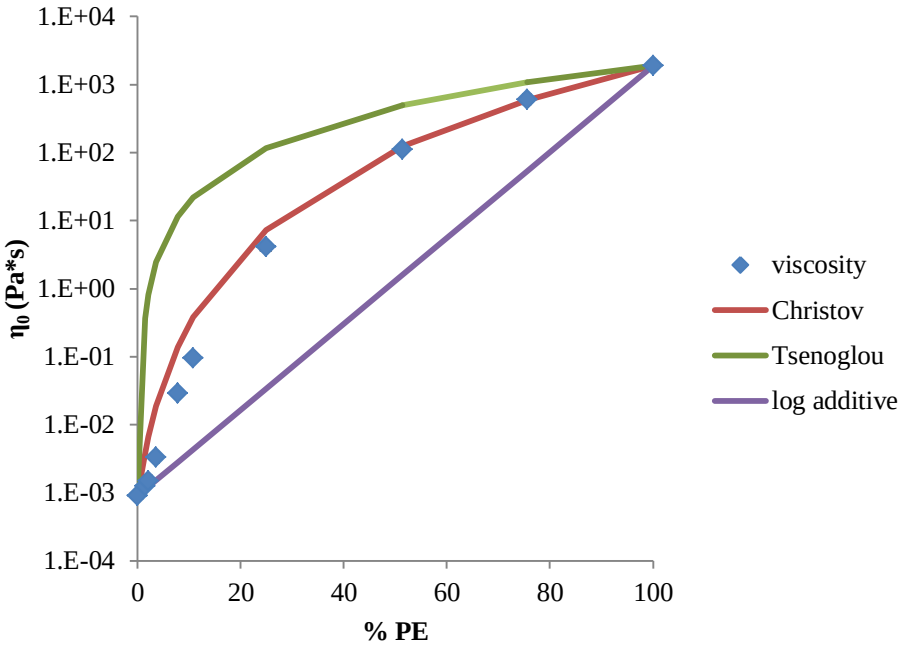

Figure 32: Zero shear viscosity (η_0) vs. composition (% PE) for blends of 72K PE and wax, with the curves predicted for the Christov, Tsenoglou, and log-additive models. An exponent of 4.3 was arbitrarily generated in order to obtain the lowest possible R^2 between the values predicted by the Christov equation and the data collected.

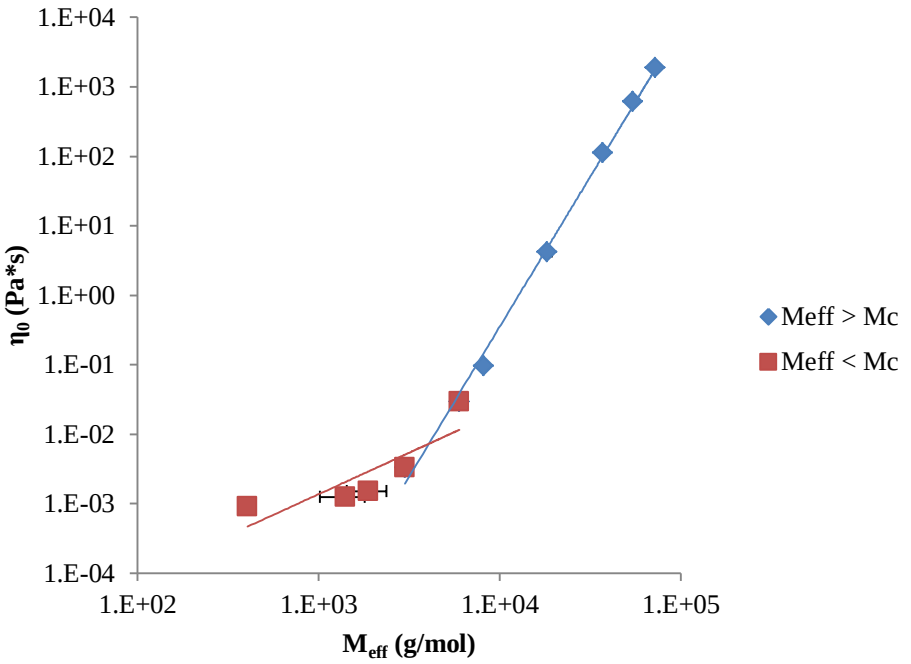

Figure 33: Zero shear viscosity (η_0) vs. effective molecular weight (M_{eff}) for blends of 72K PE and wax with power law fits

Table 16: Linear and exponential factors of the power law fits of Figure 33

	$M_{eff} > M_c$			$M_{eff} < M_c$			*Intercept,* M_{eff}*
	K	α	R^2	K	α	R^2	
$\eta_0 = KM_{eff}^{\alpha}$	1.98×10^{-18}	4.31	0.996	3.64×10^{-7}	1.19	0.727	4074

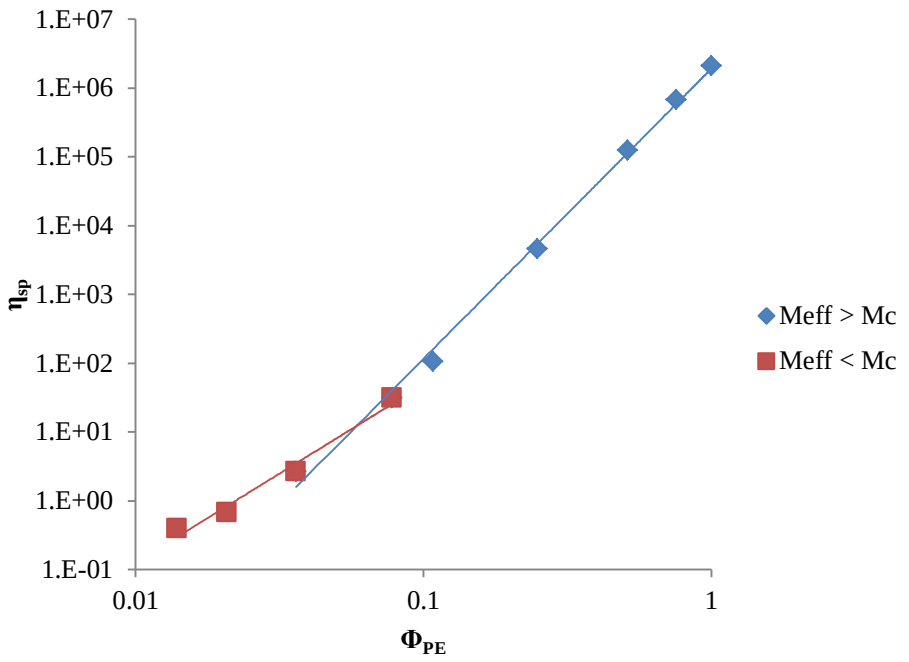

Figure 34: Specific viscosity (η_{sp}) vs. volume fraction of PE (Φ_{PE}) for blends of 72K PE and wax with power law fits

Table 17 Linear and exponential factors of the power law fits of Figure 34

	$M_{eff} > M_c$			$M_{eff} < M_c$			*Intercept,* Φ_e
	Y	z	R^2	Y	z	R^2	
$\eta_{sp} = Y\Phi^z$	1.90×10^6	4.21	0.997	1.88×10^4	2.59	0.979	0.0588

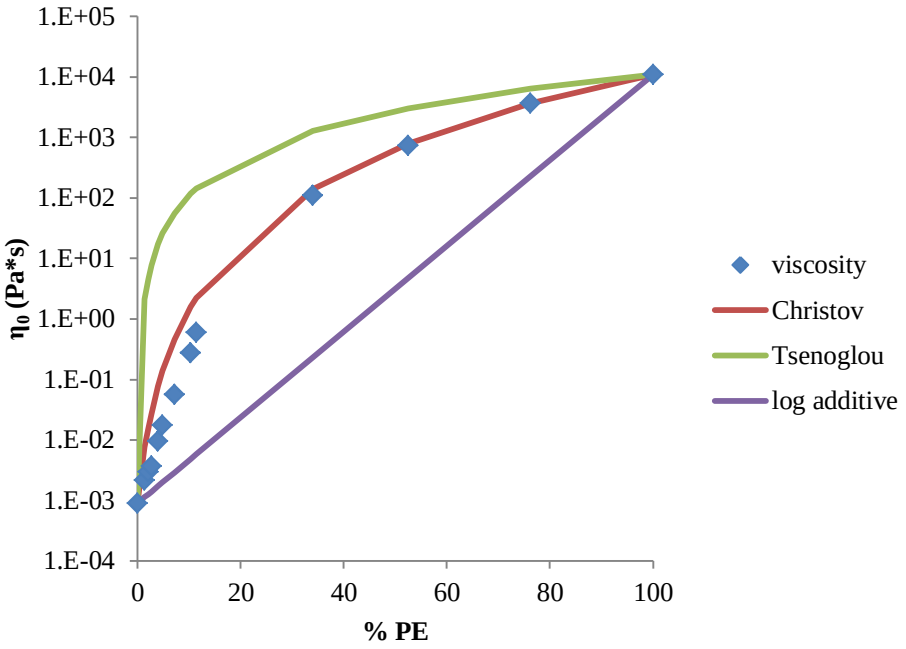

Figure 35: Zero shear viscosity (η_0) vs. composition (% PE) for blends of 115K PE and wax, with the curves predicted for the Christov, Tsenoglou, and log-additive models. An exponent of 4.2 was arbitrarily generated in order to obtain the lowest possible R^2 between the values predicted by the Christov equation and the data collected.

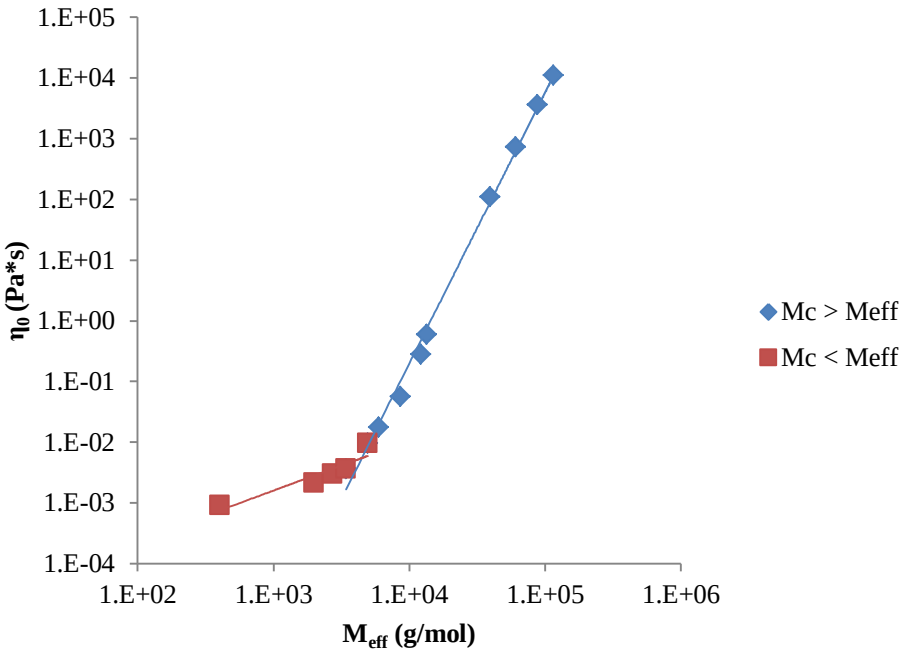

Figure 36: Zero shear viscosity (η_0) vs. effective molecular weight (M_{eff}) for blends of 115K PE and wax with power law fits

Table 18 Linear and exponential factors of the power law fits of Figure 36

	$M_{eff} > M_c$			$M_{eff} < M_c$			*Intercept,* M_{eff}*
	K	α	R^2	K	α	R^2	
$\eta_0 = KM_{eff}^{\alpha}$	2.82×10^{-19}	4.46	0.995	5.40×10^{-6}	0.824	.8611	4473

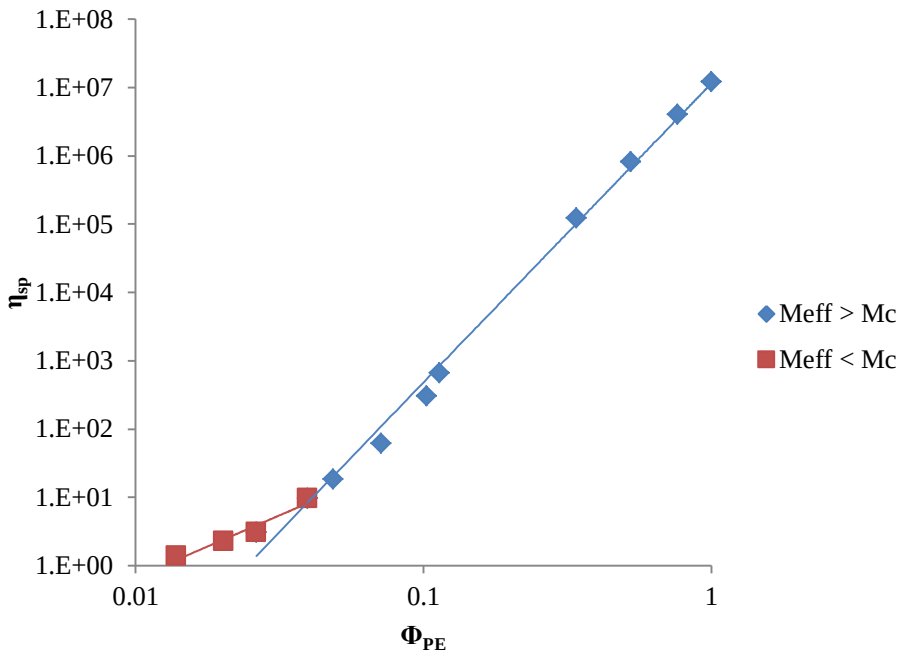

Figure 37: Specific viscosity (η_{sp}) vs. volume fraction of PE (Φ_{PE}) for blends of 115K PE and wax with power law fits

Table 19: Linear and exponential factors of the power law fits of Figure 37

	$M_{eff} > M_c$			$M_{eff} < M_c$			*Intercept,* Φ_e
	Y	z	R^2	Y	z	R^2	
$\eta_{sp} = Y\Phi^z$	1.14×10^7	4.38	0.995	2.92×10^3	1.82	0.949	0.0393

125K PE and Wax blends

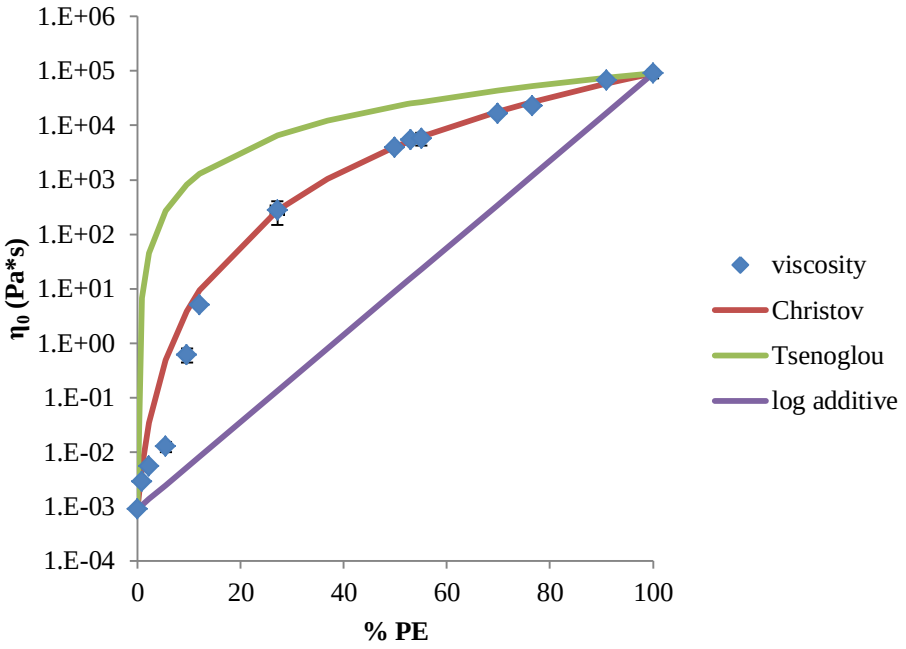

Figure 38: Zero shear viscosity (η_0) vs. composition (% PE) for blends of 125K PE and wax, with the curves predicted for the Christov, Tsenoglou, and log-additive models. An exponent of 4.6 was arbitrarily generated in order to obtain the lowest possible R^2 between the values predicted by the Christov equation and the data collected.

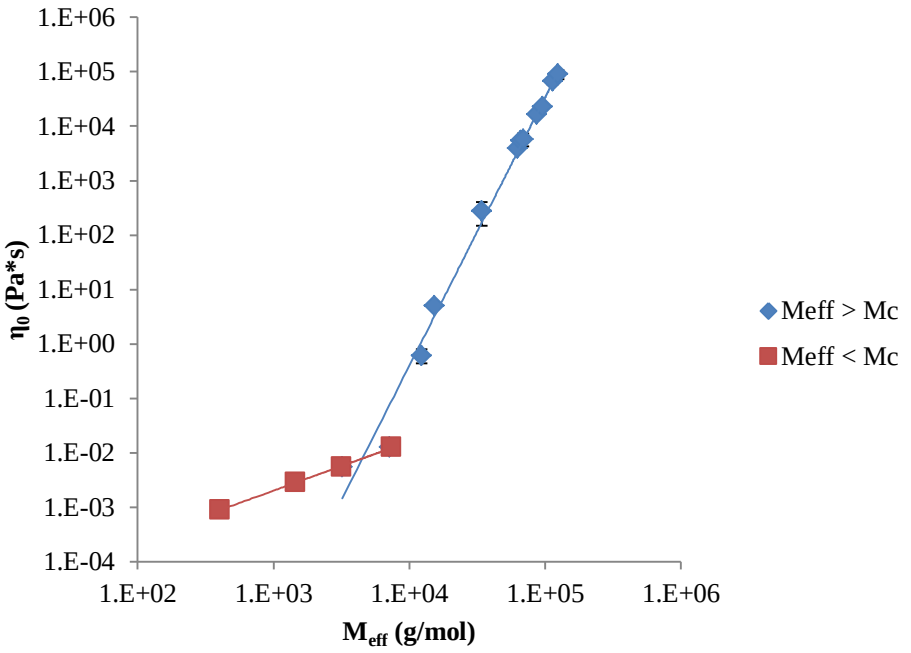

Figure 39: Zero shear viscosity (η_0) vs. effective molecular weight (M_{eff}) for blends of 125K PE and wax with power law fits

Table 20: Linear and exponential factors of the power law fits of Figure 39

	$M_{eff} > M_c$			$M_{eff} < M_c$			*Intercept,* M_{eff}*
	K	α	R^2	K	α	R^2	
$\eta_0 = KM_{eff}^{\alpha}$	7.84×10^{-21}	4.93	0.985	3.98×10^{-6}	0.902	0.999	4514

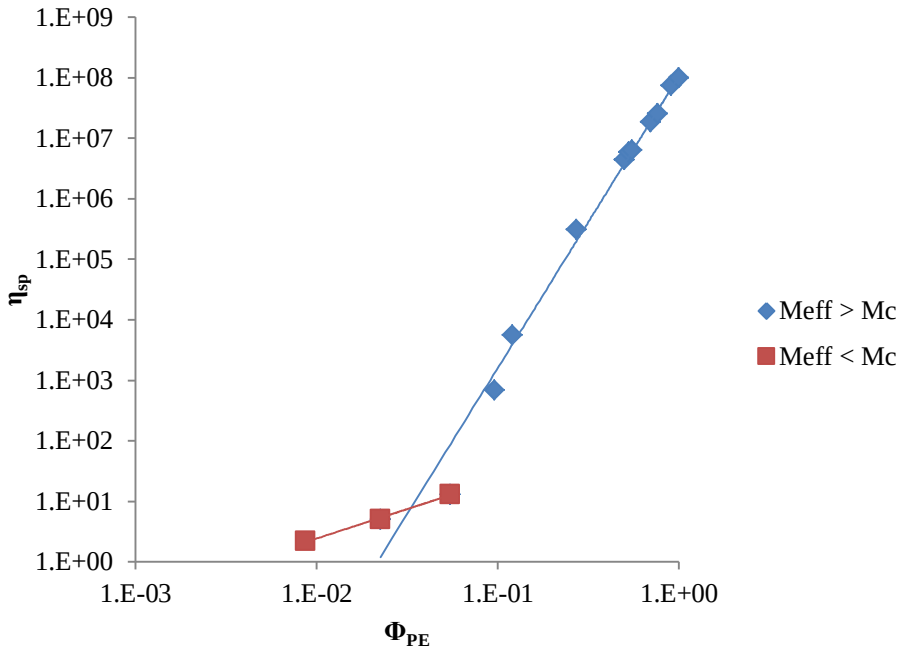

Figure 40: Specific viscosity (η_{sp}) vs. volume fraction of PE (Φ_{PE}) for blends of 125K PE and wax with power law fits

Table 21: Linear and exponential factors of the power law fits of Figure 40

	$M_{eff} > M_c$			$M_{eff} < M_c$			*Intercept,* Φ_e
	Y	z	R^2	Y	z	R^2	
$\eta_{sp} = Y\Phi^z$	1.06×10^8	4.82	0.984	2.14×10^2	0.972	0.997	0.0331

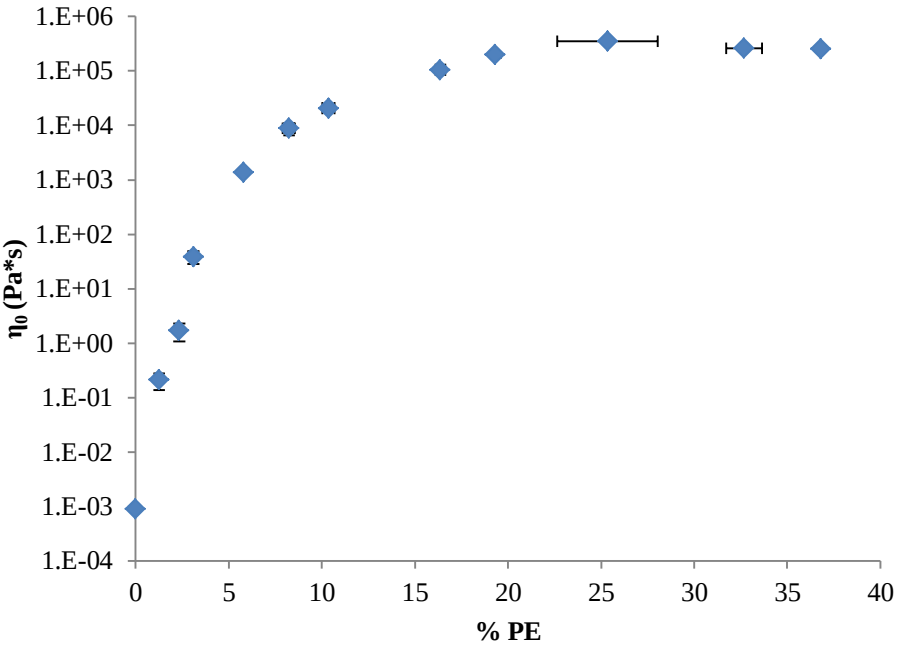

Figure 41: Zero shear viscosity vs. % PE for blends of UHM$_w$PE and wax.

No fits have been attempted to the data in Figure 41 as all the theories here used for determining η_0 as a function of composition require a known of viscosity for the pure components. Measurement of the viscosity of pure UHM$_w$PE is beyond the capacity of the tools available. The manufacturer lists outright the UHM$_w$PE's melt flow index (MFI) as "undefined".[2] In fact, most work concerning UHMwPE blends with other

[2] MFI is a measure of the mass of polymer (in grams) that flows in ten minutes through a capillary of specific length and diameter at specific temperature (above the polymer's T_m) and pressure. This measure approximates viscosity. The method is described in ASTM D1238 and ISO 1133, but was not used in these experiments.

polyethylene, even those using wax, tend to employ another solvent (decaline, xylene, etc.) to form the mixture. This is necessary for forming blends of higher UHMwPE concentration than can be achieve by conventional melt mixing. A point of significance in Figure 41 is the measured decrease in viscosity for concentrations greater than 25% UHM_wPE. This may be a result of the samples slipping between the plates of the rheometer due to their very high viscosities. However, samples of greater than 25% UHM_wPE also exhibited aberrant thermal behaviors in the PE-rich phase's melt and recrystallization enthalpies (noted in *3.3.2. Thermal Results and Phase Behavior*). Therefore, there may be a structural cause for the decreased viscosity, perhaps due to inadequate mixing at such high UHM_wPE content. As such, for rheological considerations, the two highest compositions of UHM_wPE are disregarded.

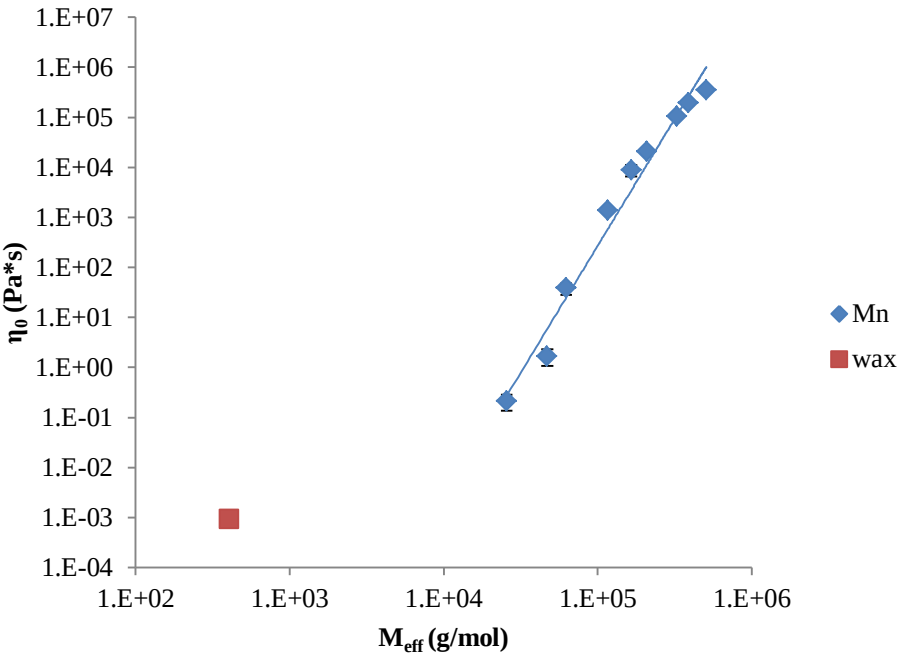

Figure 42: Zero shear viscosity (η_0) vs. effective molecular weight (M_{eff}) for blends of UHM_wPE and wax with power law fit

Table 22: Linear and exponential factors of the power law fit of Figure 42

	$M_{eff} > M_c$		
	K	α	R^2
$\eta_0 = KM_{eff}^{\alpha}$	1.21×10^{-23}	5.07	0.973

In the case of Figure 42, a fit is applied only to the higher values of viscosity, as the M_{eff} never goes below 3800 g/mol in the tested compositions. The only data point below M_c is for pure wax.

Also, note the decreasing slope the curve that begins at the higher M_{eff} values. At compositions higher than these (25% and greater), the measurement of viscosity actually shows a *decrease*. Again, this may be attributed to the beginning of slippage of the

samples between the plates of the rheometer, thus marking an effective limit to the capabilities of the rheometer used. Therefore, the power law exponents may be *greater* than those presented here.

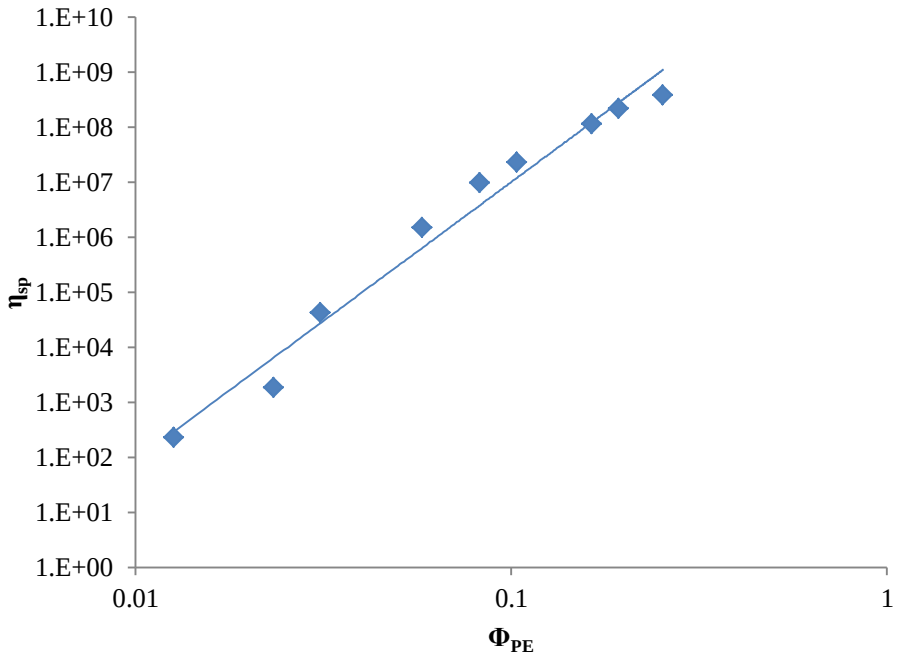

Figure 43: Specific viscosity (η_{sp}) vs. volume fraction of PE (Φ_{PE}) for blends of UHM$_w$PE and wax and power law fit

Table 23: Linear and exponential factors of the power law fit of Figure 43

	$M_{eff} > M_c$		
	Y	z	R^2
$\eta_{sp} = Y\Phi^z$	1.14×10^{12}	5.05	0.977

When the PE/wax systems are considered in terms of conventional melt-blend theories, the best fit to data comes from the Christov equation. However, in order to provide a good fit of the equation to the data, a purely empirical exponent must be applied in the equation. This exponent is determined by generating the smallest R^2 values of the Christov equation to the actual data. Even so, the Christov fit varies substantially from the experimental values at low PE concentration.

As such, these systems should not be considered in terms of any of these theories, which unsurprisingly fail to predict the data for the entire composition range. These types of equations rely on dynamic symmetry in the polymer components; such symmetry does not exist when one component has a molecular weight below that needed for entanglement in the melt (i.e. the paraffin wax) while the other has a molecular weight greater than the critical value (i.e. the HDPE).

The combined plots of specific viscosity as a function of concentration show a shift up and to the left (to higher specific viscosity and lower concentration) with increasing molecular weight of the PE in solution (Figure 44). This is to be expected since higher molecular weights of similar polymer have lower critical concentrations for entanglement. That is, the factor *Y* in Equation 41 is a function of the polymer's molecular weight.

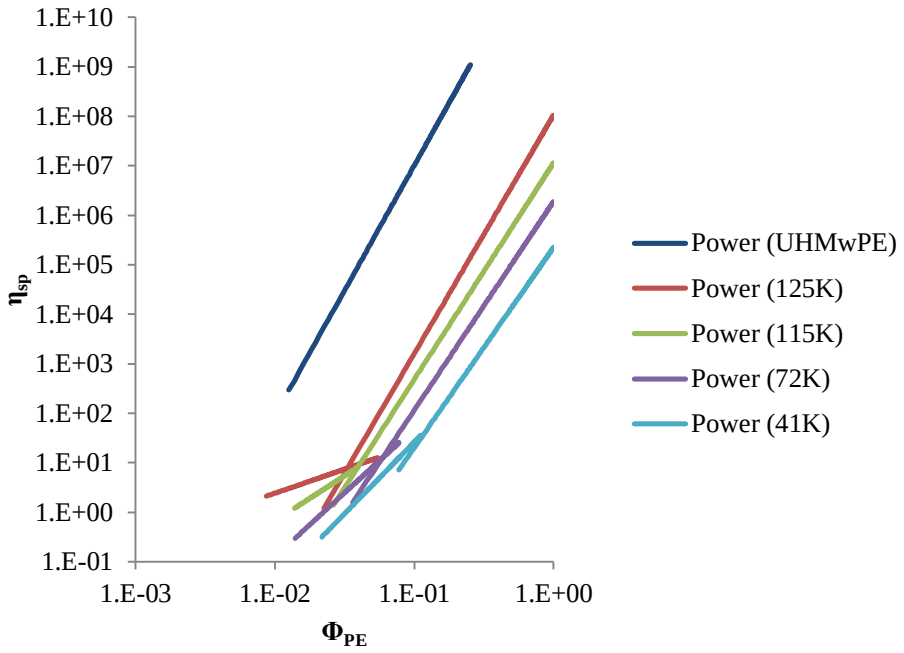

Figure 44: Overlay of the power law fits of specific viscosity (η_{sp}) vs PE concentration (Φ_{pe}) for all the blends of PE and wax

Table 24: Power law fit exponent *z* for the concentrated regime and Φ* critical concentration for the grades of PE

PE M_w (g/mol)	*z exponent for $M_{eff} > M_c$*	*Φ* from intercept*
$41x10^3$	4.05	0.125
$72x10^3$	4.22	0.0588
$115x10^3$	4.38	0.0393
$125x10^3$	4.82	0.0331
$2x10^6$	5.05	

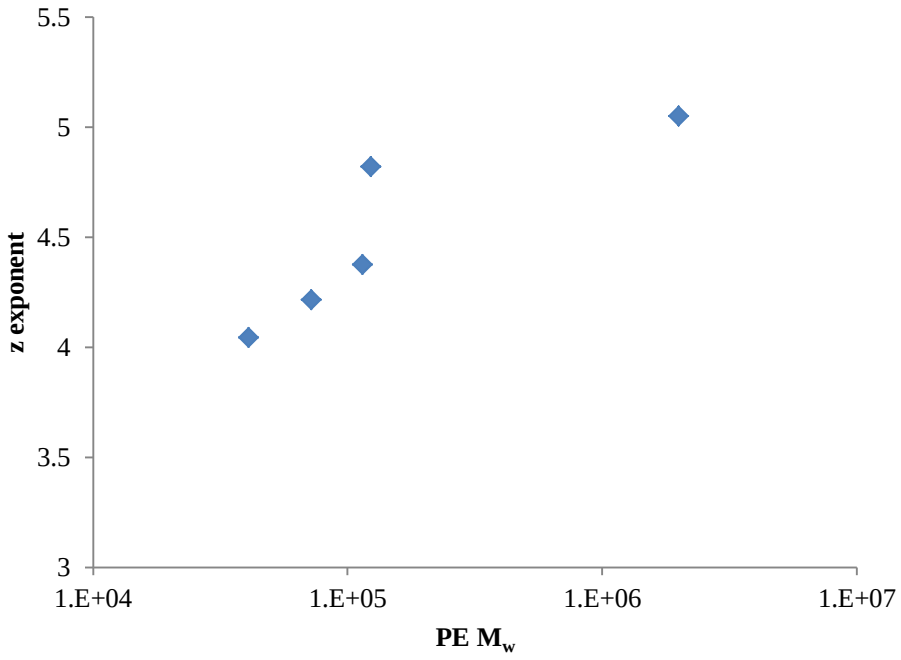

Figure 45: Exponents z from the power law fits of $\eta_{sp} = Y\,\Phi^z$ for the different PE molecular weights

From Figure 45, it is evident that the exponent *z* shows some dependence on molecular weight. Additionally, the exponent for 125K PE lies significantly higher than those of 41K PE, 72K PE, 115K PE, and UHM$_w$PE. This is similar to the behavior of the zero-shear viscosities of the melts in Figure 25, and likely has the same origin, specifically LCBs in 125K PE.

The power law fits for low concentrations tend to be poor matches to the data. The causes of this are threefold. Firstly, the rheometer is less accurate for samples of extremely low viscosity, with noise becoming a major factor in measurements. Secondly, as the concentrations decrease, the degree of mobility available to PE chains increases, both during mixing and during shear in rheometry. While the overall average composition holds valid, the local concentrations have wider variation (especially in

terms of M_{eff} which amplifies volumetric concentration) for low concentration samples than for high concentration. Thirdly, and most significantly, the low concentration region actually covers a range of concentration regimes (dilute, semi-dilute, semi-dilute entangled), each with their own characteristic exponents. Therefore, the power law fit for the low concentrations should only be taken as a means of generating a rough critical value for the start of the concentrated regime, about which there is more concerned here.

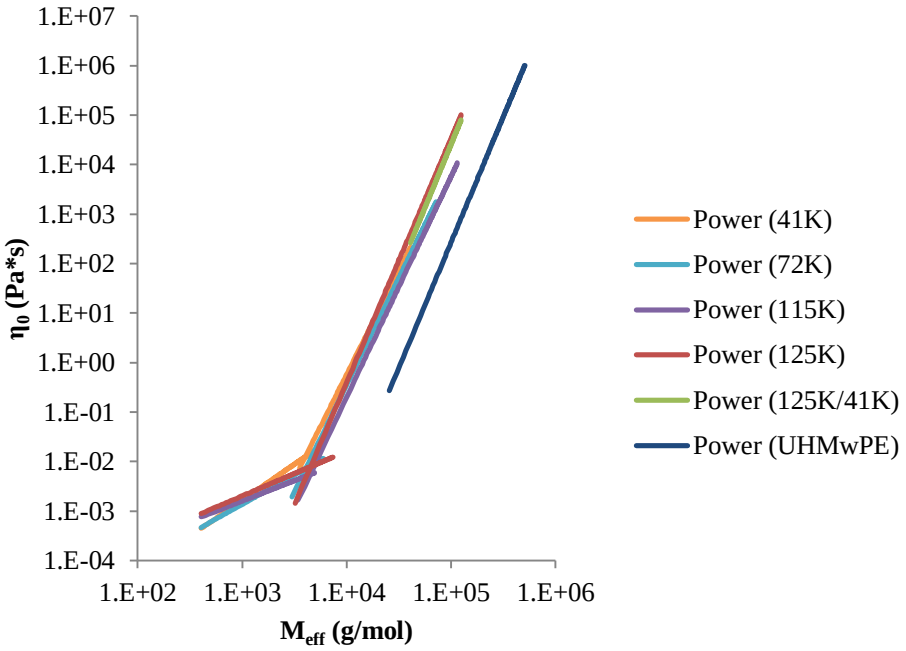

Figure 46: Overlay of the power law fits for zero shear vistcosity (η_0) vs effective molecular weight (M_{eff}) for all the blends

Table 25: Power law fit exponent α for the concentrated regimes and critical effective molecular weights M_{eff}* of the grades of PE

PE M_w (g/mol)	*α exponent for $M_{eff} > M_c$*	*M_{eff}* (g/mol) from intercept*
$41x10^3$	4.19	4016
$72x10^3$	4.31	4074
$115x10^3$	4.46	4473
$125x10^3$	4.93	4514
$2x10^6$	5.05	

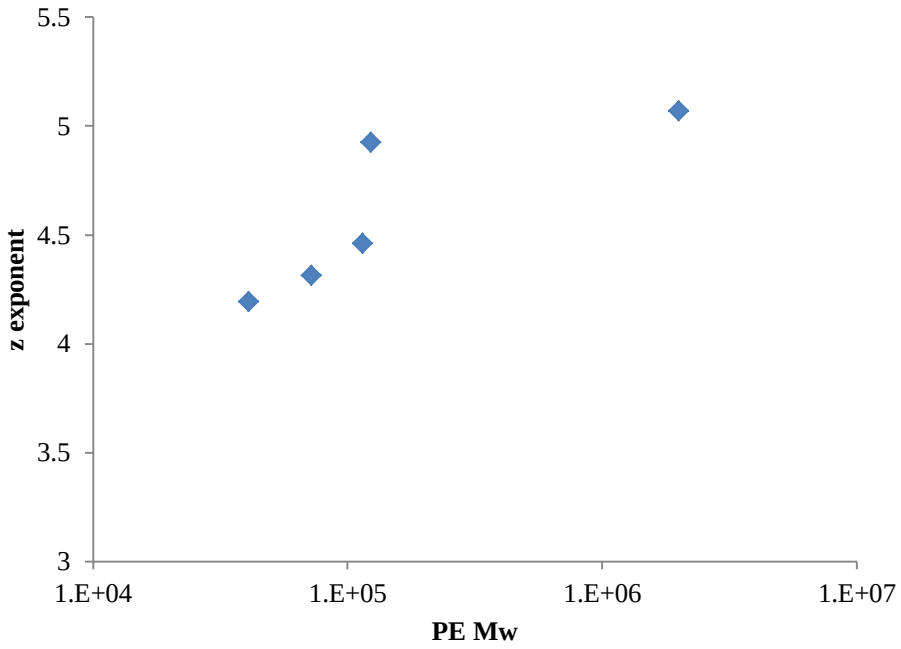

Figure 47: Exponents α from the power law fits of $\eta_0 = K M_{eff}^{\alpha}$ for the different PE molecular weights

The combined plots of zero shear viscosity as a function of molecular weight overlay each other with a fair degree of consistency (Figure 45). This consistency includes the data from the blend of 125K PE and 41K PE (control blend). The only noticeable exception is that of UHMwPE which shifts to a higher value of molecular

weight for a given viscosity. This consistency indicates that M_{eff} (which is itself a function of the polymer's molecular weight and concentration) may be a reliable predictor of blend viscosities for blends of HDPE and wax, even when the wax molecular weight is below the critical molecular weight for entanglement. However, the exponents of the fits to the regions above the critical molecular weight differ sufficiently from those predicted by melt blend theory (which is normally around 3.6 for conventional PEs but can go as high as 4.2 for LCB metallocene PEs) as to render them invalid beyond use in identifying the critical effective molecular weights, being empirical in nature. As with specific viscosity as a function of concentration, the exponent α has some level of dependency on the polymer's molecular weight (Figure 47).

A final approach to analyzing the data comes from Equation 42, where $\eta_0 = K'M_w^{\,b}\Phi^a$. Equations of the form $\eta_0 = K\Phi^a$ can be determined directly from the data. Indeed, the data for η_{sp} as a function of concentration is a direct derivation of η_0 as a function of concentration. Hence, the raw data for both are not presented here.

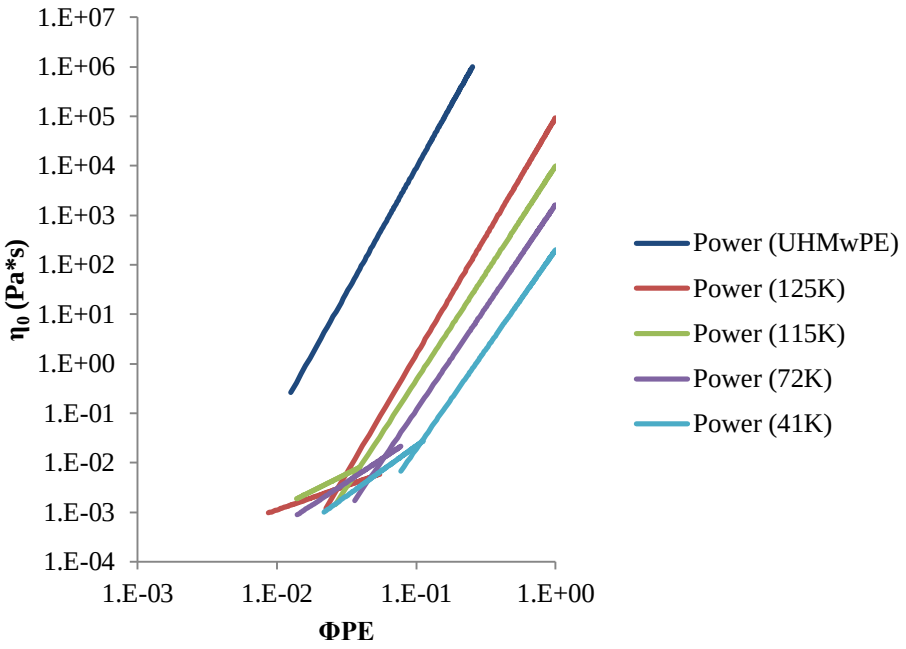

Figure 48: Overlay of the power law fits for zero shear vistcosity (η_0) vs PE concentration (Φ_{pe}) for all the blends

Table 26: Power law fit exponent *a* for the concentrated regime and Φ* critical concentration for the grades of PE

PE M_w (g/mol)	*K factor*	*a exponent for $M_{eff} > M_c$*
$41x10^3$	200	4.02
$72x10^3$	$1.64x10^3$	4.15
$115x10^3$	$9.993x10^3$	4.33
$125x10^3$	$9.37x10^4$	4.79
$2x10^6$	$1.03x10^9$	5.05

A relation between the linear factor in the above power law fit and the molecular weight of the polymer may be defined by

Equation 44

$$\eta_0 = K\phi^a = K' M_w^b \phi^a$$

where it follows that $K = K' M_w^b$. This equation was solved for the 41K, 72K, and 115K mixtures. The PEs in these three types of mixtures are expected to have similar molecular architectures (as determined from their pure melt viscosities in Figure 25). The solution for Equation 44 for these three PE was found to be $\eta_0 = 6.538 \times 10^{-16} M_w^{3.799} \Phi^a$, where a is the exponent determined from the plot of η_0 as a function of concentration for the given PE.

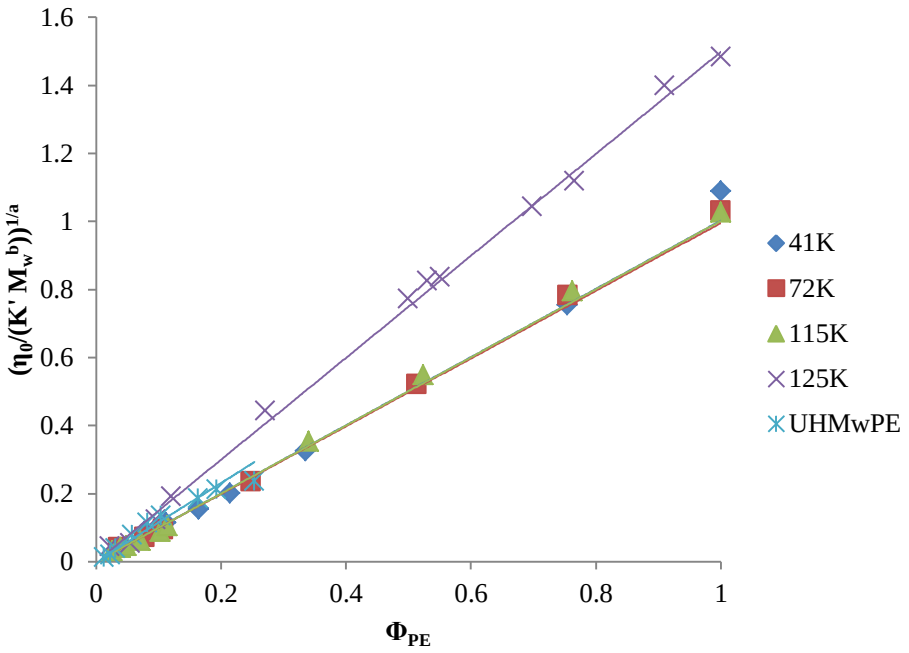

Figure 49: Master curve of the solution $\eta_0 = 6.538\text{x}10^{-16} M_w^{3.799} \Phi^a$ fitted for all PE systems used in this study. The solid lines are linear fits to the data.

From the plot of the viscosity data normalized to this solution, it is shown that a uniform equation for determining the viscosity of concentrated solutions of conventional PEs (41K, 72K and 115K) exists, with near-perfect overlap between the three data sets. Furthermore, regardless of the molecular architecture of the PE, the normalized viscosity approaches zero as concentration approaches zero, as shown for all five grades of PE used in this study. 125K PE and UHMwPE both possess stronger dependencies of normalized viscosities on concentration in concentrated solutions than for 41K, 72K, and 115K, as demonstrated by their higher slopes, which equate to greater values of K' ($4.53\text{x}10^{-13}$ for 125K and $9.86\text{x}10^{-16}$ for UHMwPE).

In terms of Equation 43, $\eta_0 \sim [M^{(df+2)/df}]^{(d+2)/2}$, given that the system has d=3, d_f is determined to be 1.58 for these conventional PE, which is between the fractal dimensions

of a swollen chain with excluded volume ($d_f = 1.67$) and solutions of stiff chains ($d_f = 1$). That is, in terms of structure, $\eta_0 \sim M^{3.8}$ is close to $\eta_0 \sim M^{3.67}$, which is the predicted relationship for swollen chains in solution with excluded volume. [105] Notably, this fractal dimension method does not always hold true, as the exponent has been observed to vary from 3.3 to 3.7 for concentrated solutions of flexible polymers. [88]

For all of these power law fits, a core issue remains, preventing a unified theory. The power law exponent for concentration is a function of the molecular weight. This increase in exponent value for molecular weight in systems of similar polymer/solvent has been observed previously for PEO in water. K.W. Ebagnninin et al reported for concentrated solution of PEO in water (forming a semi-dilute network), exponents of 4.08 for PEO = $4x10^5$ g/mol, 4.41 for PEO = $1x10^6$ g/mol, and 4.89 for PEO = $4x10^6$ g/mol. [106] These exponent values are of a similar scale to those found for the PE/paraffin wax systems.

A particular factor known to increase the exponent for viscosity as a function of composition for concentrated solutions is solvent quality. As solvent quality decreases, the exponent increases from 3.914 for athermal solvents to ~4.5 for good solvents [107] to 4.67 for theta solvents, and higher for poor solvents. This provides a possible explanation for the increase in exponent with molecular weight if the solvent quality of paraffin wax for PE decreases with increasing PE molecular weight. This explanation seems questionable however as no liquid-liquid phase boundaries are observed in the phase diagrams deduced from the thermal data (*3.3.3. Phase Diagrams*). Such boundaries would be expected for polymers in a poor solvent. As such, the cause of the

correlation between increased exponent value and increased polymer molecular weight remains uncertain.

3.5. Conclusions

3.5.1. Thermal Overview

For DSC temperature cycles across all mixtures of PE with wax, the PE-rich phase peak melting and recrystallization temperatures shift as a function of concentration, these temperatures increasing with increasing PE content in a given blend. This indicates a miscibility of wax in PE across all compositions. Contrariwise, the wax peak temperature points are not constant, but vary irregularly, establishing no clear trend with respect to sample composition, and remaining proximal to peak temperatures for pure wax. This has been reported previously for other blends of PE with paraffin wax. This indicates that PE is not forming a single phase system with the wax. Therefore, the system of PE and paraffin wax can be considered to have the characteristics of either a semi-miscible polymer melt or of a polymer solution for which the PE is the solute and the wax is the solvent.

This conclusion is supported by the heat values for the phase transitions in the blends as a function of their compositions. For each of the samples, a linear fit to the recrystallization or melting heat for the wax phase as a function of composition intersects the x-axis before wax content reaches 100%. This indicates that at a certain composition,

all the wax in the sample is absorbed into the PE-rich phase, resulting in a single-phase material. In the reverse, the postulate that PE is *not* absorbed into the wax phase is supported by the intercept at 0 of the heat values for fusion and recrystallization of the PE-rich phase as a function of composition. Again, both of these indicate a semi-miscible polymer melt or a polymer solution for which the PE is the solute and the wax is the solvent.

From the thermal data for phase transition temperatures and phase transition enthalpies, it is determined that PE and wax form a semi-miscible blend for all systems examined. In the solid solution, wax exists as an independent phase until the PE composition reaches a critical value beyond which the wax is completely absorbed into the PE rich phase. In the liquid solution, the PE and wax form a single phase, with no liquid-liquid phase separation. This is consistent with a mixture that exists as an ideal solution in the melt but a non-ideal solution in the solid state. Previous studies on this type of system have shown similar results, but without determining the comprehensive phase diagrams shown herein. This type of phase diagram should exist for any binary mixture of PEs, regardless of molecular structure, as long as one component has a molecular weight below the molecular weight of entanglement in the melt.

Both these data sets (for transition temperatures and transition heats) provide supporting information for the Deformation Induced Phase Segregation process, discussed in the next chapter.

3.5.2. Rheological Overview

Considering the zero-shear viscosity to be a function of the effective molecular weight of the mixture, allows the results for the zero-shear viscosities of the solutions of the different PE in paraffin wax to overlay each other fairly well (with the exception of the UHMwPE), where the traditional plots of specific viscosity or zero shear viscosity as a function of concentration show large quite variation between the different PEs.

By solving the relation $\eta_0 = K\Phi^a = K'M_w^b\Phi^a$, the three conventional polyethylenes formed a unified curved for the normalized viscosities. All five PE showed a molecular weight dependence of viscosity $\eta \sim M^{3.8}$. This is indicative of a concentrated solution of either long flexible chains, or - more closely - swollen chains with excluded volume. However, in the normalized plot, only the conventional PE lie on the defined curve; the 125K (in which LCB is deduced) and UHMwPE lie above the curve. However, all five data sets intercept the origin at 0% PE.

An additional issue in generating a general theory for the rheology of PE/wax systems is the dependence of the exponent of the concentration on the PE's molecular weight. As the molecular weight of the PE increases, so does the exponent. Increasing value in the exponent is normally indicative of decreasing solvent quality for the polymer. However, for the values of exponents found herein, liquid – liquid phase separation would be expected in the phase diagram. No such separation was observed during the DSC sweeps, supporting the postulate that the mixture remains homogenous in the melt for all PE molecular weights.

CHAPTER 4: DEFORMATION INDUCED PHASE SEGREGATION

4.1. DIPS: Introduction

Currently, conventional separation of wax from a blend with PE is accomplished primarily by Thermally Induced Phase Separation, or TIPS. Previous work has used TIPS for creating micro-porous structures within HDPE [43] [60] [63]and UHM_wPE [59] [61]. TIPS has also been exploited for using a gel of UHM_wPE in paraffin as an energy storage media [62] [63]. However, the TIPS process is rather slow, and does not result in full segregation, just local separation. Other methods demonstrated include shear induced phase separation near the critical melting temperature of the blend or cloud temperature of the solution [40] and capillary extrusion though the latter method is applicable only to immiscible PE/PE blends [24].

Early in this thesis work, blends of 70% PP 350 and 30% C105 PE wax were produced and extruded through a capillary, collecting the fiber on a winder. During one of the production sessions, with the extruder's ram stopped, collection of the fibers on the winder was able to continue, drawing them directly from the melt through the capillary. The resultant fibers were exceedingly thin and produced at a remarkably high draw ratio. In the pursuant investigation of this phenomenon, drawing more of these thin fibers by hand, it was noted that the surface appeared to deform in an unexpected manner. For closer examination, the neat-drawn fibers were sectioned and imaged in SEM. Under this magnification, they displayed a distinct shell or coating that was not present in the undrawn ram-extruded fibers (Figure 50).

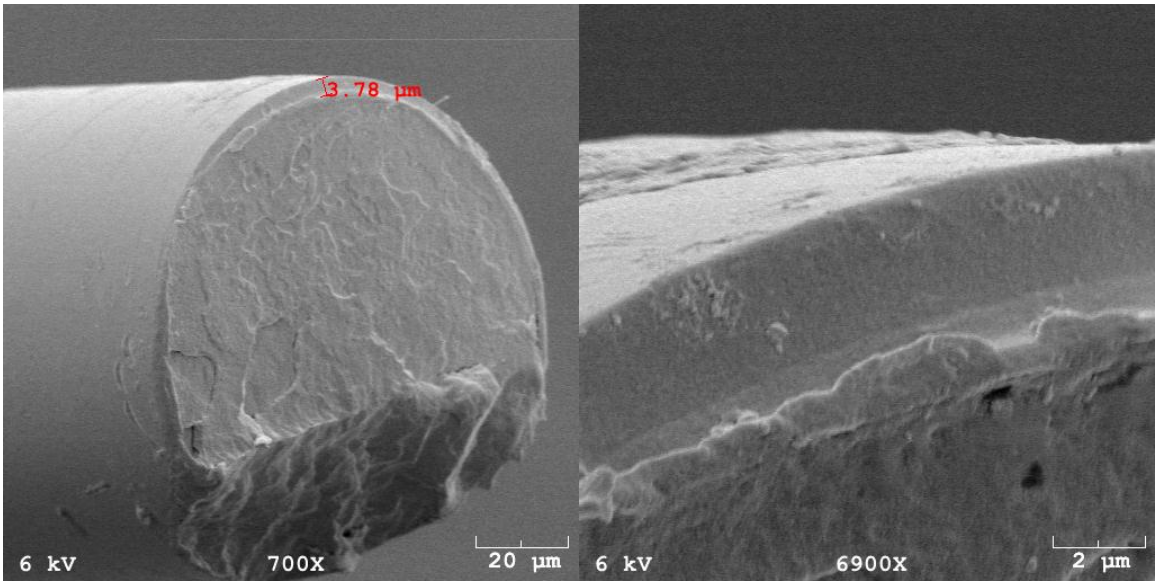

Figure 50: Cross-section of jet drawn fiber produced from a blend of 70% PP 350 / 30% C105 PE wax

From these observations, it was theorized that the tensile stress exerted during the jet-drawing from the melt squeezed the matrix of polymer blend, causing the lower viscosity material to migrate to the outer surface. This appeared similar to the manner in which a sponge filled with water behaves when it is stretched or compressed. This phenomenon was referred to as Deformation Induced Strain Segregation, or DIPS. If this effect were validated and if exploitation of this effect proved feasible, it would potentially offer a completely new method of inducing segregation in polymer blends.

Early on, it was surmised that to execute this technique successfully, the initial blend must be co-continuous. If the blend were not co-continuous, there would be no pathway for the lower viscosity material to flow out of the matrix.

Drawing of fibers may prove a viable method of producing this type of phase segregation. However, noting that compression caused by tensile stress appeared to be the immediately final or proximal cause of segregation, segregation via compression was chosen as the more practically applicable and industrially promising subject for research.

In the segregation process adopted, a sample is placed under compression. One surface of the sample, a surface perpendicular to the applied compressive force, is carefully kept unobstructed. This is dissimilar to the compressive force normally undergone during industrial molding. If an isotropic pressure were applied, as would routinely occur during compression molding in a standard mold, there would be no driving force vector to cause the wax to flow perpendicularly to the applied force. (The vector sums would equal zero.). Additionally, there would be no place for the wax to go. In contrast, the process adopted specifically provides an escape route for wax squeeze out.

It was observed that during the drawing of a fiber, the matrix contracted perpendicularly to the axis along which the drawing force was applied. This was a byproduct of the matrix elongation along that axis as it is drawn. Noting that during the compression of a film or slab, the matrix elongates perpendicularly to and contracts parallel to the axis along which the compressive force is applied. It was theorized that the same physics that caused the wax to coat the fiber during draw should cause wax to surround the outside of a slab of similar material during compression, always being driven in a direction that is perpendicular to the axis of applied force.

The loss of wax during various stages of processing (mixing, compression, drawing, etc.) is a known phenomenon. Processing systems are normally configured in

such a way as to minimize this "leakage." However, the devices were specifically configured to encourage this effect in the compression procedure. Significantly, the purpose was not to drive the wax out of the PE crystallites, but rather to drive out only the wax that existed as an independent phase.

In order to accomplish this, discs 10 mm in diameter and 1.5 mm thick were prepared from a blend of 25% UHM_wPE / 75% wax. These discs were then compressed to a thickness of 0.25 mm employing a range of temperatures under the procedure described in *3.2.4. Compression Molding*. These temperatures represented different regions of thermal behavior for the blend as determined by DSC, depicted in Table 27.

Following this compression samples were taken from the resulting film and analyzed for composition by TGA. It was found that for temperatures above the wax melting temperature, but below the melting point of the PE-rich phase, severe segregation could be induced wherein the material furthest away from the center of the sample constituted almost nothing but wax. Further, there was exhibited a clear transition from PE-rich material to wax-dominated material as a function of radial distance. This segregation decreased with increasing temperature, and essentially disappeared upon reaching temperatures at or above the melting temperature of pure PE at which point the phase structure became essentially uniform across the sample (Figure 51). Thus, the temperature for which this process is most efficient proved to be above the melting temperature of the wax, but below that of the PE matrix.

Table 27: Temperatures for compression and region of thermal behavior. T_m(PE rich) is the melting temperature of the PE rich phase while T_m(PE) is the melting temperature of the pure PE.

Compression Temperature, T (°C)	*Region targeted*
90	T_m(wax) < T < T_m(PE rich)
120	$T \approx T_m$(PE rich)
130	T_m(PE rich) < T < T_m(PE)
140	$T_m \approx T_m$(PE)
180	$T > T_m$(PE)

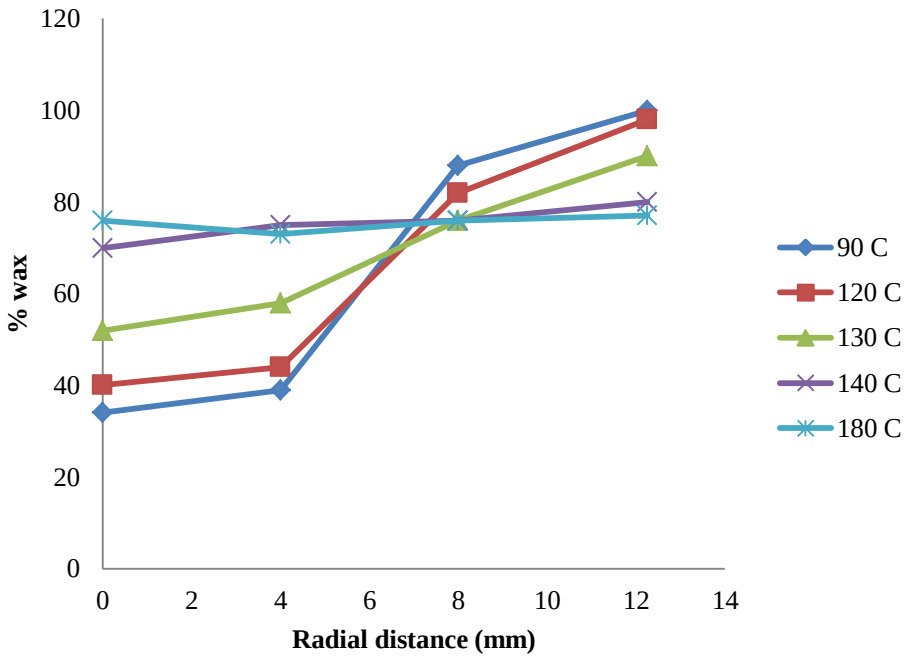

Figure 51: Wax content of compressed discs of a 30% UHM_wPE / 70% wax blend as a function of radial distance

DSC thermal sweeps were performed on a number of the samples. Dual melting peaks for the PE rich region were resolved for materials compressed near or above T_m(PE rich) but below T_m(PE). This implies that two crystal types were formed correlating well

with results obtained from ultra-drawing of LM_wPE/UHM_wPE films, in which the drawn films displayed two high-temperature melting peaks rather than the single peak exhibited by the neat film. [51] [52] This supports the postulate that compression and drawing result in similar crystalline deformations.

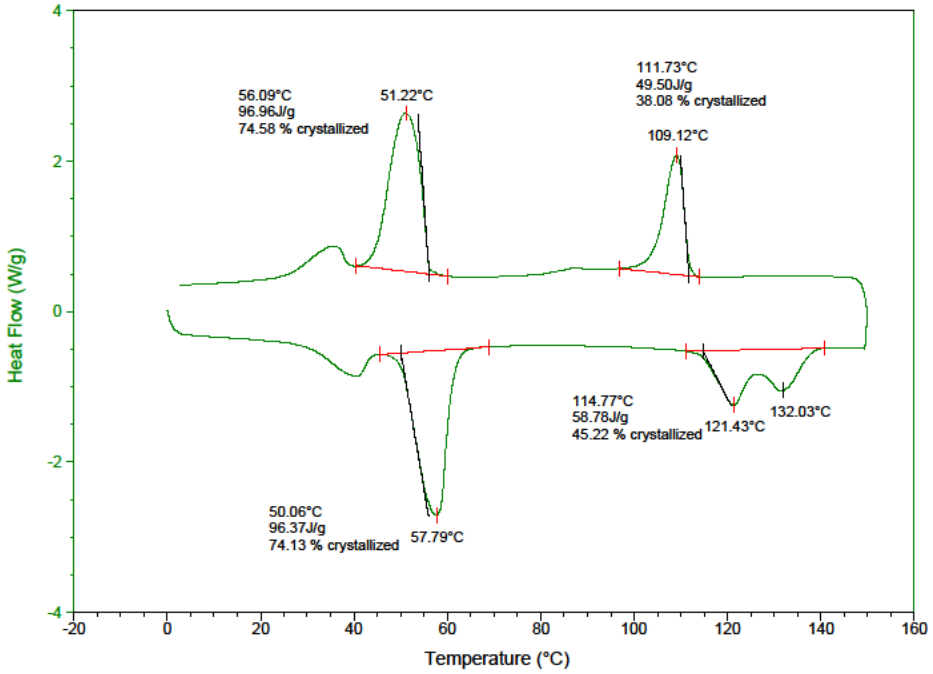

Figure 52: DSC sweep of a film of 25% UHM_wPE / 75% wax compressed at 130 °C. The sample is taken from a half-radius distance.

Attempts have been made to induce this type of phase separation by hot-drawing extruded fibers employing an Instron® production and testing device. However, characterization of such fibers produced proved difficult. The only functional means of identifying phase segregation in such fibers is by microscopy, but to do this the fibers must be sectioned, and sectioning such samples has proven problematic. This sectioning

difficulty applies also to fibers jet drawn directly from the melt. Nevertheless, combination of the two drawing techniques enables a range of drawing ratios and rates to be applied to the fiber, though only the Instron gives temperature control along the entire length of the fiber during drawing. However, the contemporary Instron's drawing rate is limited to only 5 cm/sec versus that of jet drawing, which can go as high as several meters per second, being limited only by the draw rate the melt can sustain without rupturing. Nevertheless, both processes remain valuable as they provide a means of processing and gauging the basic mechanical properties of ultra-drawn UHM_wPE/wax fibers. [53] Furthermore, being able to reliably reproduce DIPS by drawing an extruded fiber has a large number of possible industrial applications.

Ultimately, it was determined that the most effective means of depicting the dynamics of DIPS was by measuring by TGA the overall composition changed across the PE-rich region of a sample, as produced and characterized in the compression procedure described in *4.2.3. Compression Molding*.

4.2. Material Preparation and Characterization

4.2.1. Melt Mixing

In order to make the blends that would later be used in the DIPS study, the same techniques were used as described in *3.2.1. Melt Mixing*. In fact, all of the blends used in this part of the study were also used in the thermal and rheological studies. The

compositions selected for use in the DIPS study included blends of 75%, 50%, and 25% 125K PE (designated as P75, P50, and P25 respectively); and blends of 35%, 25%, and 10% UHM_wPE (designated as X35, X25, and X10 respectively). These samples were then compressed to individually to specific temperatures and ratios as documented on Table 29. The temperatures corresponding to T_m as determined by DSC and the initial compositions as measured by TGA for each of the blends are given on Table 28.

Table 28: Blend compositions and melting temperatures for compression molding

Blend	*Neat Composition from TGA (% PE)*	*T_m of PE-rich phase from DSC (°C)*
P75	75.91	126.5
P50	49.91	121.6
P25	27.12	119.1
X35	36.80	125.3
X25	25.34	123.7
X10	10.36	120.7

4.2.2. Thermogravimetric Analysis

TGA was performed using a both a Thermal Analytics Q5000 TGA and a Thermal Analytics Q500 TGA. This analysis was done to determine the composition of samples following compression in the study of DIPS, utilizing the same technique as that used to verify sample compositions as in *3.2.2. Thermogravimetric Analysis*. The TGA measurements were performed on the PE-rich disc resulting from compression as described in *4.2.3. Compression Molding*.

4.2.3. Compression Molding

The press used to create samples is the same as in *3.2.4. Compression Molding*. To create discs for compression in examining the Deformation Induced Phase Segregation (DIPS), a Teflon sheet was situated upon a large steel plate. Upon the surface of the Teflon sheet were positioned stainless steel washers (inside diameter = 13.5 mm, height = 2 mm), thereby forming an array of miniature molds. Small chunks (~0.3 g) of the sample material were placed inside each washer. A second Teflon sheet was then positioned on top of the samples.

Then the entire system was hoisted onto the bottom plate of the (preheated) hot press and the bottom press plate was elevated until the top plate of the press made only slight contact with the top Teflon sheet, this contact just sufficient to permit heat transfer. From that point forward, the procedure is the same as for preparing samples for parallel plate rheometry as described above.

The hot press was also used to drive the previously postulated deformation-induced phase segregation, referred to herein as DIPS. (This phenomenon shall be later discussed in further detail.)

The methodology to demonstrate and measure this phenomenon comprises a series of different tests using the previously prepared sample discs. Table 29 details conditions used in compressing the samples.

Table 29: Compression ratios and temperatures used for examination of DIPS

Compression temperature	*Compression ratio*		
	2x	*4x*	*20x*
100 °C	A1	B1	C1
T_m	A2	B2	C2
180 °C	A3	B3	C3

The first step of the procedure is to prepare a clean, polished aluminum sheet. Upon this sheet is rested a plate of tough, flat, incompressible material having an orifice in its center such that the aluminum plate forms the bottom surface of a small testing chamber and the orifice walls form the side walls of the chamber. In the center of this orifice is placed the previously prepared disc-shaped sample to be processed and examined. Over the top of the plate containing the sample rests a Teflon sheet thereby forming the top surface of the small chamber.

The plate orifice must be sufficiently large to permit a small amount of wax to be pressed out of the sample laterally in all directions without contacting the walls of the orifice. The thickness of the incompressible plate determines the compression ratio that will be exerted upon the sample. In these tests, plates of 1 mm, 0.5 mm and 0.1 mm were employed generating compression ratios of 2, 4, and 20, respectively.

The press is then preheated to one of three specific temperatures depending upon which test series is to be executed, as shown in Table 29. For the first test series, the press is preheated to 100 °C. For the second series, the press is preheated to the melting temperature of the blend to be compressed (This would be in the 120 to 125 °C range for the blends used). For the third test series, the press is preheated to 180°C.

Once the press is pre-heated, the entire assembly (aluminum sheet, sample, incompressible plate, and Teflon sheet) is placed upon the lower platen of the hot press.

The lower platen is then elevated until the top platen only slightly contacts the Teflon sheet, this contact just sufficient to permit heat transfer. The system is held in this configuration for five minutes to allow the sample to equilibrate. Then the plates are rapidly compressed together until they achieve two metric tons of pressure as measured by an installed analog pressure gauge. After one minute in that state, the assembly and sample are removed from the press and quenched in ice water.

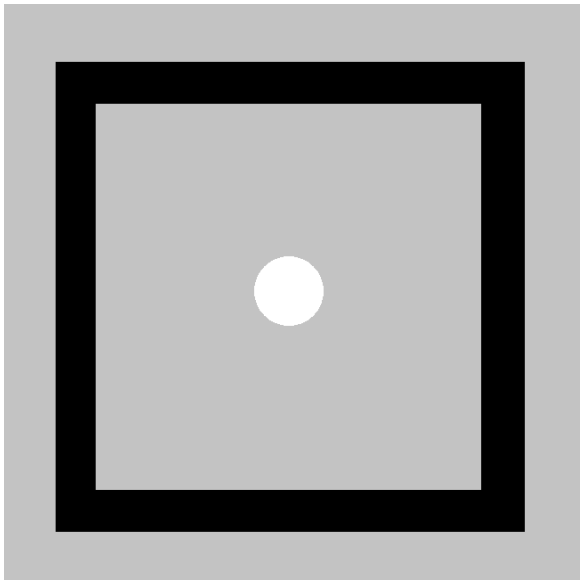

Figure 53: Simple schematic of the set-up used for testing DIPS samples. Grey is the underlying aluminum sheet. Black is the mold that determines the compression ratio, and white is the sample to be compressed.

The goal of the process is to exactingly compress the sample, and precisely determine the amount of wax remaining in the sample after the procedure. Most of the

ejected wax is extruded onto the floor of the chamber. However, in recovering samples after compression, wax material was sometimes found clinging to the top and/or bottom surfaces of the sample. . To precisely remove the entirety of the wax from the exterior of sample, the main disc was pealed from the aluminum sheet, using a razor blade to tease the material from the metal surface. A light abrasion was then applied by hand for 30 seconds to the top and bottom surfaces of the samples to remove residual wax. Tissue paper is used as the abrasive as it will easily remove wax from the surface, but has little effect on the underlying PE-rich material. A quick rinse in water and acetone removes any residual paper material that may have adhered to the sample surfaces. (Neither of these solvents interacts with polyethylene.)

An example of a typical sample resulting from a compression procedure may be found in Figure 54. On the left, the PE-rich portion of the sample remains adhered to the aluminum sheet, with a clearly defined region of squeezed-out wax surrounding it. Notice also the thin, clear region between the wax-residue and the PE-rich sample. Upon quenching, the sample undergoes a degree of strain relaxation, rapidly snapping back and separating from the more brittle surrounding wax. On the right, some material remains adhered to the Teflon top sheet. This material is purely wax. Note the lateral striations in the waxy material evident on the Teflon sheet. This indicates that some segregated wax remains on the top and bottom surfaces of the main sample disc, but irregularly so. This wax deposit is removed by the abrasion procedure described above.

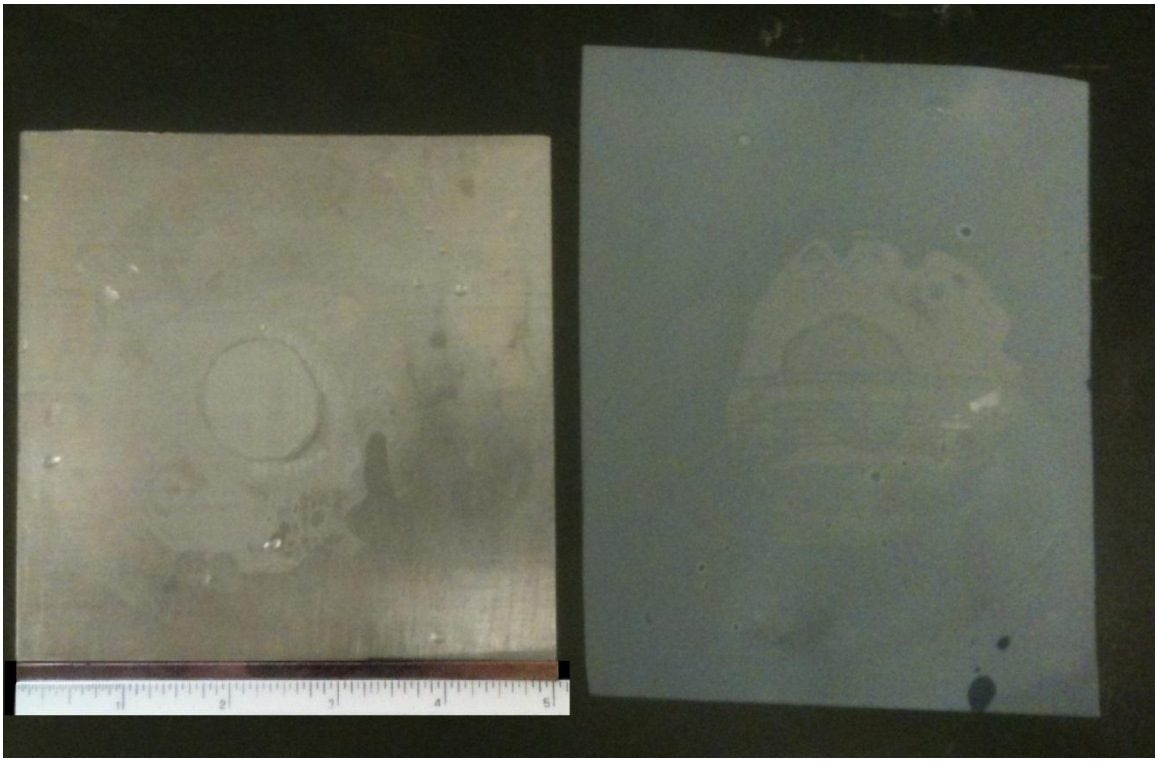

Figure 54: A sample of 10% UHMwPE and 90% wax compressed at 100 °C and a compression ratio of 20, then quenched in water. Scale bar is in inches.

The resulting sample from these procedures can then be examined by TGA, DSC, or microscopy to determine its structure and composition, and thereby measure the amount of material that was squeeze from the sample and resolve any structures related to the phenomenon.

A key difference in compression configuration for DIPS from the configuration used to make typical mold samples is that the material comprising the top surface is different from the material comprising the bottom surface of the chamber. This makes collecting, imaging, and measuring the resulting samples much simpler because the PE rich samples are more inclined to adhere to the aluminum than to the Teflon after

quenching. Without this difference, some of the samples would tend to break or tear when being separated from the mold. In addition, by having only one Teflon sheet, any effects caused by compression of the Teflon itself were reduced.

4.2.4. Etching and Microscopy

Morphology determination for PE/PE blends is more difficult than for most blend types as the two components are chemically identical and therefore vulnerable to the same types of solvents. X-ray photoelectron spectroscopy, nuclear magnetic resonance spectroscopy, and other methods for determining local chemistry are not feasible because they lack the spatial resolution needed, are unable to differentiate the two components, or require bulk amounts of fluorescing material (which are quite expensive). Phase-sensitive Atomic Force Spectroscopy can differentiate the local phase structure of these types of blends, and has been used to do so [108], but the surface to be examined must be extremely smooth. Ultimately, examination of the blend by optical microscopy (OM) and scanning electron microscopy (SEM) are the best techniques available to determine morphology. However, prior to examination under microscopy, it is frequently beneficial to section and partially or selectively etch the sample. These two steps will determine the quality of the image generated from microscopy.

Two sectioning methods were found feasible: sectioning by fracturing in liquid nitrogen, and sectioning by cutting with a microtome. Fracturing in liquid is practical for bulkier samples. In this method, the sample is first submerged in liquid nitrogen for 30 minutes. After it is fully equilibrated, the sample is either struck with a hammer (for

irregular geometries) or snapped between tweezers (for slabs or thick fibers). For smaller samples, such as drawn fibers, cutting the sample with a microtome is far more practical. Generally, liquid nitrogen fracture is preferred to cutting as the resulting cross-section is of a much higher quality.

Following sectioning, samples may be partially etched to improve the contrast between the different phases. The first method for etching is permanganic, which preferentially attacks the amorphous component of the polyethylene. [47] [108] [109] [110] In permanganic etching, two parts sulfuric acid and one part ortho-phosphoric acid are combined with 2 wt% potassium permanganate. The surfaced desired to be etched is then immersed in this solution for 10 hours under gentle stirring. Following etching, the sample is washed first with sulfuric acid, then with water, and finally with methanol to remove any residual permanganate.

The second method for etching employs cyclohexane. By heating the cyclohexane to above the wax's melting temperature, but below that of the PE-rich phase, the wax may be selectively removed. In this case, the sample surface for examination is immersed in cyclohexane at 75 ºC for 10 hours under gentle stirring. Following dissolution, the sample is placed overnight in an oven at 50 ºC under vacuum to extract any residual solvent. [53] [59] This is the method of etching preferred for most of the samples examined herein.

Optical microscopy was performed using a Motic SMZ-168 reflective microscope; scanning electron microscopy was accomplished using a Hitachi S-800 SEM. Optical microscopy allows for low-magnification examination of samples. In general, it is useful for identifying color or shade dependent variations in a sample (rather

than topological variations as for SEM), and sample dimension determination (i.e. fiber diameter). For resolving features on a smaller scale, SEM is necessary. SEM is useful for direct imaging of the phase structure of a blend. However, as is true for any polymeric material, a layer of gold needs to be sputtered onto the sample prior to placing it in the SEM to prevent charging of the sample surface. SEM images in this text were sputtered with an Au-Pd coating and examined under a 6 kV beam.

4.3. Results and Discussion

4.3.2. DIPS Investigated

There are three ways of considering the composition data before and after compression. The first is in terms of absolute compositions; that is, the measured percent values for PE content. This has the advantage of bringing into focus the change in composition in relation to the overall composition. The second is in terms of the change in absolute composition; that is, the difference in measured PE percent values. This has the advantage of isolating the change in composition itself. The third is in terms of relative wax composition; that is, the change in wax composition as normalized to the initial wax composition. This is to say if a sample started with 20% wax and ended with 15% wax, it has lost 20% of its initial wax content. This approach has the advantages of being an intuitive, easily visualized, and easily communicated means of measuring the degree to which the target material has been removed in relation to its initial content.

Previous publications verify that paraffin wax can melt and recrystallize without destruction of the PE-rich network. Furthermore, while the temperature is 100 C and the wax phase is melted but the PE-rich phase remains solid, the capillary forces between the network of PE and the wax prevent the liquid wax therein from flowing freely. Therefore, baring the application of another force (i.e. compression) blends of PE and wax will normally maintain their compositions and morphologies at all temperatures. [62] The exact phase diagrams of these blends at steady state were previously developed in this study and are shown Figure 23 for the P# type blends and Figure 24 for the X# type blends.

From Compression of P75

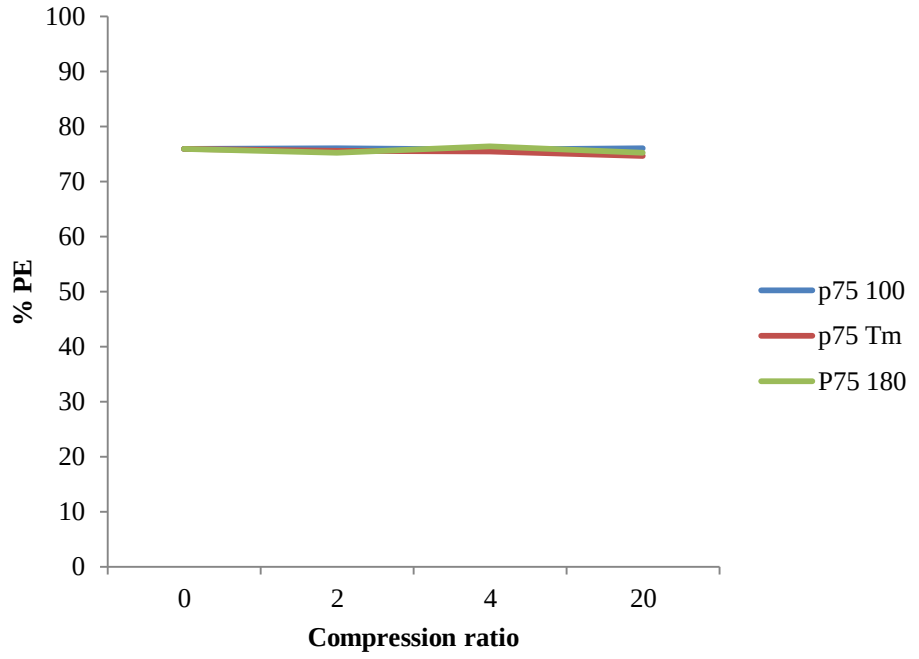

Figure 55: Absolute % PE composition of P75 samples at different compression ratios

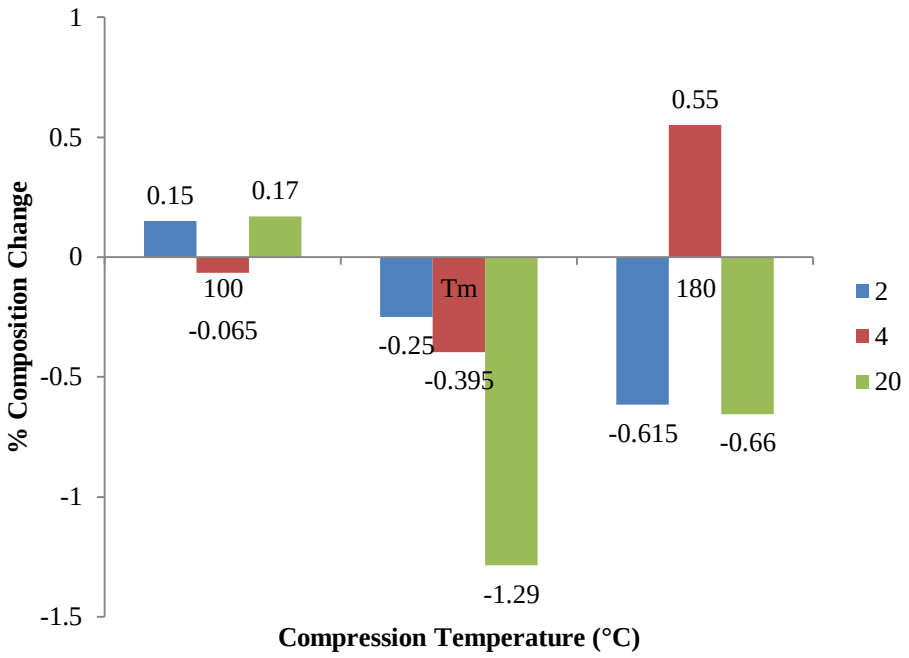

Figure 56: Absolute change in % PE composition of P75 samples at different compression ratios

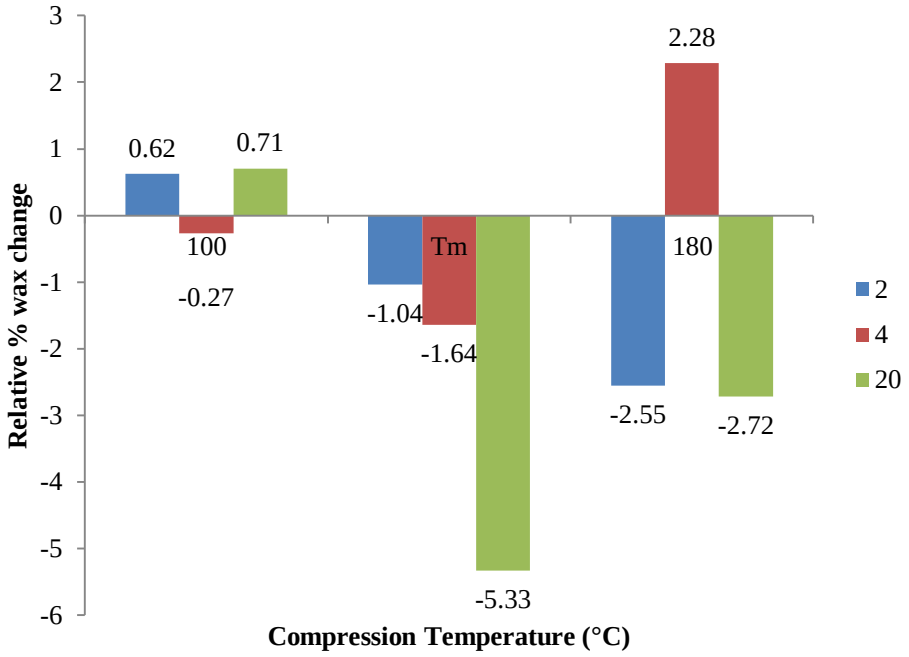

Figure 57: relative change in % wax composition of P75 samples at different compression ratios

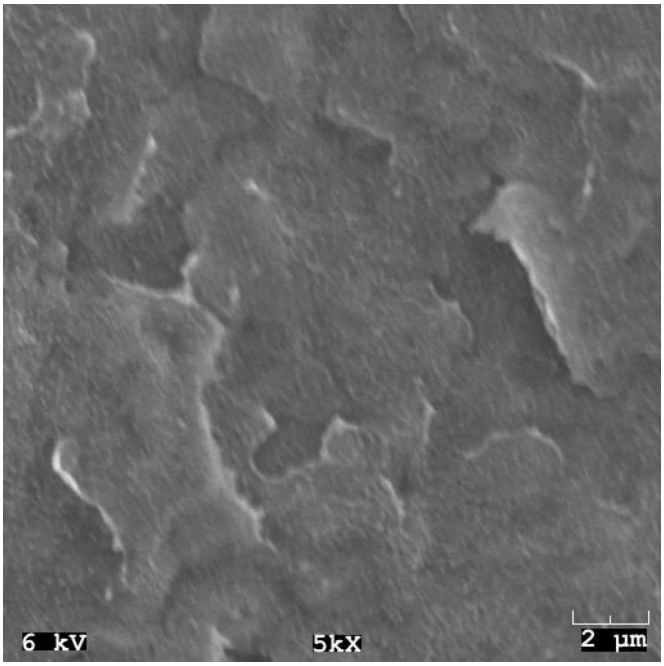

Figure 58: Morphology of P75 samples taken by SEM at 5K magnification and 6 kV.

From plots of the sample compositions as a function of both the compression ratio and the compression temperature for the P75 blend (Figure 55 - Figure 57), it is determined that negligible, if any, "squeeze out" of the wax phase occurred. SEM examination of the samples shows a near uniform phase structure with little or no isolated wax phase present (Figure 58). Furthermore, the compositions of the P75 samples approach that for which the wax phase no longer exists independent from the PE as determined from DSC of approximately 85%.

From Compression of P50

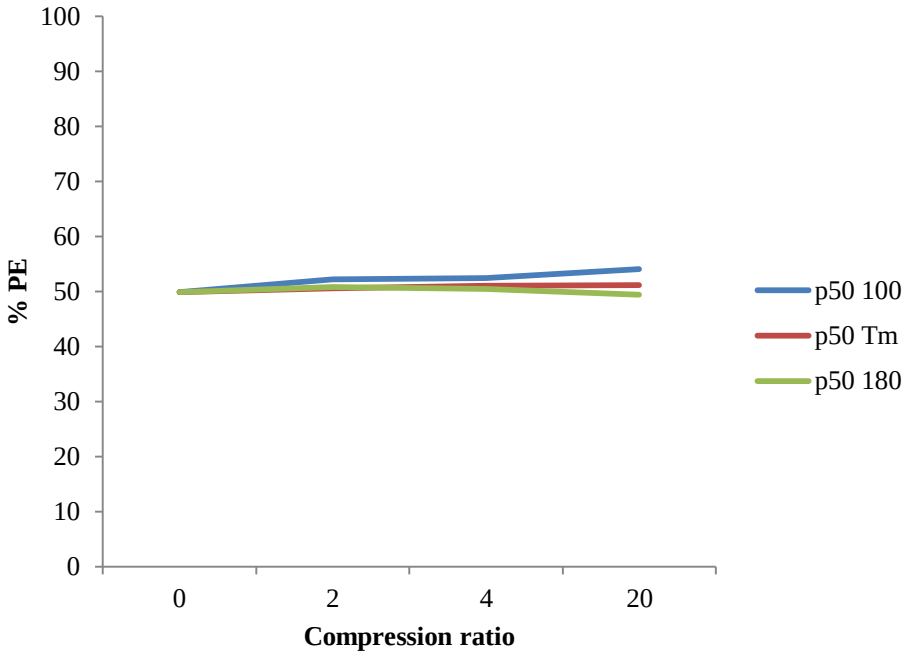

Figure 59: Absolute % PE composition of 50 samples at different compression ratios

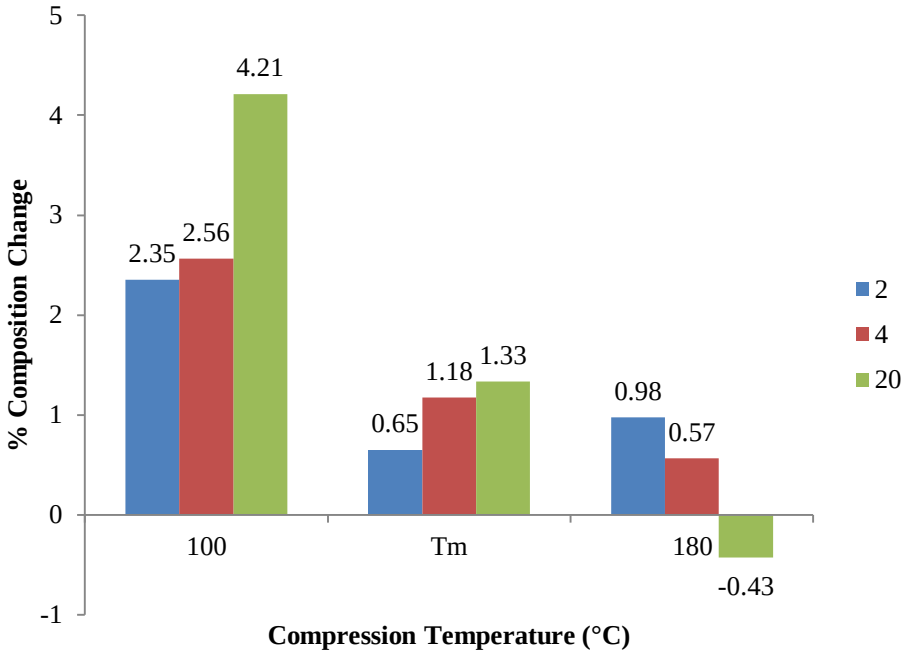

Figure 60: Absolute change in % PE composition of P50 samples at different compression ratios

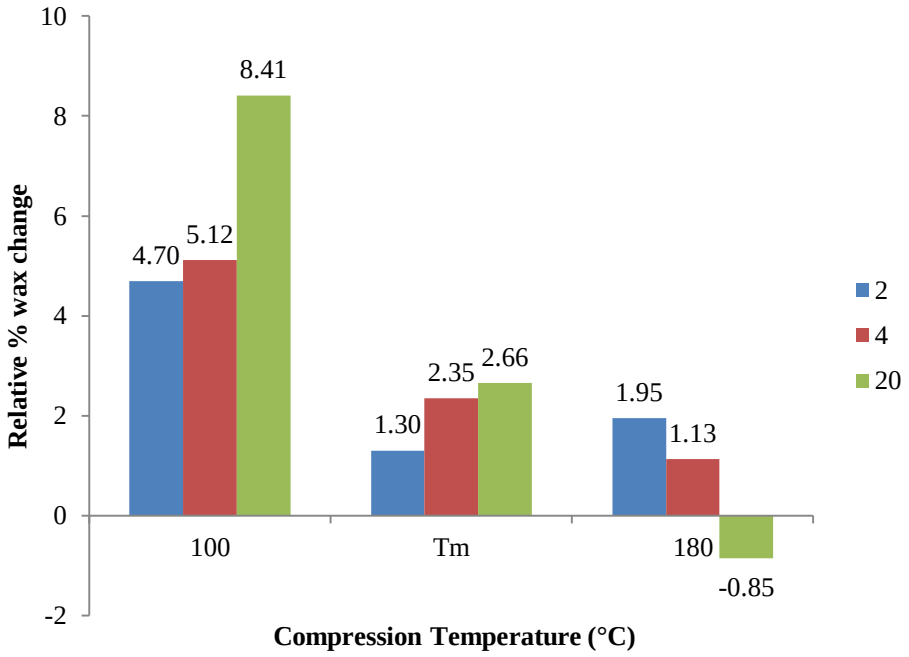

Figure 61: relative change in % wax composition of P50 samples at different compression ratios

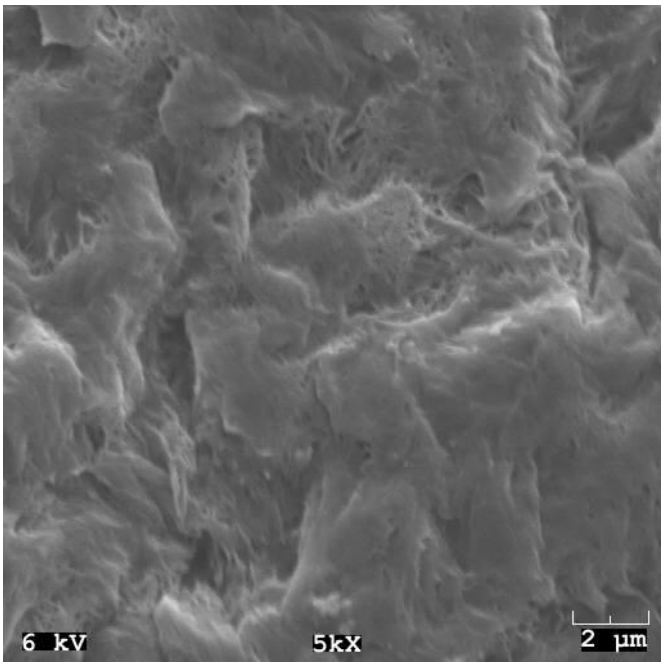

Figure 62: Morphology of P50 samples taken by SEM at 5K magnification and 6 kV

From plots of the sample compositions as a function of both the compression ratio and the compression temperature for the P50 blend (Figure 59 - Figure 61), it was determined that minor ejection of the wax phase occurred, with the amount of wax expelled increasing with compression ratio for a given temperature and decreasing with temperature for a given ratio. This disgorgement is so minor that the only changes in composition eligible to be considered as be outside of the margin of error (estimated at ~2% absolute change) are those that take place at 100 °C. SEM examination of the sample shows a dense network structure with voids and channels in which the wax phase existed independent of the PE network (Figure 62). However, the wax phase was dominated by the PE-rich phase. Furthermore, the composition of the P50 samples was

well below the composition for which the wax phase no longer exists independent from the PE as determined from DSC of ~ 85%.

From Compression of P25

Samples made from blends of 25% 125K PE and 75% paraffin wax lacked sufficient mechanical integrity to be successfully collected and/or abraded after compression under most of the testing conditions used, thereby invalidating the vast majority of the TGA results for that particular blend. This lack of integrity is considered to be a direct result of the wax's influence on the mechanical properties of the blend, which are in turn contingent on the morphology present in the blend. [32] Fortunately, the initial morphology of blend was still examinable via SEM.

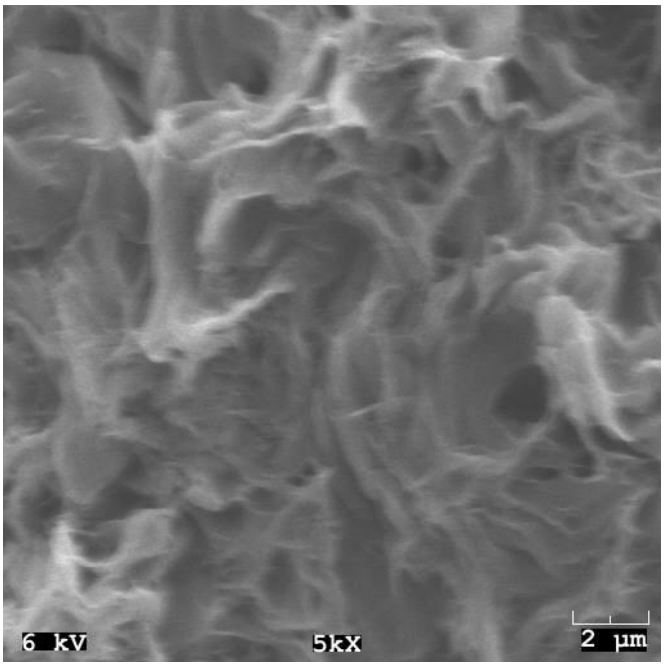

Figure 63: Morphology of P25 samples taken by SEM at 5K magnification and 6 kV

This SEM examination reveals a co-continuous PE-rich network, dominated by wax for in P25 samples. In fact this volumetric ratio of wax (voids) to PE is initially even greater than depicted above as the samples shrank substantially during drying in a vacuum oven after dissolution of the wax phase. This network appears well adapted for use in inducing DIPS. Although, as previously noted, precise collection of the compressed samples proved infeasible, the samples qualitatively displayed wax disgorgement as shown in Figure 64.

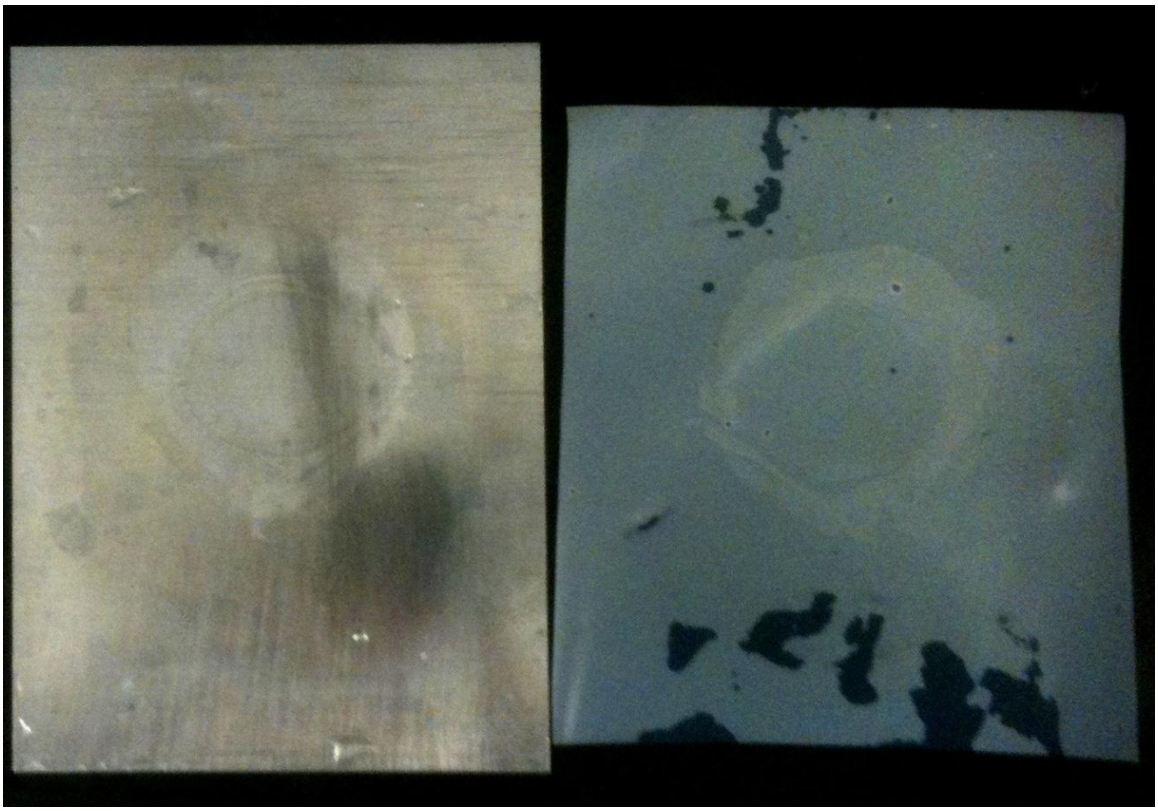

Figure 64: As-quenched sample of P25 compressed to a ratio of 20 at 100 C

From Compression of X35

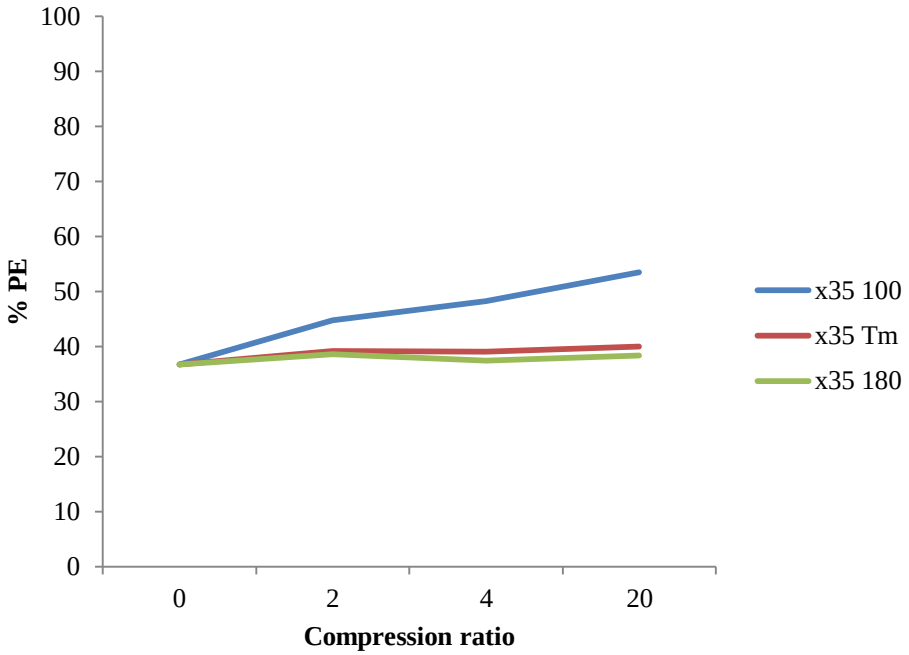

Figure 65: Absolute % PE composition of X35 samples at different compression ratios

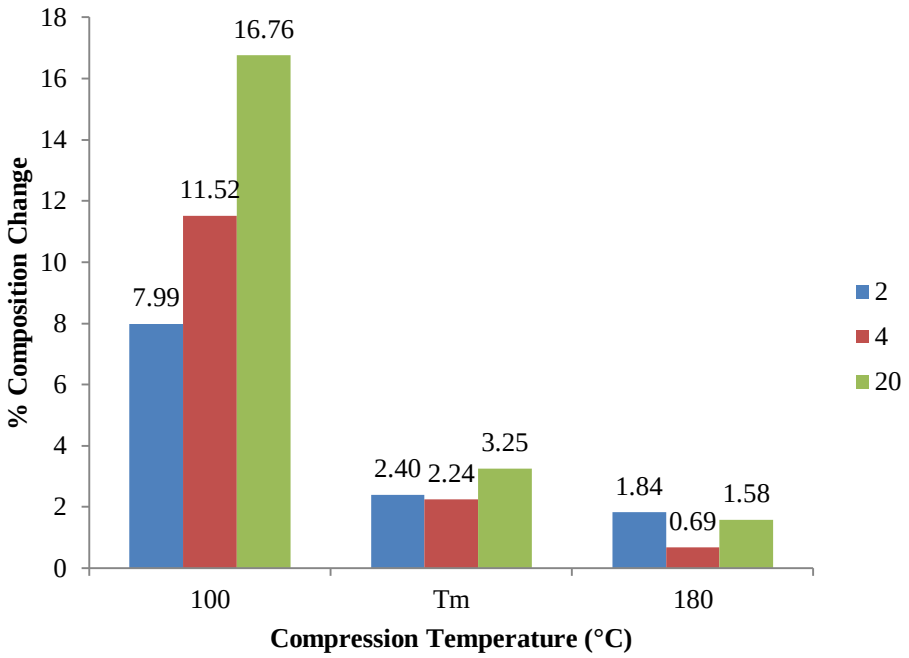

Figure 66: Absolute change in % PE composition of X35 samples at different compression ratios

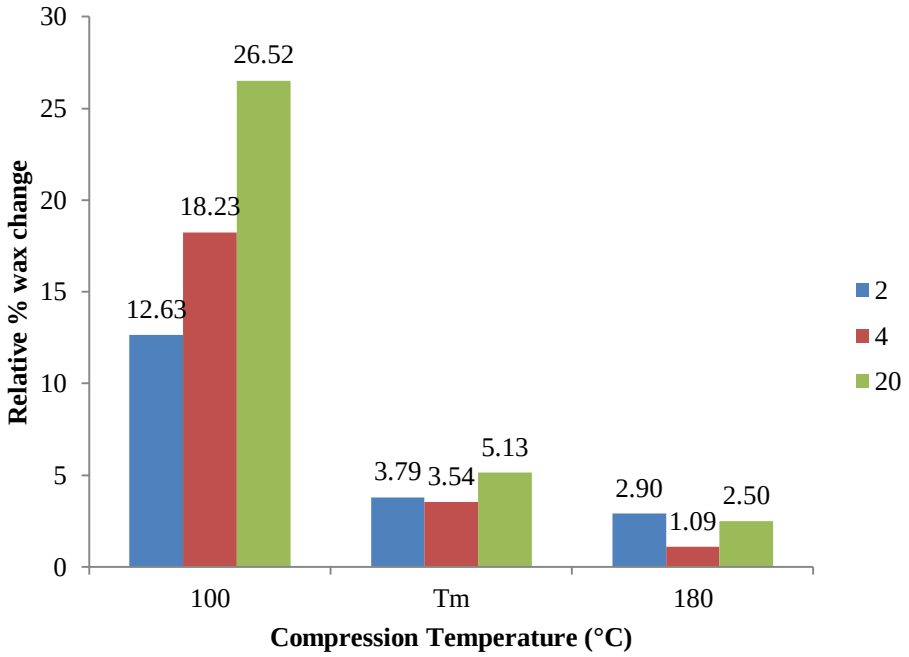

Figure 67: relative change in % wax composition of X35 samples at different compression ratios

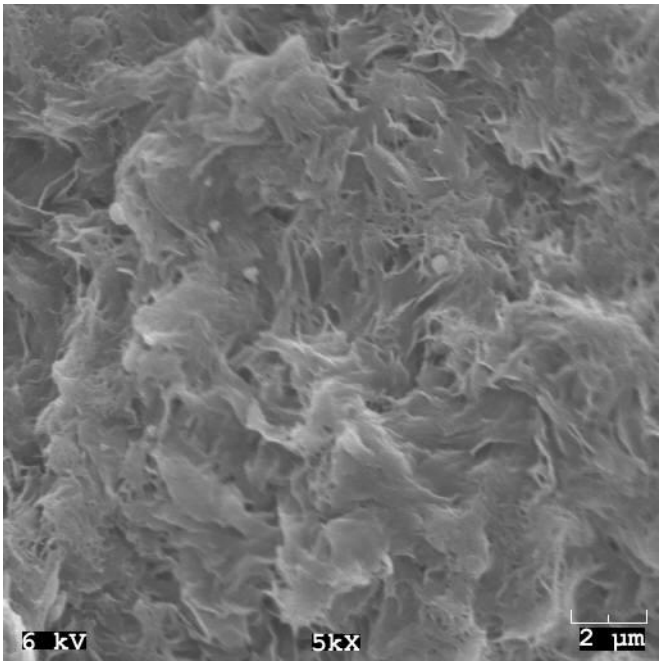

Figure 68: Morphology of X35 samples taken by SEM at 5K magnification and 6 kV

From the plots of the sample compositions as a function of both the compression ratio and the compression temperature for the X35 blend (Figure 65 - Figure 67), it was determined that substantial squeeze out of the wax phase occurred, with the amount of wax discharged increasing with increased compression ratio for a given temperature and decreasing with increased temperature for a given ratio. This squeeze out became negligible only when the compression temperature reached 180° C, well above the melting temperature for the pure PE. Squeeze out at the melting temperature itself, however, was only slight. SEM examination of the sample showed a dense network structure with voids and channels in which wax phase existed independent of the PE network (Figure 62). The composition of the X35 samples is well below the composition

for which the wax phase no longer exists independent from the PE as determined from DSC of approximately 80%.

From Compression of X25

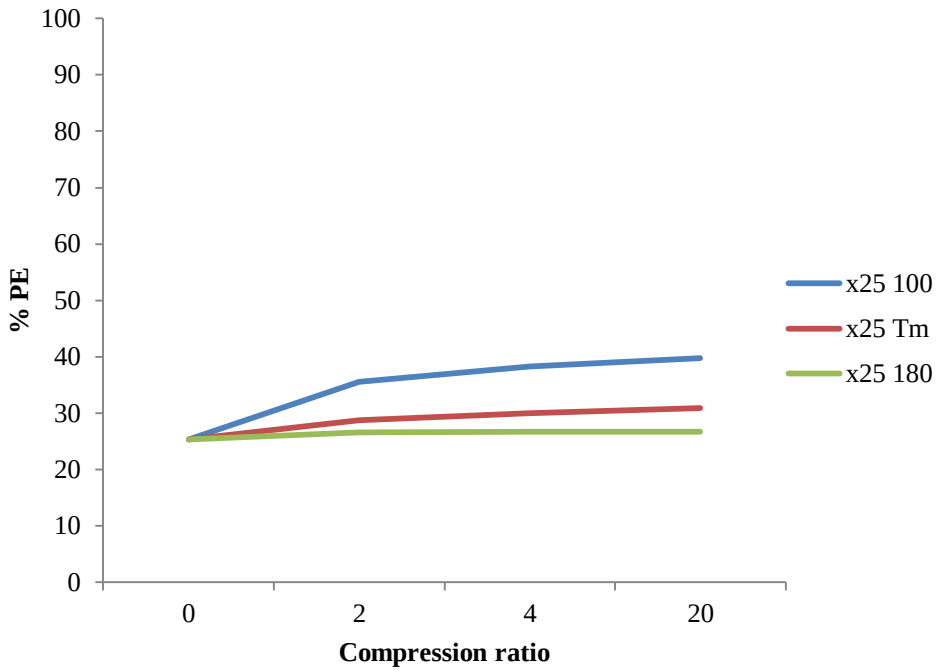

Figure 69: Absolute % PE composition of X25 samples at different compression ratios

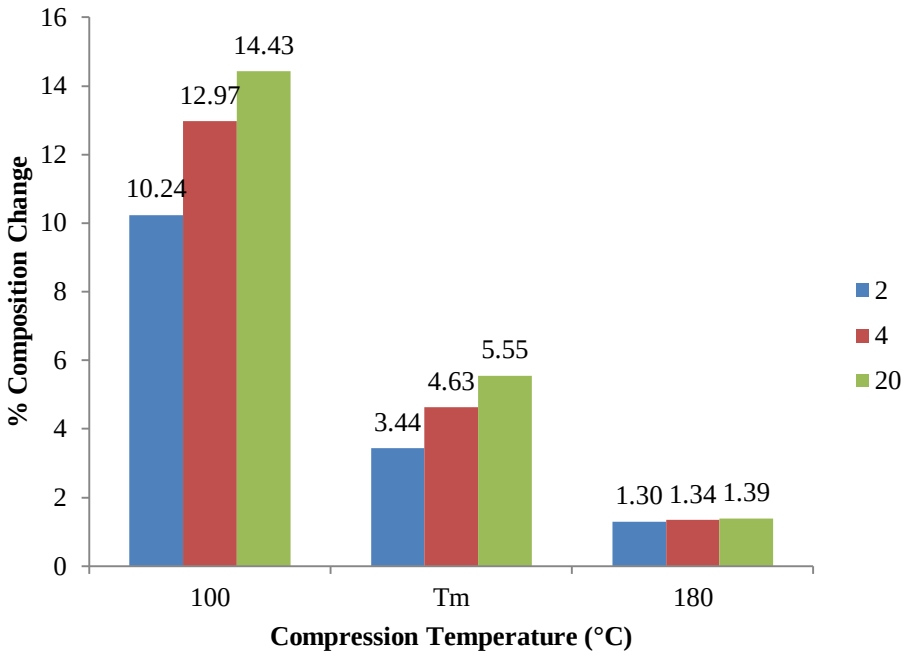

Figure 70: Absolute change in % PE composition of X25 samples at different compression ratios

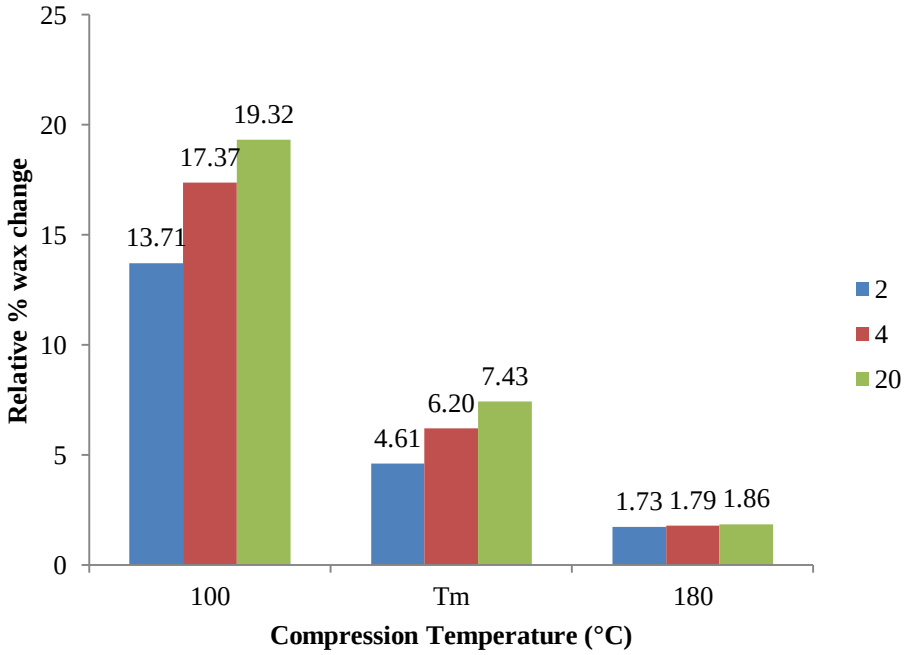

Figure 71: relative change in % wax composition of X25 samples at different compression ratios

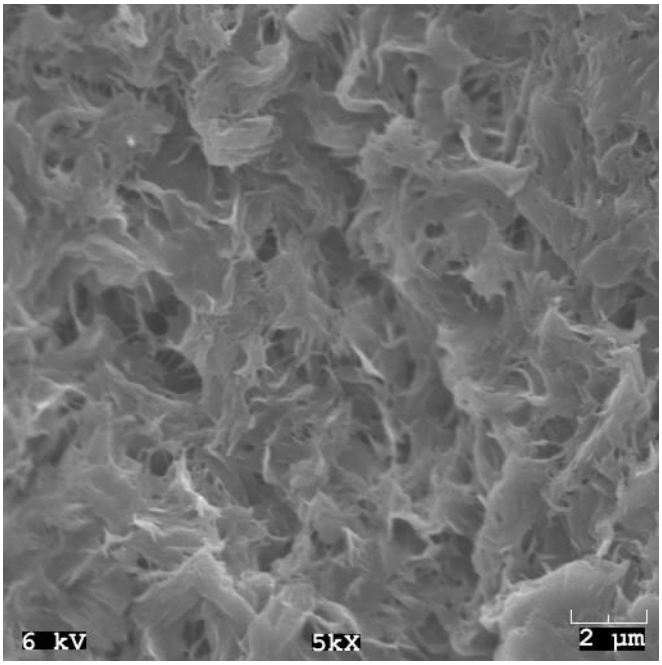

Figure 72: Morphology of X25 samples taken by SEM at 5K magnification and 6 kV

From plots of sample compositions as a function of both the compression ratio and the compression temperature for the X25 blend (Figure 69 - Figure 71), it was determined that substantial squeeze out of the wax phase occurred, with amount of wax ejected increasing with increased compression ratio for a given temperature and decreasing with increased temperature for a given compression ratio. As with the X35 samples, this squeeze out became negligible only when the compression temperature reached 180 C, well above the melting temperature for the pure PE, although squeeze out at the melting temperature itself was only slight. SEM examination of the sample shows a dense network structure with voids and channels in which the wax phase existed independent of the PE network (Figure 72). However the voids and channels take up a noticeably larger fraction of the total volume than for the X35 sample. The composition

of the X25 samples is well below the composition for which the wax phase no longer exists independent from the PE as determined from DSC of ~ 80%.

From Compression of X10

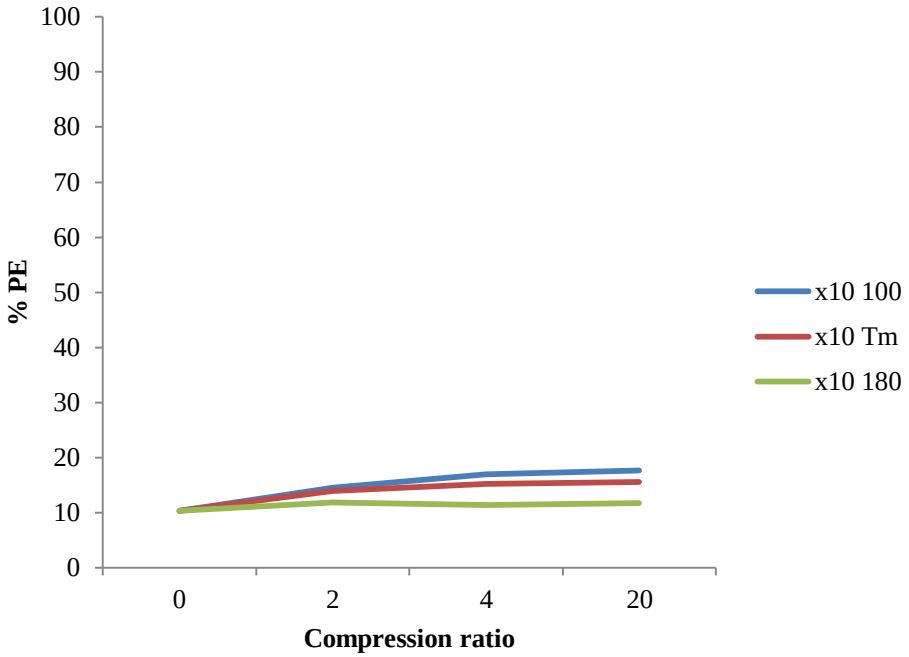

Figure 73: Absolute % PE composition of X10 samples at different compression ratios

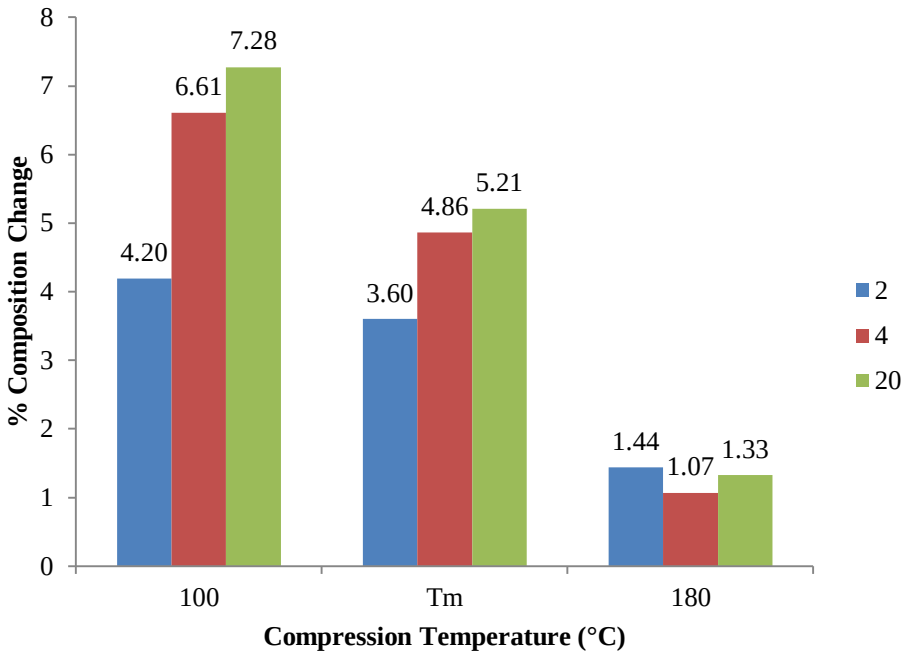

Figure 74: Absolute change in % PE composition of X10 samples at different compression ratios

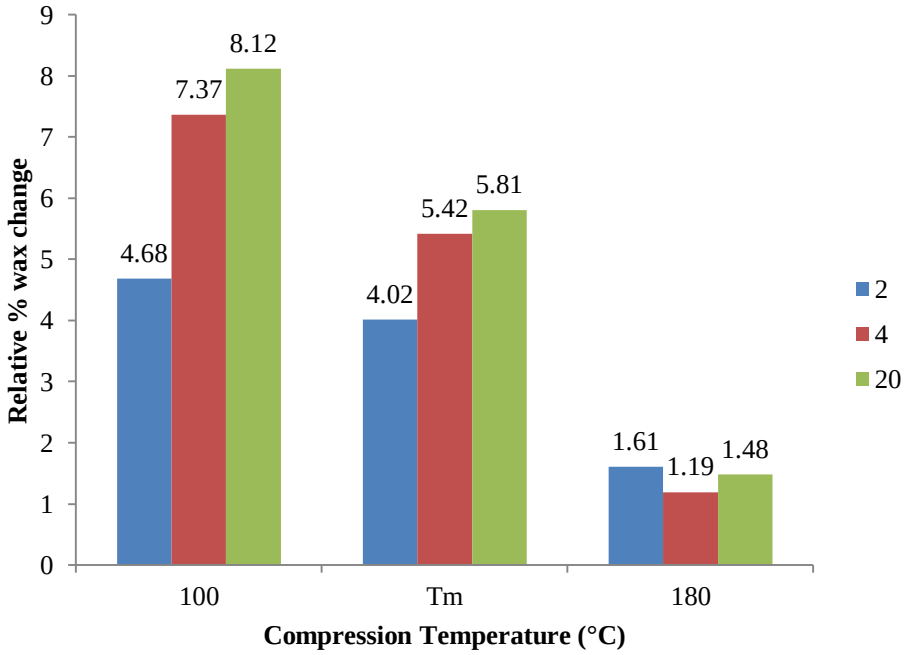

Figure 75: relative change in % wax composition of X10 samples at different compression ratios

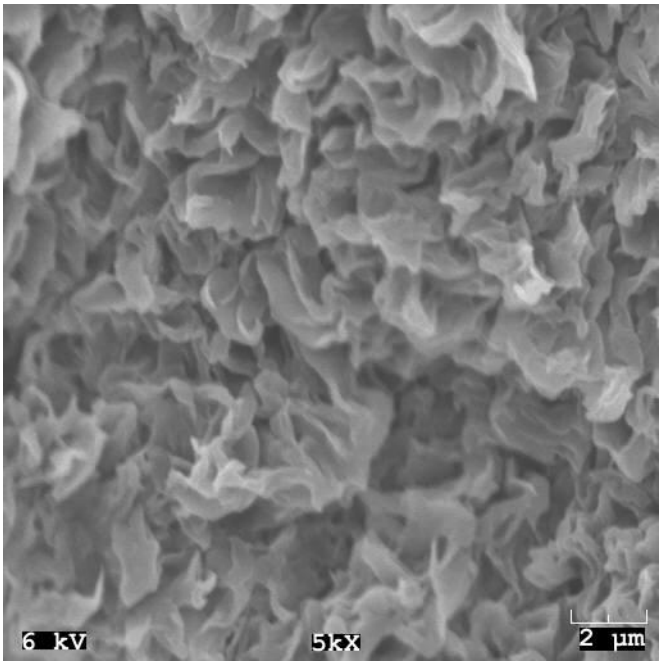

Figure 76: Morphology of X10 samples taken by SEM at 5K magnification and 6 kV

Like P25 samples, the X10 samples were difficult to collect following compression, but unlike P25 collection did remain viable. From plots of sample compositions as a function of both the compression ratio and the compression temperature for the X10 blend (Figure 73 - Figure 75), it is determined that substantial squeeze out of the wax phase occurred in the sample, with the amount of wax squeezed out increasing with compression ratio for a given temperature and decreasing with temperature for a given ratio. As with the X35 samples, this squeeze out became negligible only when the compression temperature reached 180° C, well above the melting temperature for the pure PE. However, unlike previous samples, squeeze-out remained substantial at the melting temperature. SEM examination of the sample shows a network structure dominated by voids and channels in which the wax phase existed

independent of the PE network (Figure 76). Like the P25 samples, this fraction of void would be initially even greater than that imaged as the sample shrank during drying, though less so than for P25. The composition of the X10 samples is well below the composition for which the wax phase no longer exists independent from the PE as determined from DSC of approximately 80%.

4.3.3 Compression Overview

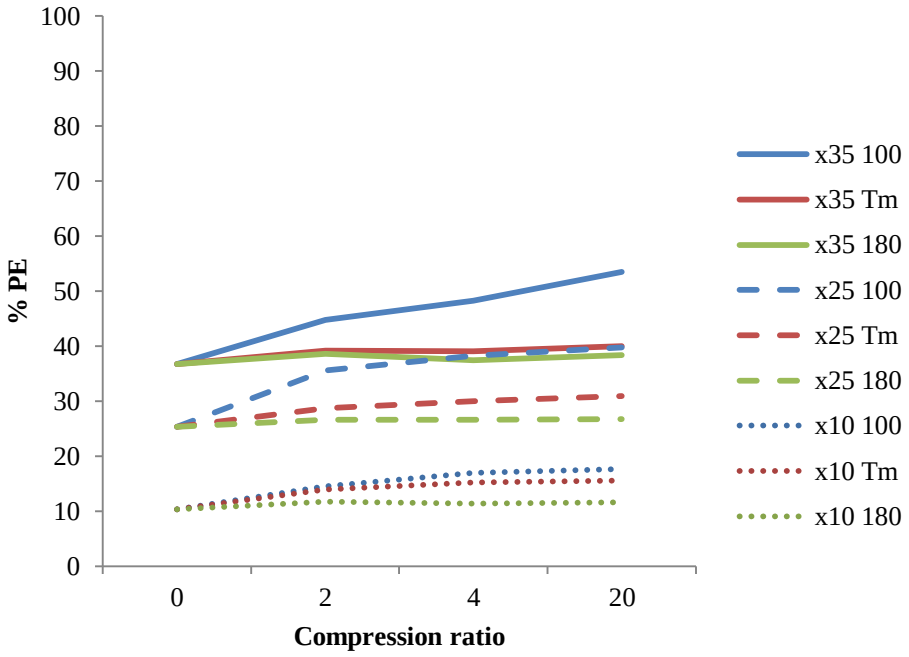

Figure 77: Absolute % PE composition of all X# samples at different compression ratios

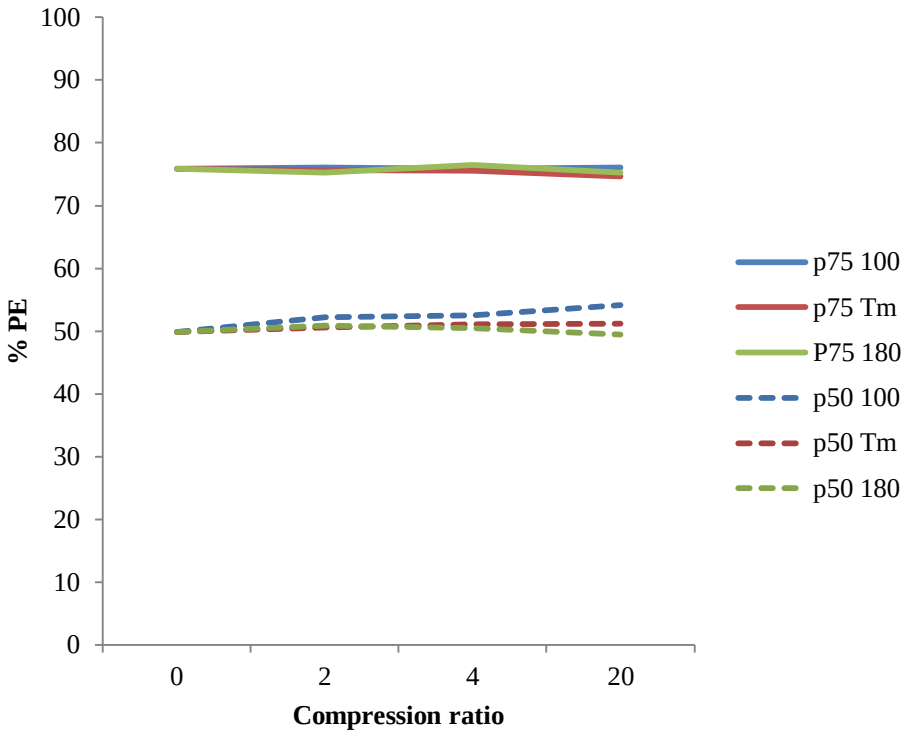

Figure 78: Absolute % PE composition of P# samples at different compression ratios

By examining Figure 77 and Figure 78, it is apparent that X35 possessed the greatest absolute and relative squeeze-outs of wax from the samples. The least absolute and relative squeeze-outs of were for P 75. The degree to which squeeze out occurred in a given sample depended upon:

- *The temperature of compression*: Temperatures below the melting point of the PE-rich phase showed the greatest squeeze-out at all compression ratios.
- *The compression ratio*: Greater compression yields greater segregation of the wax phase, except for 180° C which showed no discernible change in composition for any compression ratio.

- *The composition and morphological structure of the sample*: The wax needs to be able to flow through the PE-matrix to segregate. Furthermore, the PE matrix must be strong enough as to not fully plastically deform along with the wax. (The flow of wax can be considered a type of plastic deformation as once it segregates from the sample, it will not flow back.)

The ranges of morphologies present in the mixtures are displayed in Figure 79 and Figure 80. These morphologies correspond well to those predicted by the DSC data, with regions of pure wax separate from and in a matrix of a PE-rich phase. The structures are similar to those observed for other PE networks. [50] [59] [61]

A conclusion of elastic deformation of the PE matrix is supported by the clear region separating the PE-rich disc and the segregated wax as seen in Figure 64. In more drastic cases, some of the high PE concentration samples popped themselves directly off the surface of the metal plate upon quenching as they rapidly recovered the elastic component from the strain of compression.

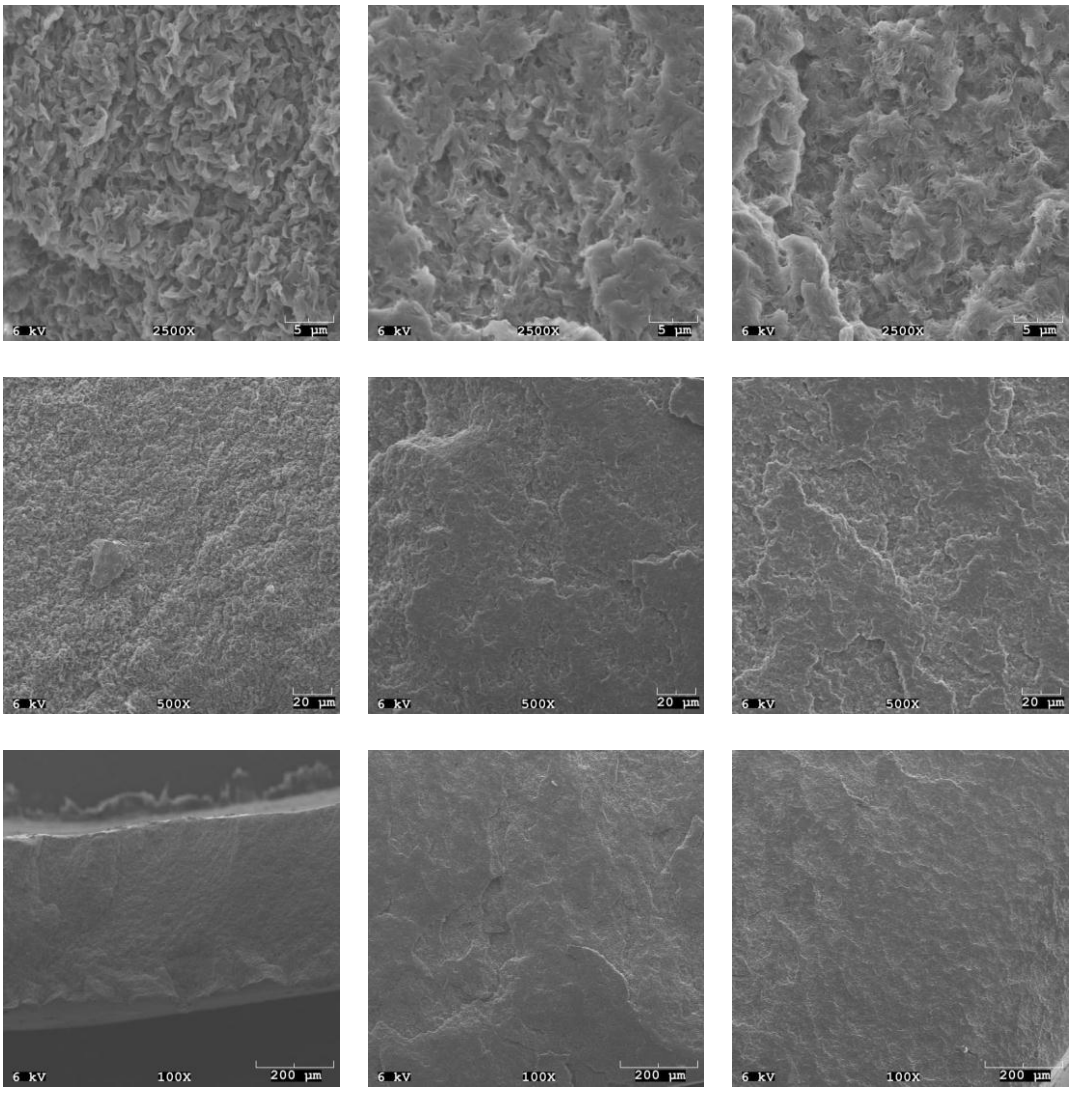

Figure 79: SEM images taken at 2500, 500, and 100 x (row 1, 2, and 3 respectively) for blends X10, X25, and X35 respectively

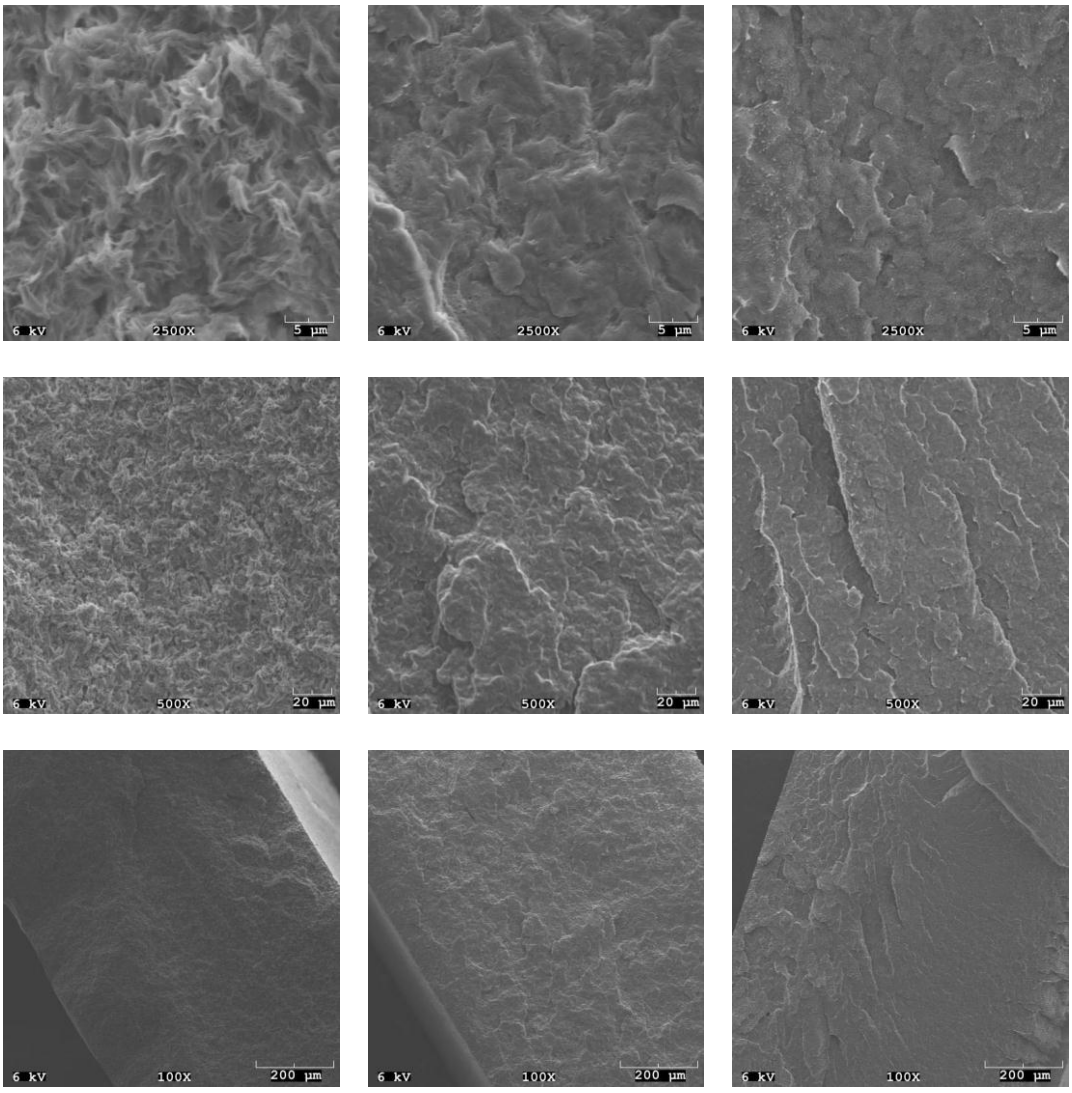

Figure 80: SEM images taken at 2500, 500, and 100 x (row 1, 2, and 3 respectively) for blends P25, P50, and P75 respectively

4.4. Conclusions

Deformation Induced Phase Segregation is the segregation of a component from a polymer blend due to the application of an anisotropic stress and resulting deformation. In this case, the stress takes the form of a compression that permits a sample to deform freely perpendicular to the compression. DIPS process occurs in blends for which the components possess greatly different melting temperatures and viscosities. Co-continuous morphology between the components is a prerequisite.

The greatest segregation of wax in PE and wax blends occurred at 100° C, with greater segregation resulting from greater compression. At the blends' melting temperatures, limited segregation arose from compression, with greater segregation again resulting from greater compression. At 180° C, only negligible segregation occurred under all compression ratios. From this, it was concluded that the PE-rich phase and wax phase act as completely independent phases at 100° C, the liquid wax being driven from the PE matrix by deformation and pressure gradient induced by compression. At melting temperatures, the elastic nature of a PE network decreases, allowing it to deform more plastically with the wax, resulting in decreased squeeze-out of the wax content. At 180°C, the PE network deforms plastically with the wax, resulting in no discernible segregation of the wax.

Furthermore, it is found that compression induced wax ejection is inherently related to the morphology of the initial blend. High-density networks associated with higher PE concentrations have reduced available mobility for flow of the molten wax, causing less segregation of wax from a sample. However, such networks possess good

elastic recovery. Low density networks at lower PE concentrations result in reduced elastic recovery of samples following compression due to decreased network strength, causing the relative amount of wax squeeze out to decrease. However, these networks possess good mobility available for the flow of the molten wax. From this it was concluded that for any given PE and wax pairing, there exists a composition and structure at which optimal squeeze out of wax is possible. This structure is postulated to be between 35% and 50% PE for the materials tested here and is optimized at a temperature above the melting transition of the wax phase, but below that of the melting transition of the PE-rich phase.

CHAPTER 5: RECOMMENDATIONS FOR FURTHER STUDY

To further the understanding of the melt and solution behaviors of similar blends, examination of the rheological properties in the dynamic state over a range of temperatures promises great benefit. Such investigations would define the time-dependent properties of the blends and thereby reveal more detail as to structure of the melts. In addition, greater focus should be paid to the low concentration regions, which were largely neglected in this study.

Within the high molecular weight PE / PE wax type systems, examination across a range of molecular weights for the waxes (the low molecular weight component and solvent in the solution) will expand the understanding of the thermal and rheological phase behaviors of this type of system. It was previously postulated that the limiting morphological factor in the solid-solid miscibility of PE and paraffin wax is the ability of the wax to incorporate into the lamellae of the PE crystallites. Therefore, for shorter wax molecules (waxes of lower molecular weight), the wax should be better able to enter the crystallites of a given PE, resulting in a more miscible solid-solid interaction. Such miscibilities could be further verified or refuted by TEM examination of the blends crystals in addition to the basic thermal DSC tests.

Simultaneously, the effects of different PE structures and molecular weights should be examined by. The new range of PEs should incorporate PEs containing a large range of molecular weights and molecular weight distributions, and varying degrees of short chain branching and long chain branching, with different architectures therein (star,

tree, brush, etc.) By expanding the range of molecular weights and molecular architectures used for both PE components, the limits of using the models described in this thesis as a means of predicting a mixture's behavior can be determined.

The types of thermal and rheological examinations performed herein and in the previous paragraphs should be expanded to incorporate other material systems of similar form such as low molecular weight methacrylates with polymethylmethacrylate. The goal would be to verify that similar phenomena occur for similar like/like systems. Specific focus should be paid to the region in which the viscous behavior changes across the critical molecular weights or critical concentrations. Also, different chemistries can incorporate different molecular dynamics (for example, molecules of stiff segments rather than a flexible chain), which in turn will result in different rheological behaviors.

A key factor in all of this will be enabling the prediction of the dependency of the exponent of concentration in $\eta \sim c^{\alpha}$ on molecular weight. As previously stated, a distinct correlation between α and polymer molecular weight has been observed for this system, and reported for other systems. However, no explanation for this correlation has been given or determined in this thesis work. By a combination of thermal phase behavior and rheological examination similar to done in this research and suggested above, a link between the α exponent and the materials phase behavior should be developed. Specifically, the expansion should be able to determine if the increase in α with increasing molecular weight is simply due to decreasing miscibility between the high (solute) and low (solvent) molecular weight components.

With regards to Deformation Induced Phase Segregation, DIPS should be examined under additional conditions and criteria. The existence and extent to which this

type of segregation can be induced due to other forms of mechanical stress/deformation should be pursued. These would include deformation due to stresses generated by drawing and twisting. Expansion of the forms of stress for which the process is viable would render DIPS immediately more attractive for a wider variety of existing industrial applications.

Additionally, the dynamics of the network phase and low viscosity phase during the segregation process should be more thoroughly investigated. Only briefly touched upon here, the manners in which the wax segregates from the bulk of a sample as a function of time, compression ratio, compression speed, temperature, etc. are quite important to the full understanding, development, and exploitation of DIPS. Further examination of processes that drive the associated segregation will enable greater efficiency and optimization. This behavior can in turn be linked to the overall phase behavior of the blend type being used in the DIPS process.

REFERENCES

[1] L. A. Utracki, "Chapter 1: Introduction to Polymer Blends," in *Polymer Blends Handbook, Vol 1-2*, Dordrecht, Netherlands, Kluwer Academic Publishers, 2002, pp. 1-122.

[2] N. Furgiule, A. H. Lebovitz, K. Klementina and J. M. Torkelson, *Polym. Eng. and Sci.*, vol. 40, no. 6, p. 1447, 2000.

[3] K. F. Wissbrun, R. H. Ball and P. J. Rossello.Belgium Patent 614,282, 22 Aug 1962.

[4] M. A. Cowan.Europe Patent 095,299, 30 Nov 1983.

[5] O. Fukui, Y. Inuizawa, S. Hinenoya and Y. Takasaki.France Patent 2,522,331, 02 Sep 1983.

[6] A. Haas and F. Raviola.Europe Patent 042,743, 13 Jan 1982.

[7] E. A. Benham, F. W. Bailey, J. D. Wehmeyer and M. P. McDaniel.United States Patent 5,378,764, 03 Jan 1995.

[8] O. E. Larsen.Canada Patent 1,120,630, 23 Mar 1982.

[9] L. Boehm, H. F. Enderle and H. Jastrow.Europe Patent 517,222, 09 Dec 1992.

[10] K. K. Showa Denko.Japan Patent 059,242, 08 Apr 193.

[11] W. R. Coutant.Europe Patent 588,147], 23 Mar 1994.

[12] L. A. Utracki and M. R. Kamal, "Ch 7 The Rheology of Polymer Alloys and Blends," in *Polymer Blend Handbook, Vol 1-2*, Dordrecht, Netherlands, Kluwer Academic Publishers, 2002, pp. 449-546.

[13] J. F. Horio, T. Fuju and S. Onogi, *J. Phys. Chem.*, vol. 68, p. 546, 1964.

[14] R. A. Bubeck, *Materials Sci and Eng R,* vol. 39, pp. 1-28, 2002.

[15] D. Yan, *Polymer,* vol. 40, pp. 1737-1744, 1999.

[16] J. Kim and et al, *Polymer,* vol. 50, pp. 4998-5001, 2009.

[17] K. Cho, B. H. Lee, H. Kyu-Myun, H. Lee and S. Choe, *Polym. Eng. Sci.,* vol. 38, no. 12, p. 1969, 1998.

[18] Y. Fang, P. J. Carreau and P. G. Lafleur, *Polym. Eng. and Sci.,* vol. 45, no. 9, p. 1254, 2005.

[19] C. Liu, J. Wang and J. He, *Polymer,* vol. 43, pp. 3811-3818, 2002.

[20] I. A. Hussein, T. Hameed, B. F. Abu Sharkh and K. Mezghani, *Polymer,* vol. 44, pp. 4665-4672, 2003.

[21] T. Hameed and I. A. Hussein, *Polymer,* vol. 43, pp. 6911-6929, 2002.

[22] J. A. Resch and et al, *Rheol Acta,* vol. 50, pp. 559-575, 2011.

[23] O. Delgadillo-Velazquez and S. G. Hatzikiriakos, *Polym. Eng. Sci.,* vol. 47, no. 9, p. 1317, 2007.

[24] R. Perez, M. Fernandez, V. Leal, P. Lafuente and A. Santamaria, *Polymer,* vol. 46, pp. 8045-8053, 2005.

[25] J. F. Vega, A. Munoz-Escalona, A. Santamaria, M. Munoz and E. P. Lafuente, *Macromolecules,* vol. 29, p. 960, 1996.

[26] L. A. Utracki, *Polym. Eng. and Sci.,* vol. 27, p. 1512, 1987.

[27] B. Neway and U. W. Gedde, *J. Appl. Polym. Sci.,* vol. 94, pp. 1730-1736, 2004.

[28] C. C. Puig, *Polymer,* vol. 42, pp. 6579-6585, 2001.

[29] M. J. Hill, P. J. Barham and A. Keller, *Polymer,* vol. 33, no. 12, p. 2530, 1992.

[30] C. C. Puig, M. J. Hill and J. A. Odell, *Polymer,* vol. 34, no. 16, p. 3402, 1993.

[31] M. J. Hill, *Polymer,* vol. 35, no. 9, pp. 1991-1993, 1994.

[32] A. S. Luyt and M. J. Hato, *J. Appl. Polym. Sci.,* vol. 96, pp. 1748-1755, 2005.

[33] M. Yamaguchi, *Polym. Engr. and Sci.,* vol. 46, pp. 1284-1291, 2006.

[34] N. Kukaleva, G. P. Simon and E. Kosior, *Polym. Eng. Sci.,* vol. 43, no. 1, p. 26, 2003.

[35] A. Valenza, F. P. LaMantia and D. J. Acierno, *J. Rheol.,* vol. 30, p. 1085, 1986.

[36] L. Bai, Y.-M. Li, W. Yang and M.-B. Yang, *J. Appl. Polym. Sci.,* vol. 118, pp. 1356-1363, 2010.

[37] K. Jordens and et al, *Polymer,* vol. 41, pp. 7175-7192, 2000.

[38] W. W. Graessley and S. F. Edwards, *Polymer,* vol. 22, pp. 1329-1334, 1981.

[39] Y.-H. Zang and P. J. Carreau, *J Appl Polym Sci,* vol. 42, pp. 1965-1968, 1991.

[40] L. Yang, R. H. Somani, I. Sics, B. S. Hsiao, R. Klob, H. Fruitwala and C. Ong, *Macromolecules,* vol. 37, pp. 4845-4859, 2004.

[41] S. M. Ghasemi and G. Mir Mohamad Sadeghi, *J. Appl. Polym. Schi.,* vol. 108, pp. 2988-2993, 2008.

[42] M. J. Hato and A. S. Luyt, *J. Appl. Polym. Sci.,* vol. 104, pp. 2225-2236, 2007.

[43] H. Matsuyama, H. Okafuji, T. Maki, M. Teramoto and N. Kubota, *J. Memb. Sci.,* vol. 223, pp. 119-126, 2003.

[44] I. Krupa and et al, *European Polym J,* vol. 43, pp. 4695-4705, 2007.

[45] E. J. Lee, J. K. Park, Y.-S. Lee and K.-H. Lim, *Korean J. Chem. Eng.,* vol. 27, no. 2, pp. 524-530, 2010.

[46] Y. Ogino, H. Fukushima, G. Matsuba, N. Takahashi, K. Nishida and T. Kanaya, *Polymer,* vol. 47, pp. 5669-5677, 2006.

[47] M. J. Hill and P. J. Barham, *Polymer,* vol. 36, no. 8, pp. 1523-1530, 1995.

[48] K. L. Lim, Z. A. Mohd Ishak, U. S. Ishiaku, A. M. Y. Fuad, A. H. Yusof, T. Czigany, B. Pukanszky and D. S. Ogunniyi, *J. Appl. Polym. Sci.,* vol. 97, pp. 413-425, 2005.

[49] J.-t. Yeh, Y.-l. Lin and C.-c. Fan-Chiang, *Macromol. Chem. Phys,* vol. 197, pp. 3531-3540, 1996.

[50] D. Xu, Y. Bin and P. Tang, *Macromolecules,* vol. 43, pp. 5323-5329, 2010.

[51] Y. Bin, L. Ma, R. Adachi, H. Kurosu and M. Matsuo, *Polymer,* vol. 42, pp. 8125-

8135, 2001.

[52] J.-T. Yeh, S.-S. Chang and T.-W. Wu, *J. Appl. Polym. Schi*, vol. 107, pp. 854-862, 2008.

[53] A. Rudin, W. J. Tchir, R. Gagnon, H. P. Schreiber and R. Callacott, *Ind. Eng. Chem. Res,* vol. 28, pp. 174-178, 1989.

[54] M. Motooka, H. Mantoku and T. Ohno, "Process for Producing Stretched Articles of Ultra-high Molecular Weight Polyethylen". United States Patent 4,545,950, 8 October 1985.

[55] M. Motooka, H. Mantoku and T. Ohno, "Process for Producing Streched Articles of Ultrahigh-Molecular Weight Polyethylene". United States Patent 4,612,148, 16 Sept 1986.

[56] Y. Ohta, H. Murase, H. Sugiyama and H. Yasuda, *Polym. Eng. Sci.,* vol. 40, no. 11, p. 2414, 2000.

[57] H. Murase, T. Kume and T. Hashimoto, *Macromolecules,* vol. 38, pp. 8719-8728, 2005.

[58] H. Murase, T. Kume, T. Hashimoto and Y. Ohto, *Macromolecules,* vol. 38, pp. 6656-6665, 2005.

[59] L. Shen, M. Peng, F. Qiao and J.-l. Zhang, *Chinese J. Polym. Sci.,* vol. 26, no. 6, pp. 653-657, 2008.

[60] J. A. Molefi and et al, *Thermochimica Acta,* vol. 500, pp. 88-92, 2010.

[61] S. Liu and et al, *J Membrane Sci,* vol. 379, pp. 268-278, 2011.

[62] U. Beginn, *Macromol. Mater. Eng.,* vol. 288, pp. 245-251, 2003.

[63] M. Y. Jeon and C. K. Kim, *J. Membrane Sci,* vol. 300, pp. 172-181, 2007.

[64] H. G. Barth and J. W. Mays (eds.), Modern Methods of Polymer Characterization, New York, NY: Wiley & Sons, p. 227.

[65] W. W. Graeslley, Polymeric Liquids and Networks: Structure and Properties, New York, NY: Francis Books, Inc, 2004.

[66] E. Guth and H. F. Mark, *Monatsh,* vol. 65, p. 93, 1934.

[67] A. Einstein, Investigations on the Theory of Brownian Movement, New York, NY: Dover Publications, 1906.

[68] G. K. Batchelor, *J. Fluid Mech.,* vol. 83, p. 97, 1977.

[69] T. G. Fox and P. J. Flory, *J. Phys. Colloid Chem.,* vol. 53, p. 197, 1949.

[70] W. Haller, *Kolloid Z,* vol. 56, p. 257, 1931.

[71] W. Kuhn, *Kolloid Z.,* vol. 68, p. 2, 1934.

[72] R. Houwink, *J. Prakt. Chem.,* vol. 15, p. 157, 1940.

[73] I. Sakurada, *Kasen Koenshu,* vol. 5, p. 33, 1940.

[74] I. Sakurada, *Kasen Koenshu,* vol. 6, p. 177, 1941.

[75] M. Rubinstein and R. H. Colby, Polymer Physics, New York, NY: Oxford University Press, Inc., 2003.

[76] L. A. Utracki and M. R. Kamal, *Polym. Eng. Sci.,* vol. 22, p. 96, 1982.

[77] L. A. Utracki, *Polym. Eng. Sci.,* vol. 23, p. 602, 1983.

[78] L. A. Utracki, *J. Rheol.,* vol. 35, p. 1615, 1991.

[79] C. M. Roland, *J. Polym. Sci., Part B: Polym. Phys.,* vol. 26, pp. 839-856, 1988.

[80] C. Tsenoglou, *Polym. Prepr.,* vol. 28, pp. 185-186, 1987.

[81] G. C. Berry and T. G. Fox, *Adv. Polym. Sci,* vol. 5, pp. 261-357, 1968.

[82] D. Nichetti and I. Manas-Zloczower, *J. Rheol.,* vol. 4, p. 42, 1998.

[83] T. G. Fox and P. J. Flory, *J. Phys. Colloid Chem.,* vol. 55, pp. 221-228, 1951.

[84] M. Aguilar and et al, *Polymer,* vol. 42, pp. 9713-9731, 2001.

[85] V. R. Raju and et al, *J. Polym. Sci. Phys. Ed.,* vol. 17, pp. 1183-1195, 1979.

[86] J. F. Vega and et al, *Rheol Acta,* vol. 118, pp. 1156-1363, 2012.

[87] E. M. Friedman and R. S. Porter, *Trans. Soc. Rheol.*, vol. 19, p. 493, 1975.

[88] J. D. Ferry, Viscoelastic Properties of Polymers, 3rd ed., New York, NY: John Wiley & Sons, 1980.

[89] M. Doi and S. F. Edwards, The Theory of Polymer Dynamics, Oxford, UK: Claredon Press, 1986.

[90] C. J. Tsenoglou, *Polym. Sci., Part B: Polym. Phys.*, vol. 26, p. 2329, 1988.

[91] M. L. Huggins, *J. Chem. Phys.*, vol. 9, p. 440, 1941.

[92] P. J. Flory, *J. Chem. Phys.*, vol. 9, p. 660, 1941.

[93] R. L. Scott, *J. Polym. Sci.*, vol. 9, p. 423, 1952.

[94] P. J. Flory, Principles of Polymer Chemstry, Ithica, NY: Cornell University Press, 1953.

[95] I. A. Hussein and et al, *Polym Degredation and Stability*, vol. 68, pp. 381-392, 2000.

[96] M. J. Hill, P. J. Barham and A. Keller, *Polymer*, vol. 12, no. 33, pp. 2530-2541, 1992.

[97] P. Smith and R. S. J. Manley, *Macromolecules*, no. 12, pp. 483-491, 1979.

[98] M. J. Hill and P. J. Barham, *Polymer*, no. 33, p. 4891, 1992.

[99] M. J. Hato and A. S. Luyt, *J. of Appl. Polym. Sci.*, no. 104, pp. 2225-2236, 2007.

[100] H. Munstedt, *Soft Matter*, vol. 7, pp. 2273-2283, 2011.

[101] M. Muthukumar, *Chem. Phys. Letters*, vol. 22, no. 1329-1334, 1981.

[102] D. S. Pearson, A. Mera and W. E. Rochefort, *Am. Chem. Soc. Polym. Preprints*, vol. 22, no. 102, 1981.

[103] W. W. Graessley, *Advan. Polym. Sci.*, vol. 1, 1974.

[104] H. Fujita and Y. Einaga, *Polymer*, vol. 31, pp. 1486-1490, 1990.

[105] J. F. Douglas and J. B. Hubbard, *Macromolecules*, vol. 24, pp. 3163-3177, 1991.

[106] K. W. Ebagninin, A. Benchabane and K. Bekkour, *J. of Colloid and Interface Sci.,* vol. 336, pp. 360-367, 2009.

[107] P. G. de Gennes, *Nature,* vol. 282, pp. 367-370, 1979.

[108] C. H. Stephens, A. Hiltner and E. Baer, *Macromolecules,* vol. 36, pp. 2733-2741, 2003.

[109] H. Kwang, D. Rana, K. Cho, J. Rhee, T. Woo, B. H. Lee and S. Choe, *Polym. Eng. Sci.,* vol. 40, no. 7, p. 1672, 2000.

[110] Y. Wang, K. Meng, X. Xie, S. Hong, C. Zhang and C. Han, *Polymer,* vol. 11, 2008.